Modelling air-water behaviour in intermittent water supply systems

Ferreira, J.P.

DOI
10.4233/uuid:1c8d5a95-b9e2-447c-af7d-b77b24c0a3f2

Publication date
2025

Document Version
Final published version

Citation (APA)
Ferreira, J. P. (2025). *Modelling air-water behaviour in intermittent water supply systems*. [Dissertation (TU Delft), Delft University of Technology]. https://doi.org/10.4233/uuid:1c8d5a95-b9e2-447c-af7d-b77b24c0a3f2

Important note
To cite this publication, please use the final published version (if applicable).
Please check the document version above.

MODELLING AIR-WATER BEHAVIOUR IN INTERMITTENT WATER SUPPLY SYSTEMS

MODELLING AIR-WATER BEHAVIOUR IN INTERMITTENT WATER SUPPLY SYSTEMS

Proefschrift

ter verkrijging van de graad van doctor
aan de Technische Universiteit Delft,
op gezag van de Rector Magnificus Prof. dr. ir. T.H.J.J. van der Hagen,
voorzitter van het College voor Promoties,
in het openbaar te verdedigen op vrijdag 21 februari om 12.30 uur

door

João Paulo BORGES COURY CAVALEIRO DE FERREIRA

Master in Civil Engineer,
Instituto Superior Técnico, Portugal,
born in Lisbon, Portugal

Dit proefschrift is goedgekeurd door de
promotor: prof. dr. Z. Kapelan
promotor: prof. dr. D. I. C. Covas

Samenstelling promotiecommissie bestaat uit:

Rector Magnificus,	voorzitter
Prof. dr. Z. Kapelan,	Technische Universiteit Delft
Prof. dr. D. Covas,	Instituto Superior Técnico, Portugal
Dr. D. Ferràs,	IHE-Delft
Onafhankelijke leden:	
Prof. dr. R. Farmani,	University of Exeter, United Kingdom
Prof. dr. ir. L. Rietveld,	Technische Universiteit Delft
Dr. M. Ferrante,	Università degli Studi di Perugia, Italy
Dr. A. Campisano,	Università di Catania, Italy
Prof. dr. ir. R. Uijlenhoet,	Technische Universiteit Delft, reservelid

Keywords: Air pockets formation, Air-water interface, Pipe-filling events, Intermittent water supply, Water pipelines
Printed by: Proefscrift-aio.nl
Front & Back: Inverted light painting, artisticly representing bubbles.

ISBN 000-00-0000-000-0

An electronic version of this dissertation is available at http://repository.tudelft.nl/.

“Se podes olhar, vê. Se podes ver, repara.”

José Saramago

ACKNOWLEDGEMENTS

At the end of this PhD, I cannot but thank and acknowledge the people who made it possible, from the professional to the most personal context. I came to TU Delft walking and I am now leaving it, literally, on two wheels.

First I would like to thank Professor Zoran Kapelan, Professor Dídia Covas and Professor David Ferras. Thank you Professor Zoran Kapelan for providing me with the amazing opportunity to carry out my doctoral studies at TU Delft. Your knowledge, encouragement and critical thinking were essential to complete this PhD successfully. Thank you Professor Dídia Covas for trusting me, now and in all the past instances, pushing me forward with motivation and never-ending support. This PhD was only possible because of you in moments way before its inception, when you sparked my interest in hydraulics and research. Thank you Professor David Ferras, for supporting me, paying attention to the details and making me a better researcher in the process. Also thank you for the discussions on hydraulics over what some people would consider an Irish "meal".

This thesis was carried out thanks to the generous financial support from the doctoral fellowship (SFRH/BD/146709/2019) funded by the Portuguese Foundation for Science and Technology (FCT).

To all my friends who helped me on this journey, thank you! To people I knew before starting this PhD journey, I need to deeply thank Filipa, along with Ori, Nuno, Sio, Stefano, for the long chats during the pandemic that kept me afloat, who incentivised and motivated me to look further despite the distance. Also, thank you André, Carreiro, Elisa, Inês, Marina and Pina for your continuous support and friendship. To Angela, Antonio, Emanuelle, Tiziana and Alexandre (yes, you are already included) who make me feel so at home in Italy and make sure I never really lose it.

I am grateful to Andrew Donnelly, Nuno Dias and Vera Marmelo who, unknowingly, helped me define the initial idea for this PhD thesis and for giving me a completely different insight into water supply systems.

Through my time in Delft and TU, to all who made 4.54 welcoming rather than a simple open space, with special thanks to Antonia, Daniel, Diana Calejas, Diana Fiorillo, Hamed and Zoë, Lais and Maikon. You made the arrival in Delft and the first months of the PhD the best I could have wished. Thank you, Raquel and Detmar for being there whenever I needed help and was home sick. Thanks to Aashna, Alex, Antonella, Job, Roberto and Sofia, who made the PhD at TU Delft such a nice time surrounded by friends. Thank you André, Andres, Anurag, Carina, Emiel, Екатерина, Guilherme, Iosif, Joana, Luuk, Roos, Tuğba, Sevda, Simon and Yana who joined for coffee, free coffee and not coffee, and all lunches, creating multiple insightful discussions and chats that made everything easier.

Alexander and Manu, thank you for spending so much time at a table due to our common interests and the peaceful and diplomatic evenings that dragged on endlessly over the board because no one dared to bite the bullet. To those who tell you to trust them,

thank you Марияна and Елица, Mário and Julia, Stephan and Zé for the uncontrollable and uncountable laughs and good moments.

Last but not least, I thank my family for being there at all times, motivating me through the hardest times, and withstanding the distance throughout this period of my life. Thank you to my grandmother Widad for making me imagine and see the positive outcomes when they were needed the most. Thank you to my siblings, Beatriz, Luís and Pedro, for the constant support. Finally, I am eternally grateful to my parents, Cristina and Paulo, for never placing barriers to my goals and for always believing in the path I am paving for myself.

CONTENTS

LIST OF FIGURES

LIST OF TABLES

LIST OF ACRONYMS

The next list describes the acronyms that will be later used within the body of the thesis:

CFD Computational Fluid Dynamics

CWS Continuous Water Supply

DDA Demand-Driven Analysis

DVCM Discrete Vapour Cavity Model

EPA Environmental Protection Agency

EPS Extended Period Simulation

EWC Elastic Water Column

EXTRAN Extended Transport (surcharge method in SWMM)

IWS Intermittent Water Supply

MOC Method of Characteristics

MSX Multi-Species Extension

PDA Pressure-Driven Analysis

RMSE Root Mean Square Error

ROI Region of Interest

RTX Real-Time Extension

RWC Rigid Water Column

SDG Sustainable Development Goals

SLOT Preissmann Slot (surcharge method in SWMM)

SPH Smooth Particle Hydrodynamic

SV-E Saint-Venant Equations

SWMM Stormwater Management Model

VOF Volume of Fluid

WNTR Water Network Tool for Resilience

WSS Water Supply System

LIST OF SYMBOLS

The next list describes the symbols that will be later used within the body of the thesis:

Constants

g	Gravitational acceleration (m s^{-2})
R	Gas constant (J K^{-1} mol^{-1})

Greek symbols

β	Pressure-flow rate relation for PDA
Δ	Variation
γ	Specific weight (N m^{-3})
ρ	Density (kg m^{-3})
θ	Pipe angle with horizontal (°)

Subscripts

AP	Air Pocket
atm	Atmospheric
av	Average
c	Critical
f	Final
i	Initial
j	Orifice index
max	Maximum
min	Minimum
p	Pipe
r	Relative
w	Water

Variables

$\overline{A}$ Average flow area variation (m^2)

A Flow cross-section area (m^2)

a Air entrainment factor (-)

b Air entrainment exponent (-)

c Pipe wave celerity ($m\ s^{-1}$)

c_1 Pipe constraint coefficient (-)

C_{drag} Drag coefficient (-)

C_d Discharge coefficient (-)

C_r Courant number (-)

D Pipe diameter (m)

d Orifice diameter (m)

E Pipe Young modulus of elasticity (Pa)

e Pipe wall thickness (m)

F Froude number (-)

H Pressure-head (m)

K Water bulk modulus (Pa)

k Polytropic coefficient (-)

L Pipe length (m)

l Longer axis air pocket length (m)

n Coefficient describing air pocket depth (-)

p Pressure (Pa)

Q Flow rate ($m^3\ s^{-1}$)

$Q^{friction}$ SWMM's friction component of the flow rate ($m^3\ s^{-1}$)

$Q^{inertia}$ SWMM's inertial component of the flow rate ($m^3\ s^{-1}$)

$Q^{pressure}$ SWMM's pressure component of the flow rate ($m^3\ s^{-1}$)

r Air pocket radius (m)

R_e Reynolds number (-)

S Cross section area (m^2)

s	Orifice cross section area (m^2)
S_f	Friction slope (-)
T	Temperature (K)
t	Time (s)
T_s	Preissmann slot width (m)
U	Average flow velocity ($m\ s^{-1}$)
V	Volume (m^3)
x	Spatial coordinate along the pipe axis (m)
Y	Orifice expansion factor (-)

SUMMARY

Water supply networks represent key infrastructures to provide safe, reliable, drinking water with adequate pressure to communities, thus ensuring people's health and well-being. These networks can be operated continuously or intermittently. Continuous water supply (CWS) is characterised by delivering permanently pressurised piped water to consumers with adequate pressure, meeting water quality standards and preventing potential contaminant intrusion. Intermittent water supply (IWS) also provides piped water, though only ensures delivery during limited periods of the day or the week, with interruptions from hours to days. This service is common in areas with limited water resources and with financial constraints. Despite the technological and management advancements in the water sector, most utilities with IWS have limited knowledge of the network performance due to unavailable or unreliable data or the lack of numerical models to better understand the systems' operation. The development of numerical models to describe the phenomena in each IWS stage (filling, supplying and emptying) is important for design, diagnosis and management purposes. Most developed research focuses on the supply stage, using models with the assumption that the pipes are continuously pressurised. Since that is not the case, a model that allows simulating free-surface and pressurised flows is necessary to describe the other two IWS stages.

The thesis aims to develop and validate a new 1D model, based on the widely used SWMM solver, capable of describing the air-water interaction during pipe-filling events in IWS systems. The specific objectives of this research are: i) to identify, understand and characterise the most relevant air pocket related phenomena during pipe-filling events in single pipes and looped networks; ii) to learn how to incorporate the air pressurisation in SWMM solver as well as iii) the different mechanisms associated with the air pocket creation; iv) to understand the model's uncertainties related to these phenomena; and v) to test the developed model in a real-life network.

To accomplish objective i) and to contribute to objectives ii) - iv), an extensive experimental data collection program is developed to understand the phenomena related to the air pocket creation during the pipe-filling event. Collected data include time series of pressure and flow rate and video recordings of entrapped air pockets, for different pipe configurations and aeration conditions. Three pipe configurations are tested: a straight horizontal pipe, a single pipe with a high point and a single-loop pipe network. Three aeration conditions end are tested: no air release, restricted and unrestricted air release.

Several novel numerical developments are gradually implemented to fulfil key objectives ii) - iv). The first is the modification introduced in the existing SWMM hydraulic solver to incorporate the air phase. A conventional air accumulator model is implemented and coupled with SWMM flow calculations. Experimental data collected during the rapid filling of a single horizontal pipe for the three referred aeration conditions are used for model calibration and validation (fulfilling objective ii). Results show that the improved SWMM, AirSWMM(v1.0), describes better the effect of air behaviour during

pipe-filling events than the original SWMM when using the EXTRAN surcharge method.

The AirSWMM(v1.0) model is improved to locate and quantify entrapped air pockets created during the pipe-filling events in single undulating pipe systems. Measurements are collected and video recordings are carried out to assess air pocket volumes for the three referred air release conditions. The stochastic nature of air pocket creation results in a range of air volumes predicted for the same aeration conditions. The new version of the model developed, AirSWMM(v2.0), is capable of simulating the air pocket creation, transport and entrainment (air and water mixing process). The stochastic nature of air pocket formation can be numerically simulated by conducting multiple runs of the new solver with different air entrainment ratios. The obtained numerical results show that AirSWMM(v2.0) can accurately locate and approximately quantify the entrapped air pocket volumes. These developments contribute to objective iii).

The AirSWMM(v2.0) model is further tested and validated using experimental data from a single-loop network laboratory setup. Experimental data consisting of pressure-head at multiple locations and video recordings of air entrapment for two high point locations and different nodal elevations, under three aeration conditions, are used. Experimental tests show that air entrapment occurs not only at the high point but along the pipe network, creating air pockets with elongated shapes and larger volumes than for single pipe systems. AirSWWM(v2.0) model results for the looped pipe network demonstrate that this model can correctly locate large air pockets with a tendency to underestimate their volumes. These developments contribute to objective iv).

The AirSWWM(v2.0) model is also tested using a case study of a real-life network published in the literature to assess the accuracy of predicted locations and volumes of the air pockets created during a pipe-filling event. For this purpose, pressure-driven analysis is implemented to better simulate the nodal demands, leading to AirSWMM(v2.1), since this feature was not originally included in SWMM. Results show that pressure-heads predicted by AirSWMM(v2.1) compare well with field data when constant spatial discretisation is used, provided the Courant number is close to 0.15. The recommendations from international guidelines for the location of air release devices (from the American Water Works Association and Deltares) are compared to the predicted air pocket locations. The locations of the estimated air pockets agree with those from the international guidelines for air valve installation. However, these locations only represent part of the air valves needed, those that are necessary for releasing entrapped air during the pipe-filling events, not accounting for other air valves important for pipe failure or conservative design purposes. These developments contribute to objective v).

Further research on AirSWMM should focus on assessing the spatial discretisation that corresponds to the best compromise between accuracy and computational effort to describe the air pocket dynamics in real-life networks. Additional numerical analyses should assess if the developed methodologies can be incorporated into the Preissmann slot pressurisation scheme. More experimental tests are needed to better quantify the air entrainment in piped flows and to analyse the effect of two-phase flows on leakage rate. Further field tests, collecting high-frequency pressure head data, should be carried out during pipe-filling events to validate the developed models.

SAMENVATTING

Drinkwaterdistributienetwerken zijn belangrijke infrastructuren om gemeenschappen van veilig, betrouwbaar drinkwater met voldoende druk te voorzien en zo de gezondheid en het welzijn van de mensen te garanderen. Deze netwerken kunnen continu of met tussenpozen worden gebruikt. Continue watervoorziening (continuous water supply, CWS) wordt gekenmerkt door het met voldoende druk leveren van leidingwater aan consumenten, waarbij wordt voldaan aan de waterkwaliteitsnormen en de instroom van mogelijke verontreinigingen wordt voorkomen. Intermitterende watervoorziening (IWS) levert ook leidingwater, maar alleen gedurende beperkte perioden van de dag of de week, met onderbrekingen van uren tot dagen. Dit komt vaak voor in gebieden met beperkte waterbronnen en financiële beperkingen. Ondanks de vooruitgang in technologie en beheer kennis in de watersector hebben de meeste nutsbedrijven met IWS beperkte kennis van de prestaties van het netwerk vanwege niet-beschikbare of onbetrouwbare data en het ontbreken van numerieke modellen om de werking van de systemen beter te begrijpen. De ontwikkeling van numerieke modellen om de fenomenen in de verschillende IWS-fases (vullen, toevoeren en legen) te beschrijven, is belangrijk voor ontwerp-, diagnose- en managementdoeleinden. Dit proefschrift onderzoekt de vullingsfase van IWS, en ontwikkeld verbeterde methodes om het gedrag van IWS netwerken beter te begrijpen, door bestaande numerieke modellen uit te breiden om tweefasige stromen op te lossen. Dit onderzoek is gedaan door een combinatie van uitgebreid experimenteel werk en het ontwikkelen van nieuwe numerieke model toepassingen

Het doel van dit proefschrift is het ontwikkelen en valideren van een nieuw 1D-model, gebaseerd op de veelgebruikte SWMM-solver, waarmee de interactie tussen lucht en water tijdens het vullen van leidingen in IWS-systemen kan worden beschreven. De specifieke doelstellingen van dit onderzoek zijn: i) het identificeren, begrijpen en karakteriseren van de meest relevante gasbel gerelateerde verschijnselen tijdens het vullen van leidingen in enkelvoudige leidingen en netwerken met lussen; ii) het opnemen van de luchtdruk in de SWMM-solver en iii) de verschillende mechanismen die samenhangen met het ontstaan van luchtzakken; iv) het begrijpen van de onzekerheden in het model die samenhangen met deze verschijnselen; en v) het testen van het ontwikkelde model in een bestaand drinkwaterdistributienetwerk.

Om doelstelling i) te bereiken en bij te dragen aan doelstellingen ii) - iv), is een uitgebreid experimenteel programma ontwikkeld om inzicht te krijgen in de verschijnselen die samenhangen met het ontstaan van gasbellen tijdens het vullen van de pijp. De verzamelde gegevens omvatten tijdreeksen van druk en stroomsnelheid, en videoopnamen van ingesloten gasbellen voor verschillende pijpconfiguraties en beluchtingsomstandigheden. Er werden drie pijpconfiguraties getest: een rechte horizontale pijp, een enkele pijp met een hoog punt en een pijpnetwerk met één lus. Er worden drie beluchtingsomstandigheden getest: geen luchtafvoer, beperkte luchtafvoer en onbeperkte luchtafvoer.

Verschillende nieuwe numerieke ontwikkelingen worden geleidelijk geïmplementeerd om te voldoen aan de hoofddoelstellingen ii) - iv). De eerste is de wijziging die wordt aangebracht in de bestaande SWMM hydraulische solver om de luchtfase op te nemen. Een conventioneel lucht accumulatiemodel wordt geïmplementeerd en gekoppeld aan SWMM-stroomberekeningen. Experimentele gegevens die zijn verzameld tijdens de vullingsfase van een horizontale pijp voor de drie eerdergenoemde beluchtingscondities worden gebruikt voor modelkalibratie en -validatie (om te voldoen aan doelstelling ii). De resultaten tonen aan dat de verbeterde SWMM, AirSWMM(v1.0), het effect van luchtgedrag tijdens het vullen van pijpen beter beschrijft dan de oorspronkelijke SWMM bij gebruik van de EXTRAN overdrukmethode.

Daarna is het AirSWMM(v1.0) model verbeterd om de ingesloten gasbellen in een enkelvoudig golvend pijpsysteem te kunnen het lokaliseren en kwantificeren .. Er worden metingen verzameld en video-opnamen gemaakt om de gasbelvolumes te beoordelen voor de drie genoemde omstandigheden waarin lucht vrijkomt. De stochastische aard van het ontstaan van gasbellen resulteert in een reeks voorspelde luchtvolumes voor dezelfde beluchtingsomstandigheden. De nieuwe versie van het op deze manier ontwikkelde model AirSWMM(v2.0) is in staat om het ontstaan van gasbellen, transport en stagnatie (het mengen van lucht en water) te simuleren. De stochastische aard van gasbelvorming kan numeriek worden gesimuleerd door meerdere runs van de nieuwe solver uit te voeren met verschillende luchtmeevoerscoëfficiënten. De verkregen numerieke resultaten tonen aan dat AirSWMM(v2.0) de ingesloten gasbelvolumes nauwkeurig kan lokaliseren en bij benadering kan kwantificeren. Deze ontwikkelingen dragen bij aan doelstelling iii).

Het AirSWMM(v2.0) model wordt verder getest en gevalideerd met behulp van experimentele gegevens van een laboratoriumopstelling met een enkel lusnetwerk. Er worden experimentele gegevens gebruikt die bestaan uit drukmetingen op meerdere locaties en video-opnamen van luchtinsluiting voor twee locaties met een hoog punt en verschillende knooppunthoogten, onder drie beluchtingscondities. Experimentele tests tonen aan dat luchtinsluiting niet alleen optreedt op het hoge punt, maar ook langs het leidingnetwerk, waardoor luchtzakken ontstaan met langwerpige vormen en grotere volumes dan bij systemen met één pijp. De resultaten van het AirSWM(v2.0) model voor het leidingnetwerk met lussen tonen aan dat dit model grote luchtzakken correct kan lokaliseren, waarbij de neiging bestaat om hun volume te onderschatten. Deze ontwikkelingen dragen bij aan doelstelling iv).

Het AirSWMM(v2.0)-model wordt ook getest met behulp van een in de literatuur gepubliceerde casus van een bestaand netwerk om de nauwkeurigheid van de voorspelde locaties en volumes van de gasbellen die tijdens het vullen van een leiding ontstaan, te beoordelen. Voor dit doel wordt een drukgestuurde analyse geïmplementeerd om de nodale eisen met AirSWMM(v2.1) beter te simuleren, aangezien deze functie oorspronkelijk niet in SWMM was opgenomen. De resultaten tonen aan dat de door AirSWMM(v2.1) voorspelde drukhoogtes goed overeenkomen met veldgegevens wanneer een constante ruimtelijke discretisatie wordt gebruikt, mits het Courant-getal dicht bij 0,15 ligt. De aanbevelingen uit internationale richtlijnen voor de locatie van luchtafblaasvoorzieningen (van de *American Water Works Association* en *Deltares*) worden vergeleken met de voorspelde locaties van de gasbellen. De locaties van de geschatte gasbellen komen overeen

met die van de internationale richtlijnen voor de installatie van luchtkleppen. Deze locaties vertegenwoordigen echter slechts een deel van de benodigde luchtkleppen, namelijk de kleppen die nodig zijn voor het vrijlaten van ingesloten lucht tijdens het vullen van de pijp, zonder rekening te houden met andere luchtkleppen die belangrijk zijn voor het falen van de pijp of voor conservatieve ontwerpdoeleinden. Deze ontwikkelingen dragen bij aan doelstelling v).

Verder onderzoek naar AirSWMM moet zich richten op het bepalen van de ruimtelijke discretisatie die overeenkomt met het beste compromis tussen nauwkeurigheid en rekenkracht om de dynamica van gasbellen in echte netwerken te beschrijven. Met aanvullende numerieke analyses moet worden beoordeeld of de ontwikkelde methodologieën kunnen worden opgenomen in het drukregelschema van Preissmann sleuven. Er zijn meer experimentele tests nodig om de luchtinsluiting in leidingstromen beter te kwantificeren en om het effect van tweefasestromen op de leksnelheid te analyseren. Verdere veldproeven, waarbij gegevens over de drukhoogte met hoge frequentie worden verzameld, moeten worden uitgevoerd tijdens het vullen van pijpleidingen om de modellen te valideren.

RESUMO

As redes de abastecimento de água são infra-estruturas essenciais para fornecer água potável segura, fiável e com pressão adequada a centros urbanos, garantindo a saúde e o bem-estar da população. Estas redes podem operar de forma contínua ou intermitente. O abastecimento contínuo caracteriza-se pelo fornecimento de água permanentemente pressurizada em condutas aos consumidores com uma pressão adequada, cumprindo os regulamentos de qualidade da água e evitando a potencial intrusão de contaminantes. O abastecimento intermitente de água (IWS) também fornece água canalizada, mas apenas assegura o fornecimento durante períodos limitados do dia ou da semana, com interrupções de horas a dias. Este tipo de operação é comum em regiões com recursos hídricos limitados e com restrições financeiras. Apesar dos avanços tecnológicos e de gestão no sector da água, a maioria das entidades gestoras com IWS têm um conhecimento limitado do desempenho da rede devido à indisponibilidade de dados, à sua baixa fiabilidade, ou à falta de modelos numéricos para compreender melhor o funcionamento destes sistemas. O desenvolvimento de modelos numéricos para descrever os fenómenos em cada fase de IWS (enchimento, abastecimento e esvaziamento) é importante para efeitos de dimensionamento, diagnóstico e gestão. A maior parte da investigação desenvolvida centra-se na fase de abastecimento, utilizando modelos com o pressuposto de que as condutas estão continuamente pressurizadas. Uma vez que tal não se verifica, é necessário um modelo que permita a simulação de caudais de superfície livre e pressurizados para descrever as outras duas fases do IWS.

A tese visa desenvolver e validar um novo modelo 1D, baseado no solver SWMM amplamente utilizado, capaz de descrever a interação ar-água durante eventos de enchimento de condutas em sistemas com operação intermitente. Os objectivos específicos desta investigação são: i) identificar, compreender e caraterizar os fenómenos mais relevantes relacionados com bolsas de ar durante enchimento de condutas em condutas simples e redes malhadas; ii) compreender e incorporar a pressurização do ar no modelo SWMM, bem como iii) os diferentes mecanismos associados à criação de bolsas de ar; iv) compreender as incertezas do modelo relacionadas com estes fenómenos; e v) testar o modelo desenvolvido numa rede real.

Para atingir o objetivo i) e contribuir para os objectivos ii) - iv), é desenvolvido um programa de recolha de dados experimentais para compreender os fenómenos relacionados com a criação de bolsas de ar durante o enchimento de condutas. Os dados recolhidos incluem séries temporais de pressão e caudal e gravações vídeo de bolsas de ar aprisionadas, para diferentes configurações de tubos e condições de arejamento. São testadas três configurações de condutas: um tubo horizontal reto, uma conduta simples com um ponto alto e uma rede de de condutas malhada. São testadas três condições de arejamento: sem libertação de ar, com libertação de ar restrita e sem restrições.

Vários desenvolvimentos numéricos são gradualmente implementados para cumprir os objectivos-chave ii) - iv). O primeiro é a modificação introduzida no atual modelo

hidráulico SWMM para incorporar a fase aérea através da implementação do modelo convencional de acumulador de ar nos cálculos de caudal do SWMM. Os dados experimentais recolhidos durante o enchimento rápido de uma conduta horizontal simples para as três condições de arejamento referidas são utilizados para a calibração e validação do modelo (cumprindo o objetivo ii). Os resultados mostram que o SWMM melhorado, AirSWMM(v1.0), descreve melhor o efeito do comportamento do ar durante os processos de enchimento de condutas que o SWMM original quando se utiliza o método de sobrepressão EXTRAN.

O modelo AirSWMM(v1.0) é posteriormente melhorado para localizar e quantificar o volume das bolsas de ar aprisionadas durante os processos de enchimento de condutas em sistemas de condutas onduladas simples. São testadas diferentes condições de enchimento numa única conduta com um ponto alto. São recolhidas séries temporais de cota piezométrica e caudal e efectuadas gravações de vídeo para avaliar os volumes das bolsas de ar para as três condições de libertação de ar referidas. A natureza estocástica da criação de bolsas de ar resulta numa gama de volumes de ar previstos para as mesmas condições de arejamento. A nova versão do modelo desenvolvido, AirSWMM(v2.0), é capaz de simular a criação, transporte e arrastamento de bolsas de ar (processo de mistura de ar e água). A natureza estocástica da formação de bolsas de ar pode ser simulada numericamente através da realização de múltiplas simulações com diferentes rácios de arrastamento de ar obtendo resultados que mostram que o AirSWMM(v2.0) pode localizar com exatidão e quantificar aproximadamente os volumes das bolsas de ar arrastadas. Estes desenvolvimentos contribuem para o objetivo iii).

O modelo AirSWMM(v2.0) é ainda testado e validado utilizando dados experimentais de uma rede malhada simples instalada em laboratório. São recolhidos dados experimentais de cota piezométrica em vários locais da rede e são efetuadas gravações de vídeo do aprisionamento de ar para duas localizações do ponto alto e diferentes elevações geométricas da malha, em três condições de arejamento. Os testes experimentais mostram que o aprisionamento de ar ocorre não apenas no ponto alto, mas ao longo da malha de condutas, criando bolsas de ar com forma alongada e volumes superiores ao observado no caso de conduta simples. Os resultados do modelo AirSWWM(v2.0) para a rede malhada demonstram que este modelo pode localizar corretamente grandes bolsas de ar com uma tendência para subestimar os seus volumes. Estes desenvolvimentos contribuem para o objetivo iv).

O modelo AirSWWM(v2.0) é finalmente testado utilizando um caso de estudo de uma rede real publicada na literatura para avaliar a exatidão da localização de bolsas de ar e dos volumes correspondentes durante o processo de enchimento de condutas. Para este efeito, é implementada uma análise de entrega de caudal em função da cota piezométrica em cada nó do modelo para melhor simular os caudais de consumo solicitados com o AirSWMM(v2.1), uma vez que esta funcionalidade não foi originalmente incluída no SWMM. Os resultados mostram que cotas piezométricas previstas pelo AirSWMM(v2.1) comparam-se bem com os dados de campo quando é utilizada uma discretização espacial constante, desde que o número de Courant seja próximo de 0,15. As recomendações das directrizes internacionais para a localização de ventosas (da *American Water Works Association* e da *Deltares*) são comparadas com as localizações previstas das bolsas de ar, obtendo um boa sobreposição entre ambas. No entanto,

estas localizações representam apenas uma parte das ventosas necessárias, necessárias para libertar o ar aprisionado durante os processos de enchimento, não tendo em conta outras ventosas importantes para efeitos de rotura de condutas ou de dimensionamento conservativo. Estes desenvolvimentos contribuem para o objetivo v).

Investigação futura sobre o AirSWMM deve centrar-se na avaliação da discretização espacial que leva ao melhor compromisso entre precisão de resultados e esforço computacional para descrever a dinâmica das bolsas de ar em redes reais. Análises numéricas adicionais devem avaliar se as metodologias desenvolvidas podem ser incorporadas no esquema de sobrecarga de fenda de Preissmann. São também necessários mais ensaios experimentais para melhor quantificar o arrastamento de ar em escoamentos em pressão e para analisar o efeito dos escoamentos bifásicos em fugas de água. Devem ser efectuados mais ensaios de campo, recolhendo dados de pressão de alta frequência, durante eventos de enchimento de condutas para validar os modelos desenvolvidos.

1

Introduction

1

1.1. CONTEXT

Water supply systems (WSS) are vital infrastructures that provide an indispensable public service to society: the provision of safe drinking water. These systems are crucial to ensure the health and well-being of the populations, being generally composed of water treatment plants, storage tanks, pumping stations, and pipes. Electromechanical equipment, like valves and pumps, and instrumentation allow the normal operation of these systems. Water utilities managing WSS need to provide enough water with sufficient pressure and comply with water quality standards.

To achieve that, water treatment, transport and distribution should be carried out with enough reliability. Water treatment level depends on the water quality at the source and often has high operation costs associated with consumed electricity and chemical reagents. Water is transported in pressurised transmission pipes by gravity or pumping, stored in tanks and distributed in networks. It is essential to efficiently operate each of these WSS phases (treatment, transport and distribution) for a sustainable management of the infrastructure. The importance of water supply for society is highlighted by having an independent target in the United Nations' Sustainable Development Goal (SDG) fully dedicated to clean water (SDG6.1), aiming to achieve universal and equitable access to water with good enough quality and an affordable price to everyone. Water supply systems can be operated continuously or intermittently, which can significantly affect their management. If an intermittent operation is in place for long enough and consumers are prepared for it, water might be available around the clock, even though it is not provided 24/7 by the utility.

Continuous water supply (CWS) is defined as an uninterrupted supply to consumers, 24 hours a day, seven days a week. Water is stored in municipal tanks belonging to the water utility and the pipe system is continuously pressurised. Supply may be interrupted for operational and maintenance purposes, typically during short periods. The benefits of this type of operation include a reliable and accessible supply system for daily and emergency uses. Water contamination is minimised since the system is pressurised, preventing water intrusion in the pipes (Farley, 2001). These benefits are essential for ensuring enough water quantity and quality for consumers.

Intermittent water supply (IWS) is characterised by irregular non-continuous water delivery to consumers. Systems operating intermittently provide water to over 1.3 billion people, which corresponds to 39% of piped water supply on premises worldwide (Charalambous and Laspidou, 2017). Climate change and water shortages together with infrastructure ageing and insufficient rehabilitation investment result in the implementation of IWS in many distribution networks as a measure to reduce leakage and to comply with water demand. Such stresses have long been felt by countries in Latin America, Africa, the Middle East and Asia. More recently, climate stress has been affecting many Mediterranean countries where CWS is predominant, especially in southern Europe, given the gradual decrease in precipitation, frequent occurrence of droughts and reduction of groundwater sources (EEA, 2021).

Intermittent water supply involves three phases - system filling, water supply, and system depressurization or emptying - and a full cycle starts with water abruptly entering the system in the filling stage. The system gets progressively pressurised, and each service connection starts to supply water to the consumer. Water going into the system

forces the air inside out during this filling stage. Water supply systems do not usually include air valves because most air is released in the consumer taps. However, undulating pipe profiles without air valves promote the entrapment of air pockets that create local head losses and lead to pipe failures in case of water hammer events. During the supply stage, water is delivered to the consumers with varying pressure. Since operating pressures are lower in IWS systems than in CWS systems, the delivered flow rate is also lower and, consequently, the time to satisfy consumer water needs is higher. When the supply stage ends, the system is closed, and the network starts depressurizing and emptying. The remaining water inside the system will be delivered to service connections or drained from the system by leaks. Often, consumers have domestic tanks to ensure the water supply during the depressurization stage. Usually, there is a predetermined time until the system is pressurised again.

1.2. INTERMITTENT WATER SUPPLY

1.2.1. CAUSES AND CONSEQUENCES

Water supply systems are not originally designed to operate intermittently but rather become operated in such a way due to management decisions motivated by several factors. IWS may present short-term benefits from the management perspective to reduce operation and maintenance costs by reducing leakage volumes and all associated costs. However, IWS motivation is not limited to governance, but also due to the lack of available water and its consequences are not restricted to higher water losses.

The causes for implementing IWS are very broad and vary from system to system, including social issues, system and utility management, and third-party causes (Simukonda et al., 2018a). The main causes are described as follows:

- **Poor governance** is usually associated with the lack of investment in due time to ensure a reliable supply, political interference in the management of the utility and poor legislation and regulation. Such decisions influence the demographics and economic dynamics that stress the water supply infrastructure (Van der Bruggen et al., 2009, Chepyegon and Kamiya, 2018, Simukonda et al., 2018a). As more people move to urban areas and rely on an overloaded supply system, the supply starts becoming compromised and tends to IWS (Klingel, 2012). **Unplanned extensions of the network** are carried out as the population agglomerate around urban centres, compromising the water supply in other locations of the system (Galaitsi et al., 2016).

- **Poor system management** is linked to how the water is distributed in the system and how the billing system is conceptualized. Utilities can have a much higher tariff to wealthier consumers, which subsidises lower-income households. Several attempts have been made to keep the tariff equal to everyone complemented with subsidies for lower-income households (McIntosh, 2003, Hanjahanja and Omuto, 2018). **Limited knowledge within the utility** is also a core problem related to poor system management because established techniques applied in continuous water supply are not necessarily applicable and provide good outcomes in intermittent situations. Several types of equipment (e.g. leak detection sensors, flow meters)

still need to be improved or rethought to address intermittent water supply problems (Mokssit et al., 2018).

- Utilities might be forced onto intermittent water supply due to **hydrological causes and lack of water** in the current climate change context. Rainfall events are becoming progressively more uncertain and areas with continuous water supply might be affected by more recurrent droughts that will compromise such supply if it is not compromising the supply already (EEA, 2021). **Poor electric power supply** affects the water supply by disrupting treatment processes and the pumping scheduled to deliver water to the network. If power outages are frequent and uncertain, the utilities' capacity to have always treated water and the means to deliver it are compromised (Vairavamoorthy et al., 2001). **Consumers' awareness** is crucial for the population not to withdraw water excessively. Doing so has two main consequences: consumers downstream are not able to withdraw their required water volume as well as the consumers withdrawing excessive water volumes usually keep water in domestic storage tanks and the residence time is high, compromising the water safety.

Intermittent water supply has operational, maintenance and management consequences for the water utilities and consumers, which are not limited to water supply times. **Operational consequences** can affect both the water utility and the consumer. The main consequences for utilities include lower operating pressures that compromise the filling process, the possibility for more recurrent pressure variations, and the existence of a multi-phase flow, whilst consumers' consequences are related to water distribution inequity across the network and water quality problems. Lower pressures than the minimum required for continuous water supply systems reduce the amount of water to be delivered (Mahmoud et al., 2017). Such low pressures create severe inequity distribution issues in the network since some customers might have continuous water supply whereas others do not receive water at all (Sharma and Vairavamoorthy, 2009, Gottipati and Nanduri, 2014). Frequent and high-pressure variations during the day not only affect the quality of service provided by the water utility to the consumers but also subject the pipes to recurring pressure variations that can accelerate the ageing and degradation of the pipe and compromise the integrity of the system (Erickson et al., 2022). Conversely, consumers' behaviour can also influence pressure variations in household connections, even when the pipe is pressurised and filled with water, which is not related to IWS (Marsili, Mazzoni, Alvisi, et al., 2023). The occurrence of multi-phase flow (water, air and sediments) in drinking water networks can increase pressure variations due to the presence of air (Ferreira et al., 2021) and accelerate the biological processes in contact with air when the pipes are empty (Bautista-de Los Santos et al., 2019). The existence of air can also exacerbate the low pressure since entrapped air introduces localized energy losses due to the reduction of the flow cross-section (Lubbers and Clemens, 2007). Water quality issues caused by sediments are quite common in domestic storage tanks since the residence time of the water in the tanks is significantly high reaching very low levels of disinfectant to prevent bacterial growth (Gonzalez et al., 2020).

Maintenance consequences are related to the increased number of pipe failures in the network and increased water losses in the system over time. Christodoulou and

Agathokleous (2012) observed pipe failures increase from 30% to 70% per year with IWS operation when compared to the reports with CWS operation. Such an alarming pipe failure rate increases water losses that the implementation of IWS is trying to reduce.

Management consequences result from domestic water meters are not as reliable in IWS as in continuous water supply systems. Air released from the systems makes meters rotate several times faster than with water due to the density difference between the fluids (Ferrante et al., 2022) and the flow rate is measured while the network is filling and the air is released through the meters. This not only induces significant measurement errors but also considerably damages the equipment, compromising even more the accuracy of the measurements (Fontanazza et al., 2015, Walter et al., 2017).

After a period of IWS operation, the consequences start exacerbating and perpetuating its causes due to even higher pipe bursts, supply disruptions and higher water losses, thus creating a negative feedback loop. Also, when the system is operated in intermittent mode for too long, reversing the operation back to CWS is a challenge.

In summary, IWS is highly unreliable and inefficient in dealing with water scarcity, high water losses and demand control. The operation of IWS systems has three different stages – water filling, pressurised supply and emptying – involving filling and depressurization of strong two-phase air-water flows. Frequent IWS cycles gradually increase pipe bursts, leakage rates, metering errors and water quality issues due to two-phase flows. Main IWS consequences are i) accelerated deterioration of pipes and equipment leading to recurring pipe ruptures and supply disruptions, ii) insufficient level of service due to low pressures or supply interruptions, iii) high water losses, iv) high risk of contamination during depressurisation and v) increased water deterioration in domestic tanks.

1.2.2. AFFECTED STAKEHOLDERS

Previously referred causes and consequences allow the evaluation of the impacts of IWS on the stakeholders, namely consumers, service providers and governmental agencies. Domestic and commercial consumers are affected by supply rationing and poor water quality from the network or due to the longer water ageing in domestic tanks.

Service providers, such as water utilities, struggle to keep reliable revenue given the water tariffs and the non-revenue water rates. Utilities are further affected by higher operational costs given the water losses in these systems, and the need to repair pipe mains and service connections. Such difficulties prevent utilities from investing and rehabilitating their systems.

Governmental agencies, including government bodies and regulators, have considerable constraints on their decision-making due to the lack of information. It is more difficult to collect data on how the system operates and how it should be monitored, being difficult to assess the required key performance indicators usually used for the decision-making process.

Practitioners cannot correctly describe IWS operation since the numerical models developed to simulate water distribution networks do not include the physical phenomena involved in this type of operation. Pipe systems and the numerical models used to simulate their behaviour were initially developed with the assumption that a CWS was in place and the systems would be operated in such a manner. However, even with the increasing prevalence of IWS, practitioners and the models they use still rely on the as-

sumption of a CWS, leaving a high uncertainty in their projects.

Since the IWS operation causes and consequences have been identified, a literature review is performed to understand the main gaps in knowledge regarding the two-phase flows in pipe-filling events and the numerical modelling of that operational stage. The literature review, the main gaps in knowledge and the outline of this thesis are presented in Chapter 2. The review first focuses on the experimental studies carried out to describe two-phase flows, followed by the numerical models available to describe pipe-filling events reported in the literature. The main research questions addressed in this thesis are outlined in the following section.

1.3. RESEARCH QUESTIONS

Chapter 2 provides the literature review that allows to identify the following gaps in knowledge:

1. Lack of experimental research on air pocket creation, transport and entrainment mechanisms during pipe-filling events;

2. Lack of 1D models capable of simulating simultaneously free-surface and pressurised flows during pipe-filling events, by incorporating the effect of air pressurization in single pipe systems;

3. Lack of fundamental understanding of 1D modelling when integrating both the effect of air pressurization and the creation, transport and entrainment of an air pocket in single pipe systems;

4. Lack of 1D models capable of simulating the air pressurization and the creation, transport and entrainment of multiple air pockets dynamics in pipe networks;

5. Lack of scientific literature describing case-study networks affected by IWS, including the identification of entrapped air pocket locations in real networks during pipe-filling events.

Based on these gaps in knowledge further explained in detail in Chapter 2, and intending to minimise the consequences of IWS, this thesis aims to answer the following main research question:

- *How can the air behaviour be described by a widely used 1D model, like SWMM, during pipe-filling events?*

To answer the main question of this thesis, five specific research questions are formulated to address the complex phenomena of two-phase flow and how to incorporate such phenomena in standard hydraulic solvers:

1. Which are the most relevant air pocket dynamic phenomena involved in pipe-filling events that need to be considered in hydraulic solvers to adequately and realistically describe observed behaviour?

2. How can the influence of air pressure in pipe-filling events be incorporated into a 1D free surface flow model?

3. How can the mechanisms of the entrapped air pocket creation be described in hydraulic solvers allowing the estimation of accurate air pocket volumes and locations?

4. What is the uncertainty of a model that integrates the most relevant air pocket dynamic phenomena when applied to pipe networks during filling events?

5. To which extent can a hydraulic solver that incorporates air pressurization and air pockets' dynamics provide estimates of entrapped air pockets' locations to determine where air valves should be installed and how does this compare to existing engineering guidelines for establishing the air valves location?

Given the lack of experimental and numerical research on air pocket entrapment, answering the above research questions requires the development of an extensive experimental research complemented by the implementation of a numerical model capable of describing the most relevant air pocket mechanisms during pipe-filling events, namely the air pocket creation, transport and entrainment. The development of 1D models incorporating two-phase flows is a step towards improving the current and future operation of IWS systems enhancing the water supply for levels of service and minimizing IWS consequences to public health.

1.4. RESEARCH OBJECTIVE AND METHODOLOGY

Given the posed research questions, the overall research aim of this thesis is:

- *To develop and validate a new 1D model, based on the widely used SWMM model, that is capable of describing and predicting, in an approximate way, the air-water interaction during pipe-filling events in intermittent water supply systems.*

This objective has been divided into the following specific objectives:

1. **To experimentally characterise pipe-filling events and the air pocket's dynamics, such as pressurization and air movement, entrainment and location, for different air release conditions.**

   An extensive experimental programme will be developed in different (three) pipe layouts to collect data and to better understand the air pressurization process. The first pipe layout is a single horizontal pipe system with four downstream end release conditions. The second is a single pipe system with an intermediate high point also tested for four downstream end release conditions. This aims to analyse how and where air pockets get entrapped during pipe-filling events through pressure measurements at three locations and video recordings on the high point. The third layout is a more complex pipe facility with a single loop, a high point and different elevations, aiming to analyse the air pocket mechanism in a network configuration.

2. **To evaluate the classic air model in an open-source software to describe pipe-filling pressurization.**

   The development of an improved numerical model based on an existing hydraulic solver, the Storm Water Management Model (SWMM), is necessary to simulate pipe-filling events in the context of IWS. This model will incorporate the classic air accumulator model and will be applied to a single horizontal pipe system with different air release conditions (the first pipe layout).

3. **To conceptualise, develop and validate a complete air pocket dynamic model for single pipes with a high point.**

   A novel methodology to describe the air pocket entrapment, transport and entrainment in pipe networks will be developed and incorporated in SWMM, the AirSWMM. The model will be calibrated and validated using the experimental data collected in the second pipe layout.

4. **To assess the complete air dynamics model for an experimental pipe network.**

   The improved air pocket model, the AirSWMM, will be tested in a simple pipe network system (the third pipe layout). Full-scale applications and limitations of AirSWMM will be discussed based on the lessons learnt with this experimental and numerical analysis.

5. **To verify the implemented model by numerically identify air pocket locations and volumes in a real-life network during pipe-filling events and the comparison with existing guidelines recommendations for air valve locations.**

   A large-scale network from the literature will be used to test the developed model. Pressure-head measurements will be compared with numerical results to validate the numerical model. Estimated air pocket locations will be compared with the air-release device recommended locations based on existing engineering guidelines.

The key innovative features of the developed work are: a) the incorporation of the air phase in a free-surface flow solver without any further intervention of the user, b) the description of entrapped air pockets creation during the pipe-filling stage, and c) a better understanding of the causes for air entrapment and pockets' locations. This is particularly relevant considering the lack of numerical models that are both computationally efficient and accurate with the interaction between free-surface flow and air-water behaviour and the shortage of theoretical recommendations for identifying potential locations of entrapped air pockets in pipes.

1.5. THESIS OUTLINE

The thesis is organised into eight chapters. Three of these chapters (Chapters 4, 5, 6) correspond to published journal papers, containing the core research work regarding the different stages of development of the numerical method and the respective validation using physical experimental data. Chapter 7 corresponds to a preliminary analysis of the recommended future research.

Each chapter corresponds to a gap in knowledge and addresses a specific sub-research question except for the experimental component which is included in each chapter with experimental tests. Table 1.1 presents the correspondence between the knowledge gaps, the sub-research questions, the chapters and the corresponding publication in an international journal.

Table 1.1: Mapping of the thesis layout, main research question, knowledge gaps and respective chapters and publications.

Main research question	Knowledge gap	Sub-research question	Chapter	Publication
How can the air behaviour be described by a widely used 1D model, like SWMM, during pipe-filling events?	Non-existence of experimental data describing air pocket dynamics in pipes.	Which are the relevant air pocket dynamics to consider?	4, 5, 6	1, 2, 3
	Lack of air pressurisation in a conventional model for a single pipe.	How can air pressurisation be incorporated into a conventional model?	4	1
	Lack of air pocket dynamics in a conventional model for a single pipe.	How can air pocket dynamics be incorporated into a conventional model?	5	2
	Lack of model testing with air pocket dynamics in a pipe network.	What is the uncertainty of the model in a pipe network?	6	3
	Lack of numerical estimates of air pocket locations and volumes.	Are the numerical air pocket estimates accurate?	7	-

Chapter 1 (the current chapter) presents the context, the complexity of IWS, and a summary of the research questions. The main objective of this project, the specific objectives, the methodology and the thesis outline are also described.

Chapter 2 offers an extensive review of the state-of-the-art concerning the main research lines on two-phase flows, including experimental and numerical contributions, in pipe systems. Previous experimental research on air pockets' movement, entrainment, dynamic effects and removal are extensively described. The different types of mathematical models to describe pipe-filling events including air-water interaction are overviewed. The main research gaps are established and identified.

Chapter 3 contains a description of the experimental facility that is used in Chapters 4-7 in terms of pipe layout, filling rate and nodal elevation. Detailed physical characteristics of the system and used instrumentation are described. The testing procedure is also detailed.

Chapter 4 focuses on the description and testing of the AirSWMM model proof-of-concept. A brief description of the Storm Water Management Model (SWMM) is provided and the details of the implemented air accumulator model and its coupling with SWMM are described. The AirSWMM model is tested in a single horizontal pipe and numerical results are compared with experimental collected data.

Chapter 5 improves on the work from Chapter 4 by proposing and implementing a novel methodology in the model for the creation, tracking and entrainment of air pockets during pipe-filling events in a single undulating pipe. Collected video recordings in the experimental facility are analysed and the entrapped air pocket volumes are estimated. Experimental and numerical pressure signals and entrapped air pocket volumes are compared.

Chapter 6 extends the application of the AirSWMM model from the previous chapter to pipe networks, attending to the mass balance of air and water in nodal junctions. Numerical results are compared with experimental data. The limitations of the application of the model to pipe networks and the entrapped air pocket volume predictions are discussed.

Chapter 7 contains a preliminary analysis of the application of the developed model proposed in Chapter 5 in a real network, validating the model with pressure-head measurements at two locations. Recommended air release device locations from international guidelines are compared with the numerical estimates of the air pockets' locations.

Chapter 8 contains the summary and the main conclusions of this research, its practical implications, and recommendations for further work. A summary of the developed work is presented. The main achievements and conclusions of the research developed are outlined. Finally, perspectives and recommendations for future work are presented.

2

Literature Review

2.1. INTRODUCTION

The existence of air in pressurised pipe systems has been experimentally and numerically studied over the last decades. This chapter aims to provide the most relevant scientific contributions on air-water interaction in pressurised systems and to identify the main gaps in knowledge in the numerical modelling of IWS systems. Section 2.2 targets experimental developments on air movement, air entrainment, air influence on pressure surges and air removal from pipe systems. Section 2.3 focuses on the representation of the described phenomena using different types of numerical models. Section 2.4 provides three case studies in which IWS is analysed and numerically described, contributing to a better understanding of what is missing in the current knowledge. Section 2.5 summarises the identified gaps in knowledge in the IWS modelling domain.

2.2. EXPERIMENTAL STUDIES

The presence of air in pipes is inevitable and has been identified as problematic (Fuertes-Miquel et al., 2019). Air can be in the shape of bubbles, plugs, slugs, annular cores, churns and in spray form, in increasing order of occupied air volume of the pipe, or simply dissolved in the water. The dissolved air in the flow affects the rheologic properties of the water (bulk modulus of elasticity, density, viscosity, and others), considerably reducing the elastic wave speed even for small air volume percentages (Chaudhry, 2014). However, air presence in a non-dissolved state, that is accumulated in localised sections, often is the cause for pipe bursts, increased friction losses, system deficient operation and, eventually, accelerated biological processes in the pipe wall that can compromise the water quality (Lauchlan et al., 2005, Ramezani et al., 2016).

Experimental research has been carried out to understand how air in different forms moves in pressurised pipes, which factors intervene on air entrainment in water flows, the influence of air pockets in pressure surges and consequent pressure variations, as well as guidelines on how to mitigate the accumulation and release the air pockets entrapped in pipe systems. Relevant experimental research is summarised here below.

2.2.1. AIR MOVEMENT

Air requires a minimum critical water flow velocity to overcome the shear stress on the pipe wall to induce movement. Several approaches have been proposed with different degrees of complexity and from different formulations. Critical flow velocities have been analysed in water transport and chemical contexts by theoretical and experimental means. The first contribution was given by Dumitrescu (1943) who developed a theoretical formulation to estimate the critical velocity in horizontal pipes for different flow rates. This formulation was further extended for vertical pipes with downward flow by Davies and Taylor (1950).

From the experimental standpoint, Gandenberger (1957) determined critical flow velocities for downwards-sloped pipes with angles higher than 9.5°, accounting for the depth of the air in proportion to the pipe diameter. A parameter n was proposed depending on the air pocket volume, V_{AP}, and the pipe diameter, D, being obtained by $n = 4V_{AP}/\pi D^3$. The critical flow velocities increase with the increase of the pipe slope up until a 40° angle is reached. From that angle onwards, the critical flow velocity decreases

as the downward pipe slope increases. Benjamin (1968) applied the same concepts to gravity currents and observed a higher critical flow velocity in experimental tests than those theoretically determined by Dumitrescu (1943).

Contrary to the previous researchers, Walski et al. (1994) showed the critical flow velocity increases after the pipe slope angle reaches 45°, being the required flow rate to induce movement considerably higher than the previously proposed. Liou and Hunt (1996) proposed an additional formulation for the critical flow velocities for horizontal pipes. Further diameters and slopes were analysed by Escarameia (2004), who focused on pipe angles from horizontal to the predominant angles in water supply and transport systems. Escarameia (2004), just like Gandenberger (1957), observed the critical flow velocity varying with the air pocket size. Pothof and Clemens (2010) extended Escarameia's work and analysed the critical flow velocity for several air pocket sizes, analysing air pockets' flows by separating between "Blow-black flows" and "Plug flows". Based on this analysis, Pothof and Clemens (2010) proposed a new critical flow velocity formulation considering the influence of the friction factor, having observed that the critical flow velocity is independent of the wall surface tension for large diameter pipes (i.e. diameters higher than 200 mm). It was also concluded the critical flow velocity varies with the Froude number, the pipe diameter, the pipe angle and the air pocket size (Pothof and Clemens, 2011).

All the previous contributions for critical flow velocities are summarised in Figure 2.1 in which the critical flow velocity, $U_{AP,c}$, is a function of the pipe angle with the horizontal plane, θ, and the air Froude number, F_g, as well as the range of diameters of each experiment, are presented in Table 2.1.

Table 2.1: Characteristic of the experimental tests to determine the critical flow velocity in terms of pipe angle, pipe diameters, air pocket size and surface tension influence.

Experiment	Pipe angle (°)	Pipe diameter (mm)	Air pocket size	Surface tension
Dumitrescu (1943)	90.0	10.0 – 70.0	No	Yes
Gandenberger (1957)	10.0 - 90.0	45.0	Yes	Yes
Davies and Taylor (1950)	90.0	12.3 – 79.4	No	Yes
Benjamin (1968)	0.0	-	No	Yes
Walski et al. (1994)	0.1 - 3.5	50.0	No	Yes
Liou and Hunt (1996)	0.0	22.9	No	Yes
Escarameia (2004)	0.0 - 22.5	105 - 150	Yes	Yes
Kent (1952)	15.0 - 90.0	102	No	Yes
Pothof and Clemens (2010)[1]	5.0 - 90	80.0 – 500	Yes	Depending on D

[1] Most tests were carried out for D = 220 mm and pipe angle of 10°.

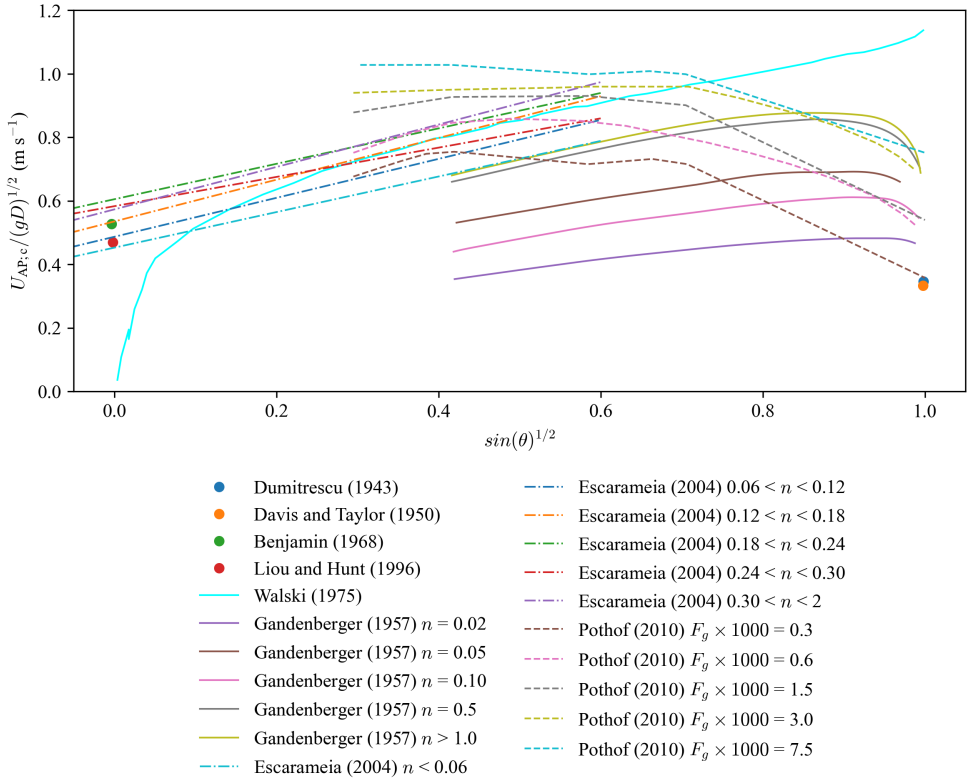

Figure 2.1: Different critical flow velocities formulations as a function of the pipe slope.

Escarameia (2004) elaborated on previous air movement research estimating the air pocket velocity once the critical flow velocity is reached, as illustrated in Figure 2.2. The air pocket's velocity showed a good agreement with the critical flow velocity for pipe angles below 6°. However, the same agreement was not observed for higher pipe angles. Further research analysed the air pockets' velocity after the flow reached the critical velocity based on the equivalent air pocket depth inside the pipe and the Froude number of the water flow. Glauser and Wickenhäuser (2009) determined the critical size of the entrapped air pockets for a constant flow rate and observed that the drag coefficient does not vary with the pocket's Reynolds number, but rather with the pipe slope and the water flow Reynolds number. However, the Reynolds number did not describe the air pocket's velocity for fixed hydraulic conditions.

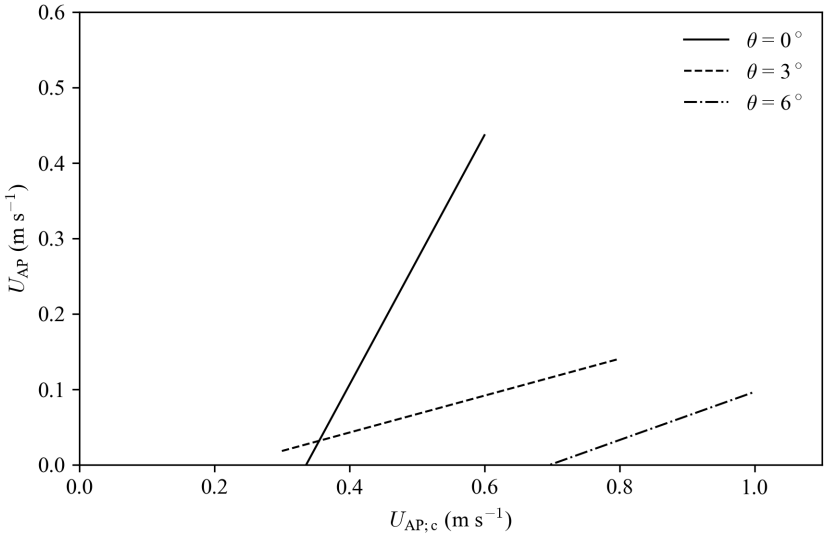

Figure 2.2: Air pocket velocity as a function of the pipe slope and of the critical flow velocity (adapted from Escarameia, 2004).

2.2.2. AIR ENTRAINMENT

Air entrainment, understood as the mixture of air within the water flow, is an even more complex two-phase flow behaviour than the air pocket movement and occurs whenever the water flow has enough momentum to emulsify part of the air pocket in the water in the form of air bubbles.

Several contributions were made with different experimental setups, considering both free-surface and pressurised flows. Air entrainment only occurs for supercritical flows (Froude number, $F = U/\sqrt{gD} > 1$) but there is still no fixed entrained airflow estimate based on the Froude number (Schulz et al., 2020). Several contributions in free surface flows (Kent, 1952, Rajaratnam, 1967, USACE, 1980) estimated the air flow rate entrained in the water in hydraulic jumps as a function of the water depth at the downstream section of the jump. Other contributions in pressurised flows (Kalinske and Bliss, 1943, Wisner et al., 1975, Rabben et al., 1983, Mortensen et al., 2011a, Schulz et al., 2020) aimed at determining the free air flow to estimate a possible time when the pipes would be air-free due to air entrainment. Mortensen et al. (2011a) analysed the scale effects on the air entrainment process and concluded that the pipe diameter does not influence the entrainment rate. Instead, the experimental facility conditions considerably affected the air entrainment process, namely whether the downstream end of the hydraulic jump causing the entrainment is fully enclosed in a pipe or a jump between pressurised and free surface flow. The physical and hydraulic characteristics of the air pocket (i.e., pressure, temperature or mass) influence the interaction at the air-water interface, greatly affecting the entrainment rate. According to the previously cited works, the air entrainment flow rate can be generically described as a function of the Froude number and of two constants, a and b, according to the following equation:

$$\frac{Q_{AP,ent}}{Q_w} = a(F-1)^b \tag{2.1}$$

where in $Q_{AP,ent}$ is the entrained air flow rate, Q_w is the water flow rate, a and b are constants that vary depending on the contribution. Each of these functions is presented in Figure 2.3, where the margin of uncertainty is highlighted. This margin corresponds to the the values air entrainment rate can take but consensual quantification is reached due to a lack of research. However, there is still no go-to contribution since the margin of imprecision is broad enough to provide considerably different results. When using these entrainment functions, users should be aware of their uncertainties.

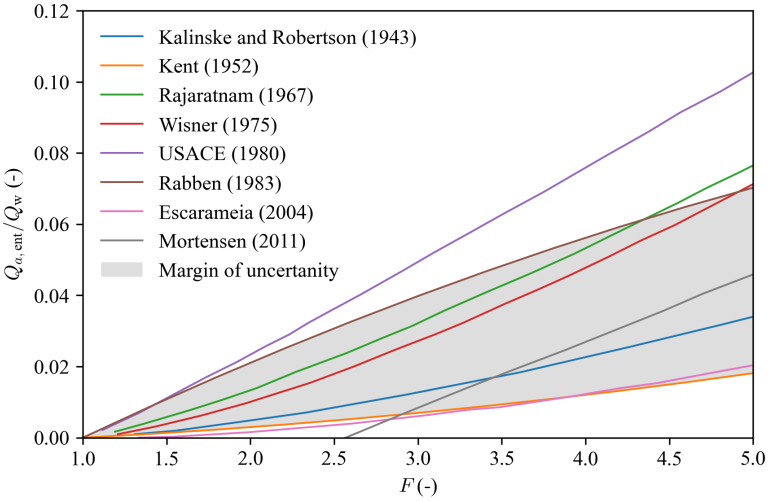

Figure 2.3: Normalised air entrainment rates as a function of the Froude number for different literature contributions and its margin of uncertainty.

2.2.3. AIR POCKETS AND TRANSIENT ANALYSIS

Entrapped air pockets in pipe systems can not only create local head losses, but cause pipe bursts in case of surge events. Once the pipes are filled, air pockets can be considered as 'in-line' or 'off-line', depending on whether they are within the main flow and prone to dragging in a no-flow structure, such as a closed branch or an air valve.

Air pockets modify several features of the pressure wave during the surge event. A pressure drop during the first wave period followed by a higher pressure rise than proposed in the literature by Joukowsky was firstly observed by Covas et al. (2006). Almeida and Koelle (1992) observed that there was a critical volume of air that led to a maximum overpressure due to pressure wave reflections caused by the air pocket compression and expansion. Kim (2008), Alexander et al. (2019) and Alexander et al. (2020) validated existing numerical models to simulate 'in-line' and 'off-line' air pockets corroborating the previous observations regarding pressure drops and overpressure.

The pressure wave period and damping are also affected by the existence of air in the pipes. Liou and Hunt (1996) determined the pressure wave celerity decreases with the

percentage of air dissolved and in free form in the water. Such behaviour was also observed for 'off-line' air pockets, corresponding larger air volumes to increasingly larger pressure wave periods (Ferreira et al., 2021). Figures 2.4 and 2.5 present pictures of the dynamics of an entrapped air pocket in a simple 'reservoir-pipe-valve' system under a hydraulic transient event, being the first image corresponding to the steady-state air pocket and the following images corresponding to the maximum overpressure and minimum underpressures during the pressure wave. A 'spring' behaviour is observed for lower air pocket volumes (Figure 2.4). Conversely, a large air-water mixture (Figure 2.5) is observed for air pocket volumes due to the collapse of the air-water interface, leading to overpressures closer to classic theory (Jowkowsky formulation). The location of entrapped air pockets has been shown as a relevant parameter since air pockets at the mid-length of the pipe seem to cause the largest overpressures (Cabral et al., 2023).

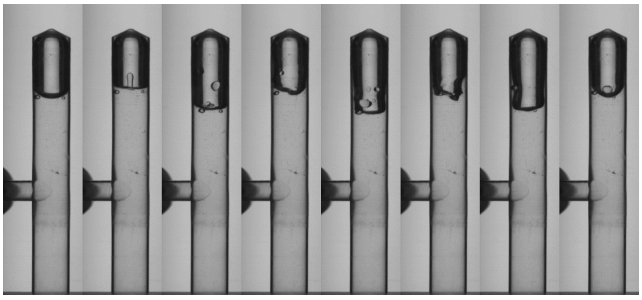

Figure 2.4: Images of an expanding and contracting entrapped air pocket during a pressurised hydraulic transient event for $Q_0 = 150\,\mathrm{l\,h^{-1}}$ and air pocket volume of $V_{AP} = 196\,\mathrm{mm^3}$ (Ferreira et al., 2021).

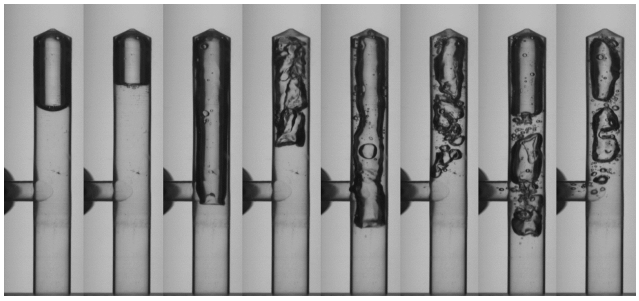

Figure 2.5: Images of an expanding and contracting entrapped air pocket during a pressurised hydraulic transient event for $Q_0 = 350\,\mathrm{l\,h^{-1}}$ and air pocket volume of $V_{AP} = 196\,\mathrm{mm^3}$ (Ferreira et al., 2021).

However, pressure variations in long pipe-filling events are still unknown and require further investigation. Ferrante (2023) observed that some pipe layouts are prone to generate larger pressure variations than others. However, no clear pattern has been identified when water hammer events occur in network filling events in IWS systems (Erickson et al., 2022).

2.2.4. AIR REMOVAL FROM PIPE SYSTEMS

Different guidelines have been proposed to remove air and air pockets from pipe systems. The studies in air movement aimed at determining the minimum required velocity to be able to dislodge and release the air from the water flow. The same process has been applied to the air entrainment in pressurised flows. Transient events have been used to detect entrapped air pockets to take measures to prevent their accumulation in such locations.

Utilities and researchers have been working towards developing better and more robust guidelines on measures to minimize the release of entrapped air in pipes. Two guidelines have been identified: one from the American Water Works Association (Ballun, 2016) and another from Deltares (Tukker et al., 2016). These guidelines recommend the main locations where to install air release valves, their type (between single, double or triple action) and size, as well as operating practices on how pipes should be filled after maintenance actions that require pipes to be emptied since these types of occurrences are prone to create large air pockets. Some of the recommendations, but not limited, for air valve locations are:

- High points – A combination of air release and air intake valves should be installed to prevent air accumulation and to provide vacuum protection in transient events or when the pipe is draining.
- Increased downslope – A combination of air release and air intake valves should be installed for the same reasons as above.
- Long ascents – Air release valves should be considered at periodic intervals to prevent having entrapped air pockets in the system for long periods.
- Long descents - Air release valves should be considered at periodic intervals to prevent having entrapped air pockets in the system for long periods.
- Horizontal pipes – A combination of air release and air intake valves should be considered to prevent stale entrapped air pockets due to low flow rates.

Despite these guidelines, researchers advocate for more effective use of air valves (Ramezani et al., 2016) and their regular maintenance actions, since they are frequently deficiently maintained (Ramezani et al., 2015). Such a problem is exacerbated for utilities with low annual budgets to comply with their maintenance plans.

In the specific case of CWS systems, designers generally assume air to be released by the consumers' taps or during the purging through fire hydrants after a maintenance intervention. Thus, using air release valves in water networks is rare despite their installations being crucial for adequate and efficient air release and admission. However, IWS systems require more air release and intake valves due to their filling and emptying stages, which are not commonly considered in the network system design, since WSS have been designed for continuous operation. The designer's assumption of the pipes being filled when simulating water supply systems affected by IWS and the decision of not reinforcing the installation of air release valves perpetrate the entrapment of air pockets and increase pressure variations due to air pocket compression and expansion

cycles. A better understanding of how and where entrapped air pockets are created and more robust guidelines for their effective control and release need to be developed. This would allow for determining where air release and intake devices should be installed to improve the operation of WSS, more particularly IWS systems severely affected by pipe-filling and emptying stages.

2.3. MATHEMATICAL MODELS

2.3.1. OVERVIEW

Numerical models with different degrees of complexity have been developed aiming at better describing the physical phenomena observed in air-water flows in pipe systems. The types of demand analyses (demand-driven and pressure-driven) that can be implemented are presented, followed by the description of each model type to simulate hydraulic conditions, the respective assumptions, applications and limitations. Models can be categorised according to the assumptions in the spatial representation of the flow, as follows.

- One-dimensional (1D) models when the pressure and velocity changes are negligible within each cross-section.
- Two-dimensional (2D) computational fluid dynamics (CFD) models can be used when cross-sectional variations are required for the analysis being carried out.
- Three-dimensional (3D) CFD model when a full description of the system or the phenomenon is required.

Three types of pipe-filling events are considered in the next sub-sections based on their air release conditions: no air release, restricted and free air release. No air release conditions are characterised by not allowing air to be removed from the pipe by an orifice or a device during the pipe-filling, allowing the air inside to compress and expand freely, without any air mass change.

Restricted air release fillings are characterised by the downstream outlets not having sufficient capacity for the air outflow at the rate of the water inflow, consequently, leading to the air pressurisation inside the pipe, once the pipe-filling starts; this is due to the downstream outlets (orifices) having a small size for the fast air release. The air volume decreases with the air compression and the air mass diminishes with the air release until the pipe system is filled with water.

Free air release fillings are those where the downstream outlets are large enough to drain the air at the water inflow rate, maintaining the air inside the pipe at atmospheric pressure. Most studies herein assume the pipes are empty before opening a valve to initiate the pipe-filling process.

This section initially presents how demand can be described in mathematical models, independently of their complexity, and is organised from the simplest steady-state 1D models to the most complex 3D CFD transient models.

2.3.2. DEMAND ANALYSES

Whenever water is to be delivered at a certain node in a model of a WSS, the user specifies which is the "base demand" at that node, that is, the water being required at that node is defined as a function of time. However, the delivered water might be lower if the available pressure at a node is insufficient to provide the required water volume; in those cases, different demand analyses depending on available pressure are necessary.

Two demand analyses can be carried out in hydraulic models: demand-driven analysis (DDA) and pressure-driven demand analysis (PDA). DDAs approaches do not consider any pressure constraint to provide the base demand and have the pressure head as an output whilst PDA approaches provide supplied volumes as a function of the required base demand, minimum required pressure and calculated pressures. DDA assumes the operational pressure at a given node is sufficient to provide the requested base demand from that node, binding the flow rate calculations in the pipes to the flow rate being delivered at the nodes. PDA requires a minimum pressure at each node to deliver water and takes the available water to be delivered as a function of the available pressure, a specified required pressure to satisfy the base demand and an exponent to describe the relation between pressure and supplied demand (Giustolisi et al., 2008).

The PDA was first introduced by Wagner et al. (1988) to better simulate pressure-deficient water supply networks with different boundary conditions. Other researchers followed up by proposing different exponents to the pressure-demand function (Bhave, 1981, Germanopoulos, 1985, Chandapillai, 1991, Fujiwara and Li, 1998, Tanyimboh et al., 2003) but all follow the model developed by Wagner et al. (1988) as presented below:

$$\begin{cases} Q_{act} = 0 & \text{for} \quad P_{av} < P_{min} \\ Q_{act} = Q_{demand}\left(\dfrac{P_{av} - P_{min}}{P_{req} - P_{min}}\right)^{\beta} & \text{for} \quad P_{min} < P_{av} < P_{req} \\ Q_{act} = Q_{demand} & \text{for} \quad P_{req} < P_{av} \end{cases} \tag{2.2}$$

where Q_{act} is the supplied nodal demands, Q_{demand} is the required nodal demand, P_{av} is the available service pressure, P_{min} is the minimum service pressure to supply demands, P_{req} is the required service pressure to satisfy the required demand Q_{demand} and β is the coefficient to simulate the concavity of the increasing delivery demand.

2.3.3. 1D EXTENDED PERIOD SIMULATIONS OR QUASI STEADY-STATE

Extended period simulation (EPS) or quasi steady-state models are versatile, easy to implement and simple models to simulate a succession of steady flows over time to analyse water quality, pressure, and leakage, and for the definition of pump schedules and control valves. The main assumptions of these models are:

- the flow can be described as a 1D flow;
- water is incompressible;
- the pipe walls are rigid;
- the water's rheologic properties remain constant;

- the friction is considered constant within the same pipe;
- in the context of pipe-filling, the waterfront (air-water interface) is assumed to be perpendicular to the pipe axis; and
- the flow has reached an equilibrium, allowing to consider pressure and flow rate to be treated as constant values between short time intervals.

The last assumption is what makes quasi-steady models not suitable to simulate unsteady events. One example of these models is EPANET 2.2 (Rossman et al., 2020) from the United States Environmental Protection Agency (US-EPA) used to simulate flows in fully pressurised pipe systems. EPANET is widely used by researchers and practitioners since it is free and open source. Several packages have been developed, such as the Water Network Tool for Resilience (WNTR), Multi-Species Extension (MSX) or the Real-Time Extension (RTX), which use EPANET's solver and expand its functionalities.

EPANET was first developed assuming a demand-driven solving algorithm, being the flow rates in the pipes and pressure heads at the nodes calculated as a function of the defined demand at the nodes. Furthermore, the first pressure-driven solving algorithm has also been developed for EPANET in the context of IWS by Ingeduld et al. (2006). Further research used EPANET with pressure-driven demand modules to optimize the water equity in the IWS context. Gottipati and Nanduri (2014) developed a uniformity coefficient to assess water equity, further improved by Ilaya-Ayza et al. (2018) as an optimization target, so that the water distribution would be as equal as possible. Nyahora et al. (2020) used this uniformity coefficient to perform a cost-benefit analysis in the rehabilitation of the benchmark Hanoi network and a case-study network of *Las Pinas* in the context of IWS; these authors noted that pipe elevation highly influenced the results due to the pressure distribution in the network. Souza et al. (2022) applied the same methodology to water distribution systems for the supply stage, having sectorized the network at several sections and introduced pressure-reducing valves to improve water distribution equity. Ayyash et al. (2024) also analysed the influence of sectorising a supply network under water scarcity conditions to assess separate supply times, concluding that such measures can significantly improve water distribution throughout the network while decreasing operating costs.

The second Joint International Conference on Water Distribution Systems Analysis & Computing and Control in the Water Industry (WDSA/CCWI) had its "battle" on the optimisation of an IWS and its operation and investments throughout the years using EPANET (Marsili, Mazzoni, Marzola, et al., 2023, Brentan et al., 2024). However, all these contributions focus on the water supply stage since the software assumes the pipes are pressurised, neglecting the IWS pipe-filling and emptying stages. This gap was already identified by Mohan and Abhijith (2020) who proposed a model with partially filled pipes using EPANET.

However, these models do not include also did not include the unsteady events of pipe-filling and neglected the presence of free-surface two-phase flows. Other limitations of these models are:

- does not allow simulating variations in time, intrinsically required when simulating unsteady events; and
- inability to simulate water flow with a percentage of air content since these assume pipes are already water-filled.

2.3.4. 1D RIGID WATER COLUMN THEORY

Rigid water column models have the same assumptions as quasi-steady state models, except that the flow can be accelerated, thus being able to simulate unsteady events. In most of these models, the air-water interface is assumed to be perpendicular to the pipe axis, also referred to in the literature as the "piston-equation".

The first contribution is attributed to Martin (1976), who observed air pressure in pipe-filling events can be considerably higher than the supplying tank head when entrapped air pockets compress and expand in a pipe with no air release conditions. Several model applications were inspired by Martin's work with different air release conditions by using an air accumulator model to simulate the thermodynamic behaviour of the air. The use of the air accumulator model for pipe-filling events requires the adoption of a polytropic coefficient (k) for the air, which is generally assumed to be $k = 1.2$ to balance fast and slow processes (Wylie and Streeter, 1993). The next contributions are organised according to their air release conditions: no air release, restricted air release and free air release conditions.

For no air release filling conditions, Malekpour et al. (2016) analysed the effects of the upstream tank head, the pipe slope, the pipe wall friction, and the liquid length variation on air pocket compression and expansion. The researchers concluded that RWC leads to maximum pressures that vary with volumes of entrapped air pockets depending on the pipe slope and friction since part of the energy gets stored in the air phase in the form of compressibility, contrary to previous results from the RWC that predicted maximum overpressures occurred for small air pocket volumes. Since then, hardly any developments have been made using RWC models. More recently, Bonilla-Correa et al. (2023) developed an analytic solution to determine the final position of the air-water interface using an RWC.

For restricted air release conditions, Izquierdo et al. (1999) simulated a pipe-filling event with several air pockets, recommending very slow manoeuvres to minimise pressure head variations. This recommendation is also used nowadays by utilities when repressurising pipes after carrying out maintenance interventions to prevent any further pipe failures in the area. Zhou et al. (2002) identified three types of air behaviours depending on the diameter of the orifice allowing for air release in the pipe. Once the waterfront advances in the pipe and reaches the downstream end of the pipe, the air either: i) cushions the filling wave significantly making the water compressibility negligible, ii) cushions the filling wave moderately, mitigating the water compressibility but with some irregularities or iii) is freely released by the orifice and water hammer is dominant. These behaviours were further analysed with different orifice diameter ratios to

better discretise and understand how pressure variations evolve (Zhou et al., 2020).

For free air release conditions, Liou and Hunt (1996) observed the importance of the upstream tank head decreases as the system length increases, since the friction also increases and reduces the water inflow over time, stabilising to a semi-steady-state flow (i.e. the flow rate keeps decreasing but the decreasing rate becomes much lower than at the early stages of the filling).

Despite the extensive research developed, RWC models have several limitations, such as:

- inability to simulate water hammer events, since the water is assumed incompressible;
- inability to simulate water flow with a percentage of air content. The fluid must be single-phased and a clear interface must exist between air and water.
- limited representation of friction, since these models usually consider a constant friction factor, independently of the flow rate;
- very complex implementation when considering multiple air pockets, making it unpractical in comparison to other models; and
- assumption of the air-water interface perpendicular to the pipe axis, unrealistic in most pipe-filling events except for fast manoeuvres.

Nevertheless, RWC models are largely used because of their simple implementation and relatively good results in pipe-filling events. However, water compressibility is not always negligible and their implementation to simulate multiple entrapped air pockets is unrealistic. These are the main reasons why the focus of pipe-filling studies shifted from using RWC to using EWC models.

2.3.5. 1D ELASTIC WATER COLUMN THEORY

Elastic water column (EWC) models are a generalisation of the RWC models, accounting for the water compressibility and the pipe wall circumferential deformation, allowing to simulate water flows with air content and dropping the assumption the column is rigid. Nevertheless, EWC still uses the air accumulator model to simulate the thermodynamic behaviour of air pockets. EWC model's main assumptions are (Almeida and Koelle, 1992, Wylie and Streeter, 1993, Chaudhry, 2014):

- the velocity and pressure variations in the pipe cross-section are considered negligible and, the flow can be described as a 1D flow;
- the pipe wall has a linear-elastic behaviour;
- friction losses are represented by steady-state friction formulations during transient events;
- the flow is single-phased;
- the pipe has its longitudinal movement constrained;

- there are no lateral in/outflows from the system; and
- in the context of pipe-filling, the waterfront (air-water interface) is assumed to be perpendicular to the pipe axis.

The water compressibility and pipe deformation are introduced in the model in the form of pressure wave celerity, c, given by the equation:

$$c = \sqrt{\frac{K}{\rho_w [1 + (K/E)c_1]}} \tag{2.3}$$

where K is the water bulk modulus of elasticity, ρ_w is the water density, E is the pipe Young modulus of elasticity and c_1 is a non-dimensional parameter that depends on the elastic properties of the pipe and its support conditions (Wylie and Streeter, 1993). When the pipe wall is considered thin, $D/e > 25$ being e the wall thickness, c_1 is obtained by the following set of equations as a function of the support conditions:

- Pipe anchored at its upstream end only: $c_1 = 1 - \mu/2$
- Pipe anchored throughout against axial movement: $c_1 = 1 - \mu^2$
- Pipe anchored with expansion joints along its length: $c_1 = 1$

whilst for thick-walled pipes, $D/e < 25$, c_1 is obtained by:

- Pipe anchored at its upstream end only: $c_1 = \frac{2e}{D}(1+\mu) + \frac{D}{D+e}(1 - \frac{\mu}{2})$
- Pipe anchored throughout against axial movement: $c_1 = \frac{2e}{D}(1+\mu) + \frac{D(1-\mu^2)}{D+e}$
- Pipe anchored with expansion joints along its length: $c_1 = \frac{2e}{D}(1+\mu) + \frac{D}{D+e}$

since the wall thickness has a small contribution to the wave celerity. The water bulk modulus varies with the presence of air in the flow and the pressure wave celerity may vary up to 50% for a percentage of 20% equally distributed air volume in the flow. Ferreira et al. (2021) also observed the same effect for isolated air pockets in pipes.

These models gained popularity when Allievi, 1903 proposed the general theory of water hammer equations and showed the flow velocity in the convective term of the moment balance equation is negligible when compared to the wave speed. These models have been used for several applications: maximum and minimum pressures calculations during water hammer events in the design of new pipe systems; and for the detection of blockage or unsealed valves (Meniconi et al., 2016, Yan et al., 2021), of leaks and bursts (Covas et al., 2005, Covas and Ramos, 2010, Louati et al., 2020, Wang et al., 2020), pipe stiffness reduction (Hachem and Schleiss, 2012) and air pocket detection (Bergant et al., 2018, Alexander et al., 2021), but several studies were developed in the context of pipe-filling events.

Marchis et al. (2010) applied an EWC model to the filling of a pipe network assuming free air release conditions (i.e. no air-water interaction), showing that these models are a viable option to simulate IWS and concluding that domestic water tanks greatly affect the consumers' demand pattern. That analysis was further improved by including the

pressure-driven analysis of nodal demand according to Eq. (2.2) to better simulate the network dynamics. Marchis et al. (2011) thus concluded IWS requires considerably more study and water distribution inequities are concerning.

Lee (2005) first proposed an EWC model to simulate pipe-filling events with air-water interaction, achieving good results and showing an air accumulator model is adequate since air pockets are considered homogeneous. Malekpour and Karney (2011) and Zhou, Liu, Karney, and Zhang (2011) used an EWC model to replicate the water compressibility effect observed by Zhou et al. (2002) and both require space-step adjustment to comply with the Courant-Fredrich-Lewys (CFL) condition to minimize numerical instabilities (Chaudhry, 2014).

For no air release conditions, Zhou, Liu, Karney, and Wang (2013) studied the thermodynamic phenomenon of white mist upon pipe pressurisation, observing EWC models still replicate the overall pressure signal while observing condensation at the dead-end. The influence of two entrapped air pockets during pipe pressurisation was also analysed by Zhou, Liu, and Karney (2013), concluding the oscillations generated from each air pocket behaving like a blockage to the flow and a compressible gas considerably increase the maximum overpressures and modify the pressure signal period. A heat transfer model was implemented in an EWC model to analyse the pressurisation of a no-air release pipe by Zhou et al. (2023), resulting in a better match of the pressure wave period. Nevertheless, better results were achieved by Martins et al. (2015) when using different polytropic coefficients for different-sized air pockets ($k = 1$ for small air pockets and $k = 1.2$ for large air pockets).

Restricted air release conditions were analysed using orifices or air valves, which can originate considerably higher pressures. Hatcher et al. (2015) compared an RWC model with an EWC model, observing RWC models overestimate extreme pressures but both struggle to simulate the pressure decay since energy losses have been an ongoing challenge to replicate in pipe-filling events (Vasconcelos and Leite, 2012). Zhou et al. (2019) simulated a restricted air release pipe with an orifice at the downstream end to replicate the experimental observations from Zhou et al. (2002). Using an EWC model allows to simulate the conditions in which the air cushioning is dominant as well as when the water hammer behaviour dominates.

Free air release conditions were analysed to determine possible consequences on the pipe integrity. Malekpour and Karney (2012) further improved their model highlighting how undulating pipe profiles with free air release conditions can cause cavitation and water column separation, leading to severe overpressures when the separated waterfronts rejoin, possibly causing pipe bursts. This is only possible when using the discrete vapour cavity model (DVCM), allowing to simulate two-phase flows in hydraulic transients (Bergant et al., 2006). The occurrence of water column separation creates air pockets in the pipes that will remain as partial blockages, causing additional local head losses and modifying the pressure waves of subsequent transient events (Malekpour and Karney, 2014c). The entrapment of entrapped air pockets due to the filling from both sides from a bypass line also generates higher pressure variations than those predicted by standard EWC models, requiring air release devices to ensure such air pockets are released (Wang et al., 2017). Those are reasons why the installation of air valves in pipes subjected to recurring transient events (like IWS systems) is advisable (Ramezani et al.,

2015).

Even though EWC models can simulate the compressibility of the water with an air-water mixture and are more versatile than RWC models, they still have some limitations:

- require a small time and space step to correctly simulate friction losses and pressure variations and to minimize numerical instabilities;
- become increasingly more complex models when phenomena like unsteady friction, two-phase flows, fluid-structure interaction and viscoelastic pipe behaviour need to be included (Bergant et al., 2008);
- need for the air-water interface to be perpendicular to the pipe axis.

The requirement for small space and time steps renders EWC models unusable, in practice, to simulate large water supply networks. Also, EWC models have been limited to conditions where the air-water interface is perpendicular to the pipe axis, which is not always the case as observed experimentally by Guizani et al. (2006). Models based on the Saint-Venant equations (SV-E) have been used to overcome such limitations since they allow the simulation of multiple air pockets.

2.3.6. 1D SAINT-VENANT EQUATIONS MODELS

Models based on SV-E can simulate free-surface flows, required to simulate pipe-filling events with low upstream pressures and not considered in previously described models. General assumptions for the development of SV-E are as follows (Chaudhry, 2008, Bousso et al., 2013):

- the pressure distribution is hydrostatic;
- the channel bottom slope is considered small so that the water depth does not vary;
- the velocity distribution in each pipe cross-section is uniform;
- the channel is prismatic; and
- head losses in unsteady flow can be described by steady-state friction formulations;

Simulating such phenomena has been proven to be demanding since several instabilities have been identified in the simulation of pipe-fillings. Yen (1986) has identified five main sources of instabilities: i) dry-bed instability, ii) supercritical-subcritical instability due to hydraulic jumps, iii) roll wave instability, iv) open-channel to pressurised flow instability and v) fully pressurised flow instabilities. Most developments have been focusing on instabilities ii) – iv) since they are the most recurrent in urban drainage and stormwater systems. However, all these instabilities are prone to happen in IWS modelling due to the nature of IWS: the pipes start with no water, hydraulic jumps can occur due to pipe slope changes incorporating air entrainment, water depth can propagate upstream due to flow hydraulic conditions, pipe pressurisation which is necessary to supply consumers and water hammer naturally occur in pressurised systems. In the context

of urban drainage and stormwater systems, two modelling techniques have been proposed incorporating SV-E: shock-capturing and shock-fitting.

Shock-capturing models have been developed assuming a single equation can reproduce free-surface and pressurised flows through a Preissmann slot, an artificial slot introduced at the pipe crown to allow SV-E to remain valid when the pipe is pressurised. Shock-capturing models do not require further methods to track the waterfront position since the water depth can be calculated independently of the flow being or not pressurised.

Within the shock-capturing category, models can be categorized into single- or two-equation depending on how the water phase is calculated. Single-equation models, like Vasconcelos and Wright (2007), solve SV-E and rely on the Preissmann slot to simulate pressurised flows. However, the incorporation of the air-water interaction is limited, and the models might require approximations to simulate pressurised flows due to instabilities or limitations in the Preissmann slot. Two-equations methods, like the one developed by Vasconcelos and Marwell (2011), simulate free surface flows with SV-E and pressurised flows with water hammer equations, having an interface between both flow types. These models allow changes in the wave celerity, improving the simulation in low-pressure flows, and have more flexibility to incorporate air-water interaction (Leon et al., 2010). However, such models are considerably more computationally demanding, difficult to implement and require more input data.

More specifically in single-equation shock-capturing models, Vasconcelos and Wright (2007) proposed a two-component pressure approach which simulates the water phase with SV-E and uses the Preissmann slot but incorporates the linear-elastic behaviour of the pipe walls to better simulate the water compressibility during transient events. However, a constant wave celerity was required as per model assumptions. The two-component pressure model has since been improved to incorporate sub-atmospheric pressures and cavitation using a MOC-DVCM, like in elastic water column models. Such a two-phase model was used to incorporate air pockets and their creation (Vasconcelos et al., 2014). However, the model did not allow keeping the air pockets in the system, information of critical importance, but air pockets would actively introduce instabilities when the calculation nodes where the air pockets would be contained got pressurised. Vasconcelos et al. (2014) identified a large gap in the literature concerning the lack of methods to describe entrapped air pockets and incorporate them in the flow calculations, but no contributions have been made since.

Shock-capturing models require the Preissmann slot method to simulate pressurised flows. Using this method i) generally inhibits simulating sub-atmospheric pressures, ii) creates mass and momentum balance problems in rapid events, iii) originates instabilities in the transition between free surface flow close to the pipe crown to within the slot and iv) does not allow to replicate the pressure wave upon a water hammer event when the pipe is pressurised. To minimize mass and momentum balance problems and numerical instabilities, the slot width must be narrow enough to prevent storage accumulation in the slot but wide enough to minimize instabilities. The recommended slot width should be:

$$T_s = \frac{g A_{full}}{a^2} \tag{2.4}$$

where g is the gravitational acceleration, A_{full} is the pipe's cross-sectional area and a is the pipe acoustic wave velocity, in these models considered to be the shallow water celerity, given by $a = \sqrt{gD}$ circular channels. Sjöberg (1982b) proposed a smooth instead of a sharp transition between the pipes to minimize instabilities, resulting in good results for gradual transient flows (Trajkovic et al., 1999). However, numerical instabilities are observed in rapid transients. Leon et al. (2009) proposed a modified Preissmann slot method by modifying the geometric transition from Sjöberg (1982b) and dividing the transition into different steps, showing a better agreement between experimental and numerical results. Malekpour and Karney (2016) analysed the source of such instabilities concluding the numerical instabilities are caused by an inadequate representation of the viscosity provided by the model. To account for all types of flows and adjust the storage effect in the slot using the Preissmann slot, Sharior et al. (2023) proposed a generalised and dynamic slot width described by a shock parameter, a decay scale and a target pipe celerity while keeping the Preissmann slot relative simplicity.

Shock-fitting models on the other hand require two sets of equations (Wiggert, 1972, Song et al., 1983, Guo and Song, 1990, Fuamba, 2002, Leon et al., 2010, Hodges, 2020), one to simulate free-surface flows and a second to simulate pressurised flows. Such distinction makes these models more versatile and generally more accurate since the calculations are carried out separately. However, a clear air-water interface tracking is required. Wiggert (1972) first proposed an interface of this kind, followed by Fuamba (2002) and Politano et al. (2007) who refined the waterfront tracking method by taking different time steps in the tracking process to allow for a smoother transition between free-surface and pressurised flow. Shock-fitting models are computationally heavier and harder to implement than shock-capturing models. For these reasons, they are not covered to the extent shock-capturing models are covered in this section.

One of the most common and widely used free-surface flow models to simulate pipe-filling events is EPA's Storm Water Management Model (SWMM). It incorporates SV-E and solves them with an implicit solver as proposed by Cunge and Wegner (1964). Several improvements have been made or proposed to the model for practical applications by the research community to better simulate pipe-filling events. Ferreri et al. (2010) analysed how SWMM performs in rapid pipe-filling events and observed there is a minimum error for a proportion between space-step, time-step and slot width. Pachaly et al. (2019) observed the most efficient space-step is a proportion between the minimum pipe length and the wave celerity SWMM considers, that being the shallow water wave celerity. Such study was extended to analyse the most accurate pressurisation method in SWMM (EXTRAN or SLOT) further discretising literature pipe systems, observing decreasing the space step (finer system discretisation) and using the Preissmann Slot method to simulate pressurised pipes leads to better results in pipe-filling events Pachaly et al. (2020).

Just like other models, SV-E models have several limitations. In a broader perspective, the main limitations of most SV-E models are:

- possible instabilities when processing flow regime transition between supercritical to subcritical flows;

- the underestimation of the wave celerity in pressurised flows since these models

rely on the Preissmann slot width to simulate pressure in pipes, which generates several instabilities (Malekpour and Karney, 2014a);

- not being able to simulate sub-atmospheric pressure forces SV-E models back to free-surface flows whenever pressure drops below the pipe diameter, even though real systems do not provide enough air intake to reestablish a free-surface flow regime (Vasconcelos et al., 2006);

- as an extension of not being able to simulate sub-atmospheric pressures, whenever pressure goes below atmospheric pressure, SV-E are not able to simulate water-column separation which can severely affect the system integrity (Malekpour and Karney, 2014c); and

- not being used to simulate two-phase flows since they do not allow a discrete ga s cavity model in the equations like EWC models.

SV-E models are still the best compromise in terms of versability regarding the phenomenon of simulating free-surface flows in pipe systems while being computationally efficient. However, there are various sources of numerical instabilities and those must be controlled to achieve accurate results. A compromise between space- and time-steps must be achieved by the Preissmann slot width if a single-equation model is used. The most used model is SWMM because it is free and open source. SWMM presents its instabilities and limitations but has been demonstrated to be robust over the years with progressive improvements to incorporate the Preissmann slot method and, eventually, progress into modelling transient events with two-phase flows, like pipe-filling using SWMM.

2.3.7. 2D AND 3D COMPUTATIONAL FLUID DYNAMICS

Computational Fluid Dynamics (CFD) models, in 2D or 3D form, are considerably more complex to implement and involve longer running times. However, they provide more insights regarding the dynamics inside the pipes, even more than with experimental measurements, since some methods are necessarily intrusive and, thus, might interfere with the measured parameters. Also, there is a disproportionate amount of 3D to 2D models, since users generally opt to fully describe the system behaviour in a 3D model, rather than assuming the third dimension can be constant.

Two-dimensional models correspond to a first higher level of complexity from 1D models, assuming the pipe properties are not constant within the same pipe cross-section, either in the vertical or lateral axis. Most contributions have taken an Eulerian approach to the topic. Liu and Zhou (2009) developed a volume of fluid (VOF) 2D model to simulate a no-air release pipe and compared its results to an RWC model results. The results in the air phase generally follow the same trend but major differences are observed in the pressure results in the water phase due to the movement of the air pocket. Zhou, Liu, and Ou (2011) further compared the previous 2D CFD model in no air release pipe-filling tests with experimental results, a RWC model and a 3D CFD model, showing all models perform similarly but with better results with the growing complexity of the models. The RWC overestimated the pressure peaks and does not accurately describe

the pressure decay and the wave period because the perpendicular waterfront assumption is invalid. Both CFD models are consistent and better replicate the pressure signal during the filing process, being the 2D model preferred due to its simplicity compared to the 3D one.

Three-dimensional CFD models have become very popular since they allow the full description of the pipe-filling process, having some contributions given in this context. In no air release pipe-filling processes, Martins et al. (2015) and Martins et al. (2017) concluded that there is an air volume that originates the maximum overpressure in the pipe-filing process and that there is a relation between the initial air volume, the pipe diameter and the pressure at the upstream end of the system. Zhou et al. (2018) analysed cases in which a disruption of the air-water interface is observed and concluded that the air-water mixture contributes to the decay of the pressure wave, which is not accounted for in 1D models. Zhu et al. (2022) used a 3D CFD model to determine the required polytropic coefficient to obtain good pressure results in a 1D model. It was observed the best-suited polytropic coefficient varies with the volume of the air pocket (also observed by Haakh (2018)) but also that unrealistic coefficients would be necessary 5% of the time to reproduce the pressure data. This would represent a considerable improvement when using 1D models, though requiring a prior 3D CFD simulation to calibrate this coefficient variation. He et al. (2022) also analysed the pipe-filling process with a slug flow to analyse the oscillatory process of the flow in a no air release configuration.

Hou et al. (2012) analysed pipe-filling events using a Lagrangian approach with a smooth particle hydrodynamics (SPH) CFD model. The model was applied to Liou and Hunt (1996) experimental data and compared to a 1D RWC model and the 1D EWC model developed by Malekpour and Karney (2014c), showing the SPH model better simulates the flow rate going into the pipe than the 1D models even though the maximum flow rate is not reached. The SPH approach provides good results but it is computationally complex for water system networks.

Overall, 2D and 3D CFD models allow to describe pipe-filling events better than 1D models and provide insights that 1D models cannot. However, these models are complex to implement and computationally expensive to simulate pipe networks, and there are too many uncertainties to justify the usage of 3D models for networks, such as leakage, illegal connections and boundary conditions. 3D models should be used to extract learnings in smaller cases and tests and improve 1D models with such insights whereas 1D models are more adequate to simulate pipe networks.

2.4. LITERATURE IWS CASE STUDIES

Three case studies on IWS networks with pipe-filling events modelling have been presented in literature and each network was simulated with a different 1D numerical model, only one incorporating the air-water behaviour. Their application also exemplifies the advantages and limitations of each model.

A RWC model was used by Romero et al. (2020) to simulate the filling of a water main with installed air valves. An air accumulator model was integrated with the RWC to account for the air pressurisation in the pipe. Results showed that the air pressure is not significant if the air valve is correctly designed since the RWC model can accurately replicate the pressure signal during the filling process. However, that only remains true when

the pipes have rising slopes. When the pipe has a downward slope, the calculated flow rate decreases considerably sooner and the air valve closes faster than the field observations and the accumulated air volume at the end of the simulation is significantly higher than expected. This is because the RWC does not allow for free surface flows.

SWMM was used to simulate an IWS pipe network by Campisano et al. (2019), incorporating both free surface and pressurised flows. Pressure-driven demand as described in Eq. (2.2) was implemented through SWMM elements and the comparison of numerical pressure results to field data demonstrated that the model was able to accurately reproduce the filling process. However, such an application did not incorporate any air-water behaviour, since it assumed free air-release conditions.

An EWC model was applied by Marchis et al. (2011) to a pipe network with domestic tanks assuming free air conditions and a perpendicular waterfront to the pipe axis. To simulate the domestic tanks, a pressure-driven analysis just like in the previous study was implemented at the nodes of the EWC model. The pressure results showed a good agreement with the measured pressure, verifying that the EWC with a pressure-driven analysis correctly describes the network filling process. Nevertheless, Marchis' model has considered unrealistic assumptions, such as i) entrapped air pockets created by two waterfronts coming from opposite sides are neglected and ii) the air pressure inside the pipes is always the atmospheric pressure. These assumptions thus ignore the possible entrapped air pocket creation and the pressure variations caused by their contraction and expansion upon transient events.

2.5. SUMMARY OF THE MAIN GAPS IN KNOWLEDGE

Despite the numerous experimental and numerical studies on air-water interaction during pipe-filling events, there are still several unresolved issues that require further research. Based on the presented literature review, five main gaps in knowledge are identified:

- **The inexistence of experimental data on air pocket creation and the lack of knowledge on the relevant air behaviour processes in pipe-filling events**

  No experimental data collected during pipe-filling events leading to air pocket creation data could be found in the literature for air-water model calibration and validation. These data should comprehend not only the entrapped air pocket volume and location but also pressures measured at different locations of the pipe system and the flow rate at the inlet pipe section.

- **Lack of available 1D models capable of simulating free-surface and pressurised flows that incorporate the effect of air pressurisation during pipe-filling events**

  Despite the existence of numerous free or commercial hydraulic solvers for free surface and pressurised flows (e.g. SWMM, InfoWorks, Mike URBAN, SewerCAD, StormCAD), none incorporates the air-water interaction, not allowing to accurately and realistically describe the air behaviour that causes pipe-filling delays and introduces additional pressure variations during pipe-filling events (Pachaly, Vasconcelos, and Allasia, 2021). Such a knowledge gap prevents a better under-

standing of the influence of air pressurisation and air release during the filling process, particularly in cases where the waterfront is not perpendicular to the pipe.

- **The inexistence of a 1D model that integrates the creation, transport and entrainment of air in pipe systems**

  Despite several specific numerical models incorporating the dynamic behaviour of the air, known as the initial air mass and the air release conditions for the numerical simulation of pipe-filling events, none integrates the mechanisms associated with the air pocket creation, transport and entrainment. Implementing a complete model with those mechanisms is important not only for scientific purposes to understand, physically describe and numerically replicate the full air-water interaction but also for the engineering practice, to define air-valve location and size based on the assessment of air pockets' size and location. The development of a novel methodology capable of describing the complete air pocket behaviour during the pipe-filling process and the respective implementation in a numerical model (SWMM) is essential to better describe pipe-filling events.

- **Lack of models capable of analysing the air pressurisation and multiple air pockets' dynamics in pipe networks**

  Despite SV-E models (e.g. SWMM) allowing the simulation of multiple air pockets in pipe networks, these models do not yet incorporate air compression and expansion or entrapment. Additionally, some RWC models have been developed to simulate pipe-filling events in single pipes when the air is located at the downstream end. However, the RWC model assumptions make their implementation too complex and case-dependent to be applied to pipe networks, since the air pocket locations need to be defined a priori. The validation of the complete air model in pipe networks is important for engineering practice.

- **Lack of numerical results on air pocket locations applied to pipe-filling events in real networks**

  To the candidate's knowledge, until today, no pipe network model capable of determining the volume and the location of air pockets created during pipe-filling events has been developed and used in pipe networks.

The above gaps in knowledge are both practical and theoretical, likely being the reason for the lack of requests for two-phase flow models incorporating air-water interaction in design, diagnosis and optimisation studies of real systems, such as IWS systems. The research questions of this thesis (in Chapter 1) focus on the experimental description of pipe filing events and their numerical simulation by developing models that reliably describe the two-phase flow observations. The research questions only focus on the technical component of IWS, not targeting the social or management causes and consequences.

3

EXPERIMENTAL DATA COLLECTION

This chapter is a compilation and adaptation of the experimental layout section of:

Ferreira, J. P., Ferràs, D., Covas, D. I. C., Kapelan, Z. (2023). Improved SWMM Modelling for Rapid pipe-filling Incorporating Air Behaviour in Intermittent Water Supply Systems. Journal of Hydraulic Engineering, 149 (4). DOI: 10.1061/jhend8.Hyeng-13137

Ferreira, J. P., Ferràs, D., Covas, D. I. C., van der Werf, J. A., Kapelan, Z. (2024). Air entrapment modelling during pipe-filling events based on SWMM. Journal of Hydraulic Research, 62 (1). DOI: 10.1080/00221686.2024.2305354

Ferreira, J. P., Ferràs, D., Covas, D. I. C., Kapelan, Z. (2024). Air entrapment modelling in networks in pipe-filling events. Urban Water Journal, 21 (6). 10.1080/1573062X.2024.2342785.

3.1. INTRODUCTION

Experimental research on different types of pipe-filling events and aeration conditions is limited in the literature as stated in Chapter 3. The experimental research developed in this thesis aims to collect data for obtaining a complete description of pipe-filling events in terms of pressure and flow rate variation along time and the characterisation of entrapped air pockets, in terms of size and location, for different pipe profiles and aeration conditions (i.e. no air release, restricted and free air release). Three pipe facilities have been assembled, namely a straight horizontal pipe, a single pipe with a high point and a one-loop pipe network. Advanced instrumentation, including high-frequency transducers, an ultrasonic flow meter and a high-speed camera, has been used in all tests. This chapter describes, in detail, the pipe facilities and their layouts, the used instrumentation and the several sets of conducted experimental tests.

3.2. DESCRIPTION OF PIPE LAYOUTS

3.2.1. EXPERIMENTAL LAYOUT #1: SINGLE HORIZONTAL PIPE SYSTEM

The first pipe facility layout aims at collecting data on the pipe-filling process under different aeration conditions, namely for no air release, restricted and free air release, to better understand waterfront progress over time in the pipe and the associated pressure variations at different locations. The pipe facility layout, depicted in Figure 3.1 and used in Chapter 4, is composed of an elevated tank that allows different initial heads, a pneumatically actuated full-bore fast opening DN20 ball valve (Ferreira et al., 2018) and a horizontal acrylic pipe with an inner diameter of 21 mm, a length of 12.4 m and a wall thickness of 2 mm. The pipe is supported throughout its length by metallic profiles to withstand its weight and minimize the vibrations due to fluid-structure interaction during pipe-filling events.

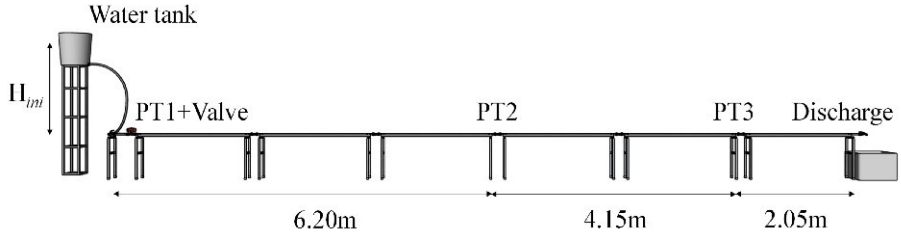

Figure 3.1: Schematic representation of the first pipe facility layout used in Chapter 4

.

Five acrylic plates with different orifice sizes were made to simulate distinct air release conditions. The orifices are circular, centrally drilled in the plate and were installed in the pipe with a gasket around each plate before the testing to prevent air release other than from the centrally drilled orifices. In this facility layout, five orifice diameters, d, were tested: d = 0 mm to simulate the case without any air release (no air release), d = 1.1 and 2.2 mm to simulate restricted air release conditions and d = 10 and 21 mm to simulate free air release conditions. The largest orifice (21 mm) corresponds, in practice,

to open-ended pipes.

Pressure measurements were carried out by three pressure transducers installed along the pipe in the following locations: (i) at the upstream end of the valve to control the tank head (PT1); (ii) at pipe mid-length (PT2) and (iii) at 2.05 m upstream of the pipe end (PT3). The location of these transducers is illustrated in Figure 3.1. Flow rate measurements were carried out at the upstream end of the pneumatically actuated valve, in the water-filled section of the pipe.

3.2.2. EXPERIMENTAL LAYOUT #2: SINGLE HIGH-POINT PIPE SYSTEM

The second pipe facility layout, used in Chapter 5, corresponds to a modification of facility layout #1 to force the creation of entrapped air pockets in the system to better characterise their creation and quantify their volume. A high point was installed at 4.75 m from the pneumatically actuated valve to entrap air pockets during pipe-filling events. The high point has a maximum height of 0.1 m above the pipe axis and is made of the same pipe material, with the same diameter as the main pipe. The pipe segments leading to the high point are sloped with a 45° angle.

Three acrylic plates with different orifice diameters from the previous facility layout were used to simulate different filling conditions: d = 2.2, 3.0, 4.5 mm. Additionally, the system was tested without the presence of an orifice at the downstream end, simulating a fully free discharge into the atmosphere (d = 21 mm) corresponding to a diameter larger than the critical according to Zhou et al. (2020).

Three types of measurements were carried out: pressure and flow rate measurements and air pocket video recordings. Pressure measurements were collected by four pressure transducers installed along the pipe as follows: (i) at the upstream end of the valve to control the tank head (PT1); (ii) before and after the pipe leading to the high point (PT2 and PT3, respectively) and (iii) at 2.05 m upstream of the pipe end (PT4). The location of these transducers is illustrated in Figure 3.2. Flow rate measurements were carried out 4.55 m from the actuated valve, just before the pipe rise to the high point, to comply with minimum distances of the flow meter for accurate measurements and due to space constraints of the experimental facility location. Video recordings were collected to detect and quantify the air pocket volume at the high point.

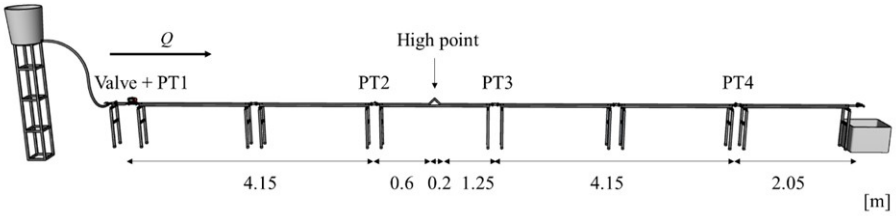

Figure 3.2: Schematic representation of the second pipe facility layout used in Chapter 5

.

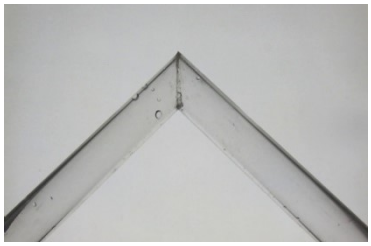

Figure 3.3: Detail of the high point installed at 4.85 m from the fast-opening valve.

3.2.3. EXPERIMENTAL LAYOUT #3: SINGLE-LOOPED PIPE NETWORK

The single pipe system with a high point has been further modified to include a single loop with the same pipe characteristics: acrylic pipes with an inner diameter of 21 mm and 2 mm thick. Pipe facility layout #3 used in Chapter 6 aims at detecting and tracking the creation of entrapped air pockets in a pipe network, quantifying their volumes and validating the developed methodology to better describe the air-water interaction.

The system layout corresponds to the schematic in Figure 3.4, where different nodes and pressure transducer locations are highlighted. The nodes' elevations vary depending on the tested configuration, having their high point and nodes' elevation specified in Table 3.1 to test the influence of pipe elevation on the air pocket entrapment process. The high point structure from the layout #2 has been installed with the high point in node 4 for Configuration 1 (C1) in Table 3.1 and in node 5 for the other configurations.

Table 3.1: Pipe elevation above or below the pipe axis of each node and high point position for each configuration, with the high point centred in the shaded node.

	Nodes elevation (m)							
Config	**1**	**2**	**3**	**4**	**5**	**6**	**7**	**8**
C1	0	0	0	0.10	0	0	0	0
C2	0	0	0	0	0.10	0	0	0
C3	0	0	-0.03	0	0.07	0	-0.03	0
C4	0	0	0.03	0	0.13	0	0.03	0
C5	0	0	-0.03	0	0.12	0	0.03	0
C6	0	0	0.03	0	0.084	0	-0.03	0

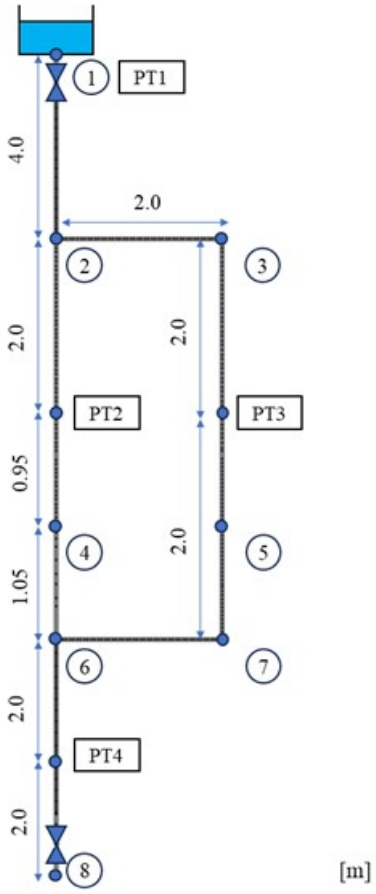

Figure 3.4: Schematic of the third pipe facility layout used in Chapter 6 with nodes' ID circled and with pressure transducers' ID squared out. See Table 3.1 for the node's elevations in different configurations.

3.3. INSTRUMENTATION USED IN EXPERIMENTS

Pressure measurements have been carried out using Siemens SITRANS P pressure sensors Series Z and Wika A-10 pressure sensors, both with a maximum measuring range of 0 - 2.5 m and a full-scale accuracy of 0.5%. The former type with a lower time response (0.1 s) was installed at the upstream section of the system to control the water level at the tank. The latter type with a high response time (1 ms) was installed at intermediate and downstream sections of the pipe to collect pressure measurements during pipe filling process. These were installed in the 'T' junctions connecting each pipe with a degree of 45° downwards to prevent air entrapment in the transducers' measuring chamber.

Flow rate measurements have been carried out by a Dynasonic ultrasonic flowmeter which has a 1% full-scale error, a time response of 0.1 s and a flowrate sensitivity of 0.0003 m.s-1. A tested electromagnetic flowmeter was not used because it would not respond as quickly as the ultrasonic flowmeter used during pipe filling events. An increased flow

rate measurement uncertainty is expected during the first filling stage, which takes only 0.4 s at the flow meter section.

Video recordings have been collected by a GoPro 7 Black camera with a resolution of 2704 x 1520 and 24 frames per second. The camera was positioned as close as possible to the high pipe and an LED panel with an intensity of 10,000 lm m^{-2} was installed in the background to provide a higher contrast between the water and the air to facilitate image processing to quantify the entrapped air volume. Coloured water could have been used but previous experience has demonstrated that the colour particles stain in the acrylic joints and could not be easily removed. A standard LED panel was used to obtain a higher contrast. The camera was installed in a tripod that remained in the same position throughout each set of tests to ensure a stable position and to minimize visualization differences between video recordings.

Pressure and flow rate measurements have been collected by an acquisition system composed of a desktop computer and two Picoscope 3424. Pressure-head and flow rate signals were acquired with a frequency of 1 kHz since the phenomena in the analysis are highly unsteady. A higher frequency is required to correctly describe variations during the filling events that could not be captured without such a fine acquisition rate.

Temperature variations observed by e.g. Zhou, Liu, Karney, and Wang (2013) during fast large pipe filling events (0.6°C) are of the same order of magnitude of the daily variations in the current tests. Still, Zhou et al. test conditions are significantly different from those tested in this research. Low pressure-head variations have been tested (between 0.3 and 1.5 m), and, in most tests, the air was being slowly decompressed, making temperature a less meaningful parameter to measure. Additionally, eventual air volume variations caused by the temperature changes would have been overshadowed by the uncertainty of air entrainment. At last, to the candidate's knowledge, temperature probes with a time response lower than the excitation period of the phenomenon (e.g. 0.1 s) are not available in the market.

3.4. DESCRIPTION OF THE PIPE FACILITY OPERATION

The three pipe facilities layouts have been operated in the same manner to ensure the system had the same initial conditions and that the tests were replicable or, given the stochastic behaviour of some two-phase flow behaviour, were conducted in equal conditions. The following procedure was used, skipping the steps with video recording in the facility layout #1:

1. Ensure the system is empty and the data acquisition system is running.
2. Check if the upstream water tank is set at the correct water level.
3. Introduce the orifice plate at the downstream end of the system, if necessary.
4. Start video recording in the camera.
5. Open the fast-opening pneumatically actuated valve.
6. Register flow rate and pressure head data for each test for 60 s, depending on the size of the used orifice at the downstream end.

7. Stop video recordings and signal acquisition.
8. Close the manual valve after the orifice plates to prevent pressure heads from rising above the transducer's limit.
9. Close the upstream fast-opening valve to disconnect the tank from the pipe system.
10. Open the manual valve and remove the orifice plate (if in use).
11. Open the compressed air ($\approx$ 0.5 bar) to flush the water in the system out.
12. Close the compressed air valve when no more water is discharged from the downstream end of the system.
13. Turn on the recirculating pump until the water tank is full again.

This procedure was repeated as many times as necessary to verify test repeatability (in the cases of facilities' layout #1 and #3) and to describe the entrainment process observed in the tests carried out in facility layout #2, as discussed in Chapter 5.

4

AIR BEHAVIOUR MODELLING IN SWMM FOR PIPE-FILLING EVENTS

This chapter is an adapted version of:

Ferreira, J. P., Ferràs, D., Covas, D. I. C., Kapelan, Z. (2023). Improved SWMM Modelling for Rapid pipe-filling Incorporating Air Behaviour in Intermittent Water Supply Systems. Journal of Hydraulic Engineering, 149 (4), DOI: https://doi.org/10.1061/JHEND8.HYENG-1313.

4.1. INTRODUCTION

Pipe-filling events are severe transient events that occur in intermittent water supply, urban drainage and stormwater systems. The severity comes from high velocities and air pressurisation and release that occurs during the pipe-filling stage of these systems. As a consequence, such mixed flow behaviour leads to increased pipe bursts and equipment malfunctioning, especially given that pressure variations can be much higher in the presence of air (Fuertes-Miquel et al., 2019). Several modelling approaches have been used to describe pipe-filling events namely rigid water column (RWC) models, elastic water column (EWC) models and even more advanced models, such as computational fluid dynamics (CFD) models.

Rigid water column models assume that the pipe is non-deformable and the liquid is incompressible. This approach was used by Martin (1976) and Cabrera et al. (1992) to analyse the pressurisation of a straight water column with an entrapped air pocket described by a simplified accumulator model. The air release with RWC models was first quantified by Zhou et al. (2002) using the theory of compressible flows (American Gas Association, 1978). Since then, several research works have also been carried out to analyse the effect of trapped and released air during pipe pressurisation, concluding that the air behaviour is indeed relevant during pipe-filling events (Romero et al., 2020). However, RWC models are not always suitable, because the wavefront profile is not always sharp and perpendicular to the pipe axis, as assumed in these models. As explained by Guizani et al. (2006), the wavefront varies with the initial water tank head H_{ini} and the pipe diameter; if the d/D ratio is too low, the assumption of a sharp wavefront from the RWC model is not valid, especially in undulating pipe profiles (Liou and Hunt, 1996).

Elastic water column models can more accurately simulate unsteady pressure variations in fully pressurised pipes or pipes with air pocket volumes much smaller than the volume of water. Zhou, Liu, Karney, and Zhang (2011) analysed the pressurisation and filling of pipes with the elastic model using the Method of Characteristics, as it is used for describing water hammer events, though with an additional piston equation to model the water-air front position. Later, Zhou, Liu, and Karney (2013) analysed the pipe-filling events with two separate entrapped air pockets. Malekpour and Karney (2014b; 2014c) also analysed the effect of blockage and pipe profile, showing that water column separation can occur. However, these researchers still assumed that the wavefront is perpendicular to the pipe axis which was shown not to be valid for low d/D ratios and sloped pipes.

Computational Fluid Dynamics models (CFD) have also been used to describe pipe-filling events. Martins et al. (2015) developed a conceptual model for pipe pressurisation on a pipe dead-end. Martins et al. (2017) further analysed the same type of system and concluded that the maximum overpressures are a function of the initial air volume, the pipe diameter and the level at the upstream tank. Zhou et al. (2018) numerically analysed the pipe-filling and verified the air-water mixing was not negligible in terms of energy losses in a dead-end pipe system. Indeed, CFD models high level of detail makes them useful for descriptive and fundamental research. However, CFD models are very demanding in terms of time and computational resources, making them unusable for standard engineering practice for water networks.

In contrast, drainage and stormwater systems fillings have been mostly studied using

free surface flow models based on Saint-Venant equations (Ferreri et al., 2010; Vasconcelos et al., 2018; Vasconcelos and Marwell, 2011). The frequently used solver for this purpose is EPA's Storm Water Management Model (SWMM), which is an open-source software widely accepted by the research and practitioner community.

SWMM was first proposed as a possible solver to simulate intermittent water supply (IWS) systems by Cabrera-Bejar and Tzatchkov (2009). Campisano et al. (2019) concluded that SWMM is better suited than an RWC model for pipe-filling events since the sharp wavefront assumption is not required in SWMM. More recently, Gullotta et al. (2021) used SWMM to determine pressure-reducing valve locations to improve water distribution equity. However, this hydraulic solver still cannot describe the air behaviour during pipe-filling events since that kind of interaction was not incorporated in the original SWMM code. Modelling this interaction is relevant in the IWS context since this kind of supply is characterised by three stages: pipe-filling stage, pressurised supply stage and emptying stage. However, only the pressurised supply stage is currently modelled, mostly by using EPANET, EPA's application for modelling completely pressurised drinking water distribution systems. EPANET model cannot describe the filling stage which has a major air-water interaction, since pipes are always fully pressurised with water, nor the pipe emptying stage, where air needs to go into the pipe.

Overall, previous research contributions noted that air behaviour is required but has never been incorporated in this kind of solver. Also, is no software to the author's knowledge that includes the modelling of air behaviour, commercial or open source.

This chapter aims to present the development and validation (with experimental data) of the improved SWMM model, capable of simulating the air pressurisation process during pipe-filling events. This is achieved by adding the air accumulator model to the SWMM hydraulic solver. Three configurations of the simple pipe system are analysed during the pipe-filling process by changing the downstream boundary condition to simulate situations with no air release (dead-end), restricted air release (smaller orifices) and unrestricted air release (larger orifices). These configurations were deemed sufficient to cover different operating configurations that are likely to occur in IWS systems. No consideration was given to more complex systems, such as pipe networks in this work, remaining to be done as part of future work.

The outline of the chapter is as follows. The collected experimental data, description of the pipe-filling phenomena and the effect of entrapped behaviour are described in Section 4.2. The original and improved SWMM model, AirSWMM(v1.0), are presented in Section 4.3. Experimental data and numerical results using EXTRAN and SLOT surcharge methods are compared in Section 4.4, showing the simulation capabilities of the model. Finally, a discussion is held on the importance of improved SWMM for future research as well as on key findings and the applicability of the proposed model to engineering practice in Section 4.5 and its conclusions are presented in Section 4.6.

4.2. EXPERIMENTAL DATA COLLECTION AND ANALYSIS

4.2.1. COLLECTED DATA

Two initial water levels in the upstream water tank of the pipe layout in Section 3.2.1 were tested: H_{ini} = 0.35 m and 1.50 m. Five orifice diameters were used as a boundary condition at the downstream end to describe different air behaviour configurations: no air release, restricted and unrestricted air release. These experimental tests were carried out to complement Zhou et al. (2020) data because this thesis aims at describing pipe-filling processes with lower ratios of H/D, comparing $H/D > 390$ from Zhou et al. (2020) to $H/D < 75$ herein. Lower ratios of H/D tend to generate lower slopped waterfronts, like those observed by Guizani et al. (2006).

Tested boundary conditions at the downstream end, with the respective final steady-state flow rates and Reynolds numbers, R_e, are presented in Table 4.1. These allow to cover flow conditions that go from laminar flow to smooth-wall turbulent flow. A total of 10 types of experiments were conducted with at least two tests for each configuration type to ensure repeatability. Tests for H_{ini} = 0.35 m and for the restricted air release configuration show zero flow rate since the flow rate was lower than the flow meter low flow cut-off.

Table 4.1: Experimental tests, steady state flow rate and respective Reynolds number.

	No air release		Restricted air release				Unrestricted air release			
H_{ini} (m)	d = 0 mm		d = 1.1 mm		d = 2.2 mm		d = 10 mm		d = 21 mm	
	Q (L h^{-1})	R_e (-)	Q (L h^{-1})	R_e (-)	Q (L h^{-1})	R_e (-)	Q (L h^{-1})	R_e (-)	Q (L h^{-1})	R_e (-)
0.35	-	-	-	-	-	-	0.28	4715	0.37	6231
1.5	-	-	0.03	488	0.08	1264	1.02	17178	1.23	20715

4.2.2. PIPE-FILLING PROCESS AND DESCRIPTION

A sample from the test with tank head H_{ini} = 0.35 m was taken to illustrate the dead end and the small and the large air release behaviours.

The observed pressure-heads, H, at three measurement locations for the dead-end configuration are presented in Figure 4.1. Upon the upstream valve opening (at t = 0 s), water flows into the pipe and no air is released. The wave front advances along the pipe and the air immediately starts to compress. While compressing, the air behaves as an energy accumulator and, once the kinetic energy of the water column from the valve opening has been transferred into potential energy in the air phase (at t = 1.3 s), the wavefront starts to move backwards as the air starts to expand. This cycle repeats itself until the kinetic energy is dissipated through friction and a final steady state is reached with a balanced air pocket pressure and water level at the tank. Hardly any difference between PT2 and PT3 measurements can be seen in Figure 4.1 since the wavefront does not reach any of the transducers and both measure the air pressure-head as a single fluid. This quasi-steady assumption is valid since the air celerity becomes $\sqrt{K_{\text{air}}^{\text{adiabatic}}/\rho_{\text{air}}} = \sqrt{142000/1.42} = 314$ m s^{-1} for adiabatic processes and becomes $\sqrt{K_{\text{air}}^{\text{adiabatic}}/\rho_{\text{air}}} = \sqrt{101000/1.42} = 267$ m s^{-1} for isothermal processes. Thus, air pressure longitudinal variation takes a maximum of 12.4 m/267 m s^{-1} = 0.046 s from the start of the air-water interface to the air pocket downstream end. Such time is of

an order of magnitude around 100 times lower than the water wavefront advance in the pipe making the spatial variation of the air pressure negligible in the current tests. Thus, whenever the air pressure-head is compared to the dead-end configuration, only data from one transducer will be presented.

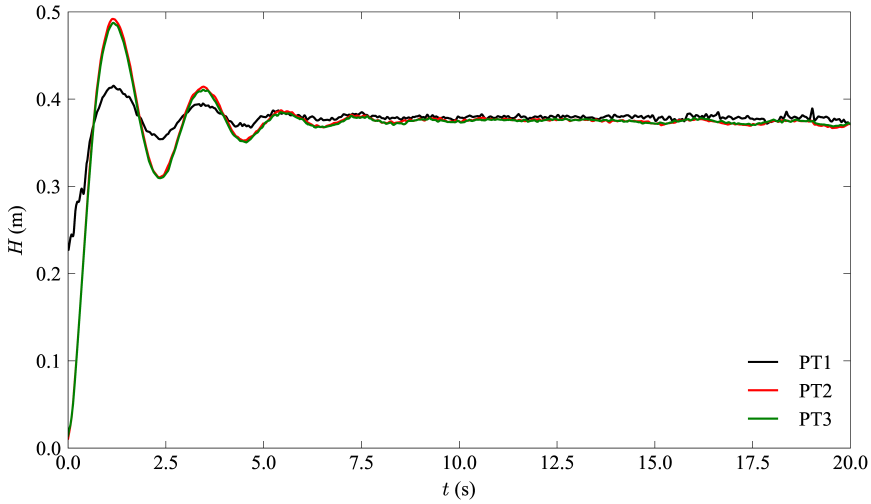

Figure 4.1: Experimental pressure-head in no air release conditions.

A sample of data collected for the pipe-filling event with a small air release configuration is shown in Figure 4.2. The registered pressure-head corresponds to the fluid pressure-head: first, the air's and, then, the water's when it reaches each transducer location. Once the valve opens (at t = 0 s), the wavefront starts advancing along the pipe and the air pressure increases. The small orifice at the downstream end allows the air release even though the air pressure-head inside the pipe reaches values similar to the ones of the water in the tank. When the air pressure inside the pipe and the tank level reach an equilibrium (approximately at t = 2 s), the flow rate severely decreases due to the smaller pressure gradient. While the wavefront progresses, the air pressure-head decreases until the wavefront arrives at each measuring location due to the air release at the downstream end. When the water arrives at each transducer, the registered pressure remains relatively constant. Air pressure decreases at a much faster pace due to its release whilst the water pressure corresponds to the water tank level subtracted from head losses until the transducer. Thus, the wavefront arrives at PT2 at t = 10 s and at PT3 at t = 34 s. When the wavefront reaches the downstream end at t = 39 s, a severe pressure surge is observed due to a small volume of air trapped at the downstream end that rapidly compresses and cannot be released as the orifice creates the same effect as a blockage, creating the observed pressure spikes between t = 39 - 55 s. Through visual observation during each test, some air volume remains in the pipe in the form of small bubbles scattered at the upper side of the pipe.

A different behaviour is observed in Figure 4.3 which shows a sample of the collected data for the unrestricted air release configuration. After opening the valve, the pipe starts

to rapidly fill and no pressurisation is observed until the water wavefront arrives at PT2 and PT3 at t = 5 s and t = 14 s, respectively. Then, the pressure head slowly increases at PT2 and PT3 until the wavefront reaches the pipe end (t = 18 s). Once the pipe end is reached, the pressure oscillates sharply due to a sudden variation in the local head loss created by the orifice. The gradual pressure head reduction after t = 18 s represents the upstream water tank emptying.

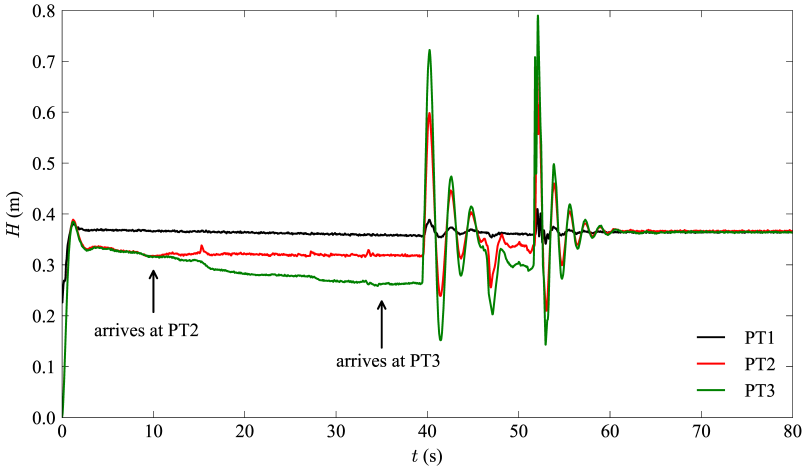

Figure 4.2: Experimental pressure-head in restricted air release conditions.

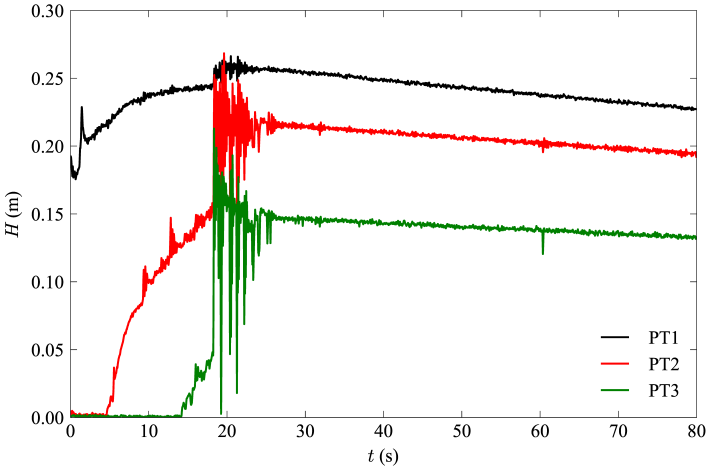

Figure 4.3: Experimental pressure-head in unrestricted air release conditions.

4.3. AIR MODELLING BEHAVIOUR

4.3.1. AIR BEHAVIOUR MODEL

The simplified accumulator model with compressible flow theory for air release through orifices is used herein to simulate the air behaviour during the pipe-filling process. In this approach, only the polytropic coefficient (which is considered constant) is required.

Water flow is considered incompressible in Saint-Venant equations. Since the air is several times more compressible than water, the variation of the air volume inside the pipe can be described by the piston function:

$$\frac{dV_a}{dt} = -Q_w \tag{4.1}$$

where V_a is the air volume inside the pipe, t is the time and Q_w is the water flow rate.

Air release formulation depends on the downstream orifice size and the air pressure inside the pipe, p_a. Considering atmospheric pressure, p_{atm}, when $p_a/p_{atm} < 1.89$, the air release from an orifice occurs in subsonic conditions and the air behaviour can be described by an isentropic behaviour (Binder, 1955). Under these conditions, airflow is described as follows (Zhou et al., 2002):

$$Q_a = C_d A_0 Y \sqrt{2g \frac{\rho_w}{\rho_a} \frac{(p_a - p_{atm})}{\gamma_w}} \tag{4.2}$$

$$Y = \left[\frac{k}{k-1} \left(\frac{p_{atm}}{p_a} \right)^{2/k} \frac{1 - (p_{atm}/p_a)^{(k-1)/k}}{1 - (p_{atm}/p_a)} \right]^{1/2} \tag{4.3}$$

where Y is the expansion factor (Martin, 1976), Q_a is the air flow rate released from the orifice, C_d is the discharge coefficient, A_0 is the cross-section area of the orifice, g is the gravitational acceleration, ρ_a is the air density, ρ_w is the water density and k is the polytropic coefficient.

In the other case, when $p_a/p_{atm} > 1.89$, the airflow through the orifice becomes chocked and a maximum airflow rate can be released:

$$Q_a = C_d A_0 Y \sqrt{2g \frac{\rho_w}{\rho_a} \frac{(p_a - p_{atm})}{\gamma_w}} \tag{4.4}$$

According to Eq. (4.4), the air volume varies as a function of the water flow rate, which in turn becomes a function of the airflow and the air compression, due to the two-way interaction between the water and the air. Therefore, the air pressure p_a and the air density ρ_a vary in time as follows:

$$\frac{dp_a}{dt} = \frac{p_a k}{V_a}(Q_w - Q_a) \tag{4.5}$$

$$\frac{d\rho_a}{dt} = \frac{\rho_a}{V_a}(Q_w - Q_a) \tag{4.6}$$

The used polytropic coefficient k is considered constant for each test. Since most transient water dynamics have an initial faster behaviour immediately after a changing

boundary condition manoeuvre, for which the flow is adiabatic, and a slower one during the establishment of the final steady state, behaving as an isothermal process, most authors propose a $k = 1.2$ for unsteady flow events in pipes (Chaudhry, 2014). Nonetheless, the polytropic coefficient value will be calibrated in this work for the three analysed pipe configurations.

4.3.2. ORIGINAL SWMM MODEL

The original SWMM model is based on the following Saint-Venant equations, corresponding to the mass and momentum continuity equations of free surface flows:

$$\frac{\partial A}{\partial t} + \frac{\partial Q_w}{\partial x} = 0 \tag{4.7}$$

$$\frac{\partial Q_w}{\partial t} + \frac{\partial (Q_w^2 / A)}{\partial x} + gA\frac{\partial H}{\partial x} + gAS_f = 0 \tag{4.8}$$

where A is the flow cross-section area, x is the length, H is the pressure-head and S_f is the friction slope.

In the numerical scheme, the water flow rate is calculated by an implicit backwards Euler numerical scheme (Roesner et al., 1988, Rossman, 2017). The solver calculates the flow rate for all the pipe segments in the system (herein referred to by pipe p) in the order in which the pipes were introduced in the input file, for each time step, t+1, and based on the previous time step, t:

$$Q_{t+1,p} = \frac{Q_{t,p} + \Delta Q_{t,p}^{\text{inertia}} + \Delta Q_{t,p}^{\text{pressure}}}{1 + \Delta Q_{t,p}^{\text{friction}}} \tag{4.9}$$

in which $Q_{t,p}^{\text{inertia}}$ corresponds to the inertial component of the flow rate which varies with the mean flow velocity in pipe p and with the flow area and flow rate changes between time steps, $Q_{t,p}^{\text{pressure}}$ corresponds to the flow rate component of the calculation in which the differential pressure between upstream and downstream nodes of pipe p, $Q_{t,p}^{\text{friction}}$ accounts for the head loss component of the flow rate calculation where only the wet perimeter (without the air) should be considered, even if the air inside the pipe p is pressurised, and p accounts for the pipe in the node sequence in analysis.

A surcharge method is required when the pipe is pressurised. SWMM version v5.1.015 includes two surcharge methods: EXTRAN and SLOT. EXTRAN surcharge method uses the continuity and the momentum equations to calculate the pressure-head, assuming a full pipe cross-section, making the convective terms of the equations equal to zero. Roesner et al. (1988) recommended a maximum time step to ensure numerical stability when using this method:

$$\Delta t = \frac{L}{\sqrt{gD}} \tag{4.10}$$

in which L is the pipe length and D is the pipe inner diameter. Vasconcelos et al. (2018) found the previous recommendation to be inaccurate for rapid pipe-filling and recommended a time step reduced tenfold:

$$\Delta t = 0.1 \frac{L}{\sqrt{gD}} \tag{4.11}$$

Conversely, SLOT surcharge method uses the Preissmann slot method to solve pressurised pipe flow while using Saint-Venant equations. An artificial slot is assumed on top of each pipe p to represent the pressurised pipe flow as free surface flow. As such, the model still uses the convective term of Saint-Venant equations but the flow area now incorporates the slot width T_s. The value proposed by Sjöberg (1982a) is used herein, as predefined in SWMM. More information on SWMM and the respective surcharge methods can be found in Rossman (2017).

Both surcharge methods should provide similar results for steady pressurised pipe flows, being the SLOT method preferential. However, such slot width does not allow to accurately estimate pressure-heads in fast unsteady pipe flows. For such dynamic events, the recommended slot width has been recommended should the following (Aureli et al., 2015):

$$T_s = \frac{gA}{c_p^2} \tag{4.12}$$

where c_p is the pipe wave celerity.

Since the wave celerity has been changed from the celerity of free surface flows to the pipe pressure wave celerity and consequently the slot width, the minimum time step must be adjusted.

Reducing the slot width requires smaller time steps to comply with Courant's number lower or equal to the unit $Cr = c_p/(\Delta x/\Delta t) \leq 1$. Thus, pipe segments of $\Delta x = 0.2$ m require a minimum time step of $\Delta t = 0.00066$ s for the pipe pressure wave celerity. Instabilities were observed for this time step, but no reference could be found on this concern. Thus, a sensitivity analysis using the original SWMM with different time steps was carried out to demonstrate that this is a limitation of the original SWMM and not of the improved version.

4.3.3. AIRSWMM(V1.0)

To incorporate the air behaviour in SWMM model, the pressure component of the flow rate calculation $\Delta Q_{t,p}^{\text{pressure}}$ from Eq. (4.9) needs to be modified:

$$\Delta Q_{t,p}^{\text{pressure}} = -g\overline{A}\frac{H_{2;t,p} - H_{1;t,p}}{L}\Delta t \tag{4.13}$$

where $H_{2;t,p}$ and $H_{1;t,p}$ are the pressure-heads at the upstream and downstream end of the pipe p, respectively at the previous time step.

The incorporation of air pressure in the model requires the consideration of three different cases: i) Case I, where both nodes of the pipe are filled with water (i.e. pressurised water column), ii) Case II, when only one side of the pipe is full of water and iii) Case III, when both nodes have free-surface flow. Case I does not require the correction of the air pressure term, since the pipe is already pressurised and no trapped air is considered. In Cases II and III, the air pressure head should be added to the pressure-head in the nodes

in contact with air for the flow rate calculation. Thus, the pressure-heads from Eq. (4.13) need to be corrected to $H = h_x + h_{\text{air}}$, where h_x corresponds to the water depth at the calculation node obtained from SWMM and h_{air} corresponds to the air pressure inside the pipe. The calculation process for the improved SWMM model is depicted in Figure 4.4. AirSWMM(v1.0) will be used as this model's name and version.

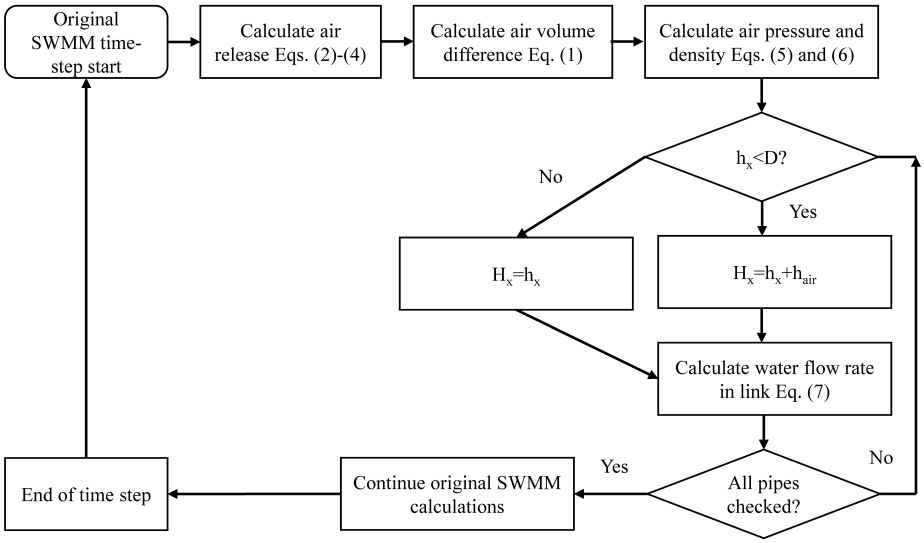

Figure 4.4: Implementation chart for the air phase calculations in AirSWMM(v1.0).

4.4. RESULTS

Three different configurations (no air release, restricted and unrestricted air release) with tank head H_{ini} = 0.35 m were simulated using both the original SWMM and the AirSWMM(v1.0) model with H_{ini} = 0.35 m. The obtained numerical results are compared with the corresponding collected data.

The experimental pipe rig could be modelled using a single straight horizontal pipe between two nodes. However, the pipe was discretised in 62 pipes segments with lengths of $L = \Delta x$ = 0.2 m between 63 nodes to improve the solver accuracy with dummy nodes between each stretch of pipe as proposed by Pachaly et al. (2020). The used time step for the restricted and unrestricted air release configurations is calculated using Eq. (4.11), resulting in a maximum time step of Δt = 0.044 s.

The water tank, upstream boundary condition, was modelled by its initial water level obtained from PT1 and by the tank geometry. Both original and AirSWMM(v1.0) models use a local head loss coefficient, K. Parameter K_{up} was introduced in the first pipe segment to represent the local head losses from the tank to the pneumatically actuated valve and parameter K_{down} was introduced in the last pipe segment to describe the orifice head loss.

The wave celerity when the pipe is pressurised was considered as c_p=300 m s^{-1}, calculated by the theoretical formula for single phase fluid (Eq. (2.3)), based on water properties (K = 2.19 GPa; ρ = 998 kg m^{-3}) and the characteristics of the pipe (E = 0.075 GPa; ν = 0.4; c_1 = 1.05), and was attributed to all segments of the pipe. The pressure wave celerity is used only used for the SLOT surcharge method with an adjusted width. Using SLOT method AirSWMM(v1.0) generated numerical instabilities demonstrated that this approach cannot be used, as such the air content in the flow has never been evaluated.

The polytropic coefficient k was observed not to vary significantly from the k = 1.2 recommended in the literature (Chaudhry, 2014). However, when no air release exists, the polytropic coefficient that best describes the observed behaviour is 1.0. This is explained by the fact that, during the pipe-filling, the adiabatic assumption for the air behaviour is no longer valid, as there is heat transfer from the water to the air and the pipe walls (Zhou, Liu, Karney, and Wang, 2013).

4.4.1. CALIBRATION AND VALIDATION

To determine the performance of the proposed changes in AirSWMM(v1.0), the tests for H_{ini} = 0.35 m of the collected data were used to calibrate the model and the second half (H_{ini} = 1.5 m) for its validation. Given the limited number of sensors in the system, no optimization was run. The calibration was carried out by using a trial-and-error approach assessing the calibration by means of minimizing the root mean square error (RMSE). The validation process was carried out by using the parameters determined during the calibration process. The pre-determined parameters are the time step, the spatial discretisation, according to Eq. (4.11). and the absolute roughness of the pipe, estimated by the steady state at the end of each test. The calibration parameters are the local head losses coefficients and the polytropic coefficient.

The time step, the spatial discretisation, the absolute roughness of the pipe, the local head loss coefficients and the polytropic coefficients used in the numerical simulations are presented in Table 4.2. As an exception, a time step of Δt = 0.001 s is required for the dead-end configuration, since the waterfront does not advance enough in the calculation nodes. This can also be confirmed with the ideal gas law $(p_f - p_i)(V_f - V_i) = kRT$ in which p is the air pressure inside the pipe, V is the air volume, R is the ideal gas constant and T is the temperature. The waterfront advances only 0.25 m, it which is hardly more than a single space step (0.2 m).

Table 4.2: Estimated SWMM model parameter values.

Model parameter	Parameter	Test				
		d = 0 mm	d = 1.1 mm	d = 2.2 mm	d = 10 mm	d = 21 mm
Δt (s)	Eq.(4.11)	0.001	0.044	0.044	0.044	0.044
Δx (m)	Model input			0.2		
Roughness (m)	Estimated			0.00076		
K_{up} (-)	Calibrated			4		
K_{down} (-)	Calibrated	10000	200	200	13	0
k (-)	Calibrated	1.01	1.15	1.15	1.2	1.2

4.4.2. NO AIR RELEASE CONDITIONS

Experimental data and numerical results for original SWMM and AirSWMM(v1.0) in the case of no air release configuration are presented in Figure 4.5.

Numerical results obtained by the EXTRAN surcharge method for the no air release configuration are depicted in Figure 4.5a. The original SWMM is not capable of simulating the observed air-water behaviour since it assumes atmospheric pressure-head ahead of the water column during the pipe-filling. The calculated pressure-head is zero until the water column reaches the location of PT3 at t = 16.0 s. When the wavefront reaches the downstream end of the pipe (t = 19.0 s), a transient pressure wave, corresponding to the filling wave going against the dead end, occurs. However, this transient phenomenon is not well described by the original SWMM model because the previous stage is not properly reproduced either. Conversely, AirSWMM(v1.0) results show a good agreement between the calculated air pressure-head and the experimental data for the first two wave periods: there is no energy loss during the pipe-filling and the air pocket behaves simply as an energy accumulator. After the first two wave periods, AirSWMM(v1.0) numerical model shows some discrepancies in amplitude and phase with the observed pressure head mostly due to the underestimation of the energy dissipation since the air behaves as a simple energy accumulator and not as a dissipator.

Numerical results obtained by the SLOT surcharge method for the no air release configuration are presented in Figure 4.5b. The original SWMM model is not capable of simulating the observed behaviour once again. Even though AirSWMM(v1.0) results with the predefined Preissmann slot show a better agreement with the collected data, obtained accuracy is not satisfactory enough as neither the pressure wave amplitude nor the period agrees well with the experimental pressure wave behaviour. Results do not improve when adjusting the slot width to the one proposed by Aureli et al. (2015). This is because, in order to use the adjusted slot, the time step needs to be significantly reduced (Δt = 0.00066 s = $\Delta x / c_p$) to comply with the Courant condition. Such a small time step leads to numerical dispersion in SWMM, which has also been observed by other researchers on SWMM community discussions. Using longer and larger diameter systems will allow to understand if the adjusted slot is adequate in a broader context. Overall, the SLOT method is not capable of describing the filling event for the no air release configuration.

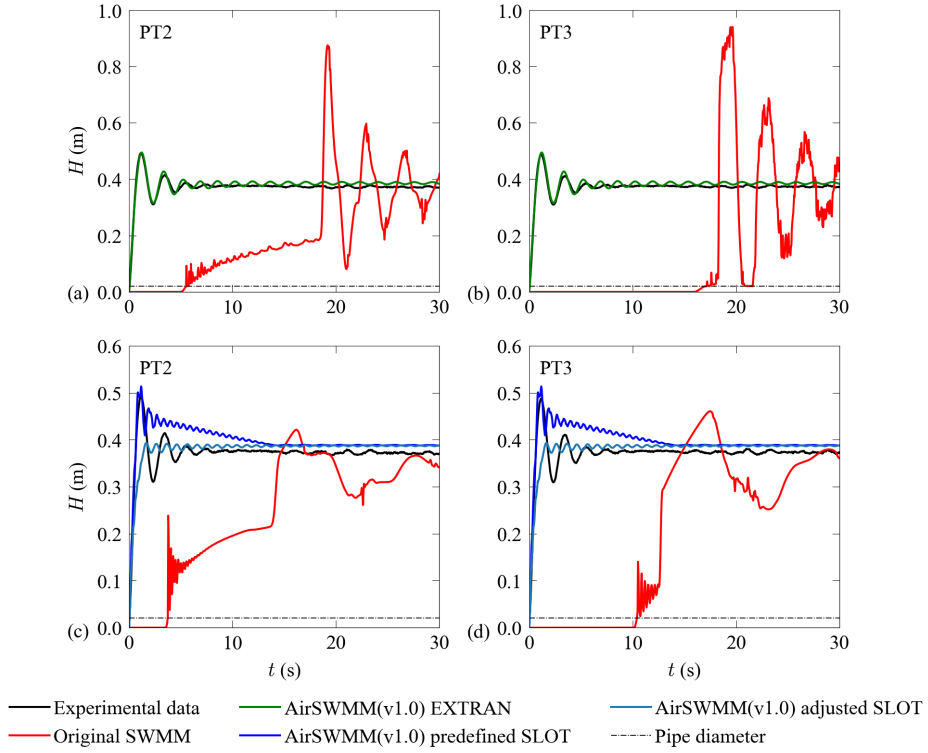

Figure 4.5: Comparison between experimental data and numerical pressure-head results for H_{ini} = 0.35 m and no air release configuration at PT2 and PT3: (a and b) with EXTRAN model; and (c and d) with SLOT method considering SWMM predefined and adjusted slot width.

4.4.3. RESTRICTED AIR RELEASE CONDITIONS

The comparison between original SWMM and AirSWMM(v1.0) results with collected experimental data for the restricted air release configuration is shown in Figure 4.6.

Results for the EXTRAN surcharge method used in two SWMM models are shown in Figure 4.6a. As can be seen from this figure, the original SWMM model cannot reproduce the air behaviour, since it assumes the air is at the atmospheric pressure inside the pipe during the filling phase. Also, the arrival time of the wavefront does not agree with collected data: the wavefront reaches PT3 at t = 12.5 s in the original SWMM model while the experimental data shows the wavefront arrives at that location at t = 34 s. When the wavefront reaches the downstream end, a transient is generated but does not have the same impact as in the no air release configuration because there is still flow going through the orifice. Conversely, AirSWMM(v1.0) (with EXTRAN surcharge method) can describe the observed behaviour reasonably well, given the good agreement with experimental data for the first overpressure caused by the air compression (t = 1 s). Once the wavefront reaches each transducer, the pressure-head stops decreasing becoming constant, since the measured pressure-head no longer corresponds to the one from the air

but from the water, belonging directly to the one from the water tank. After the pipe pressurisation (at t = 39 s), a pressure surge is observed in both pressure transducers. This corresponds, once again, to the wavefront reaching the orifice. However, in this situation, the pressure variation is only roughly approximated by the experimental results. After the pressure surge at t = 39 s, the observed pressure variations are a consequence of some small air pockets being released. While the air is released, the water flow rate is affected by an air bubble generating a pressure surge which is immediately alleviated by the air release and the restitution of the flow. The wavefront arrival time is also accurately predicted using AirSWMM(v1.0) model.

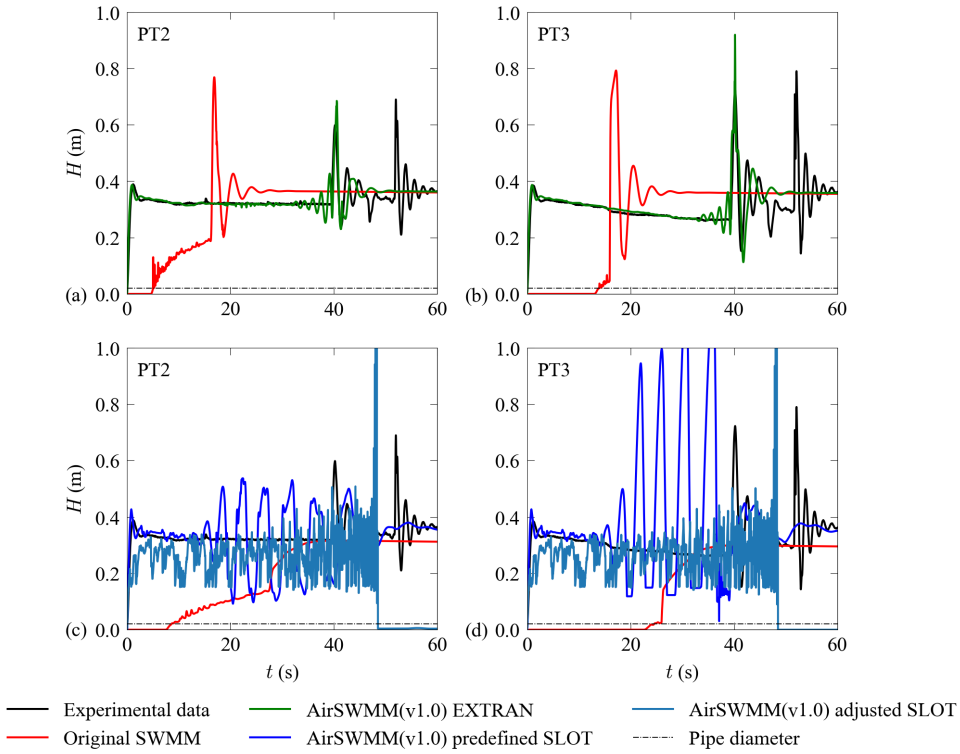

Figure 4.6: Comparison between experimental data and numerical pressure-head results for H_{ini} = 0.35 m and restricted air release configuration at PT2 and PT3: (a and b) with EXTRAN model; and (c and d) with SLOT method considering SWMM predefined and adjusted slot width.

Results obtained using the SLOT surcharge method for the restricted air release configuration are shown in Figure 4.6b. Neither the original SWMM nor AirSWMM(v1.0) can describe well the pipe-filling process for this configuration. The wavefront predicted by the original SWMM arrives at PT3 around t = 23 s, whereas the actual wavefront arrives at t = 34 s. Also, the correct steady-state pressure-head is never reached. Despite some numerical instabilities, AirSWMM(v1.0) describes reasonably well the initial stage of air pressurisation (until t = 15 s). Observed numerical instabilities are likely to be a

consequence of the flow rate variation and the pressure-head calculation with the SLOT method. These instabilities are not improved even if several calculation iterations are made for each time step. Therefore, the SLOT method is not capable of describing the pipe-filling event for the small air release configuration.

4.4.4. UNRESTRICTED AIR RELEASE CONDITIONS

Figure 4.7 shows the comparison between the experimental data and the numerical results from original SWMM and AirSWMM(v1.0) for the unrestricted air release configuration. Figure 4.7a shows the results in the case of EXTRAN surcharge method, whereas Figure 4.7b shows the corresponding result when the SLOT surcharge method is used.

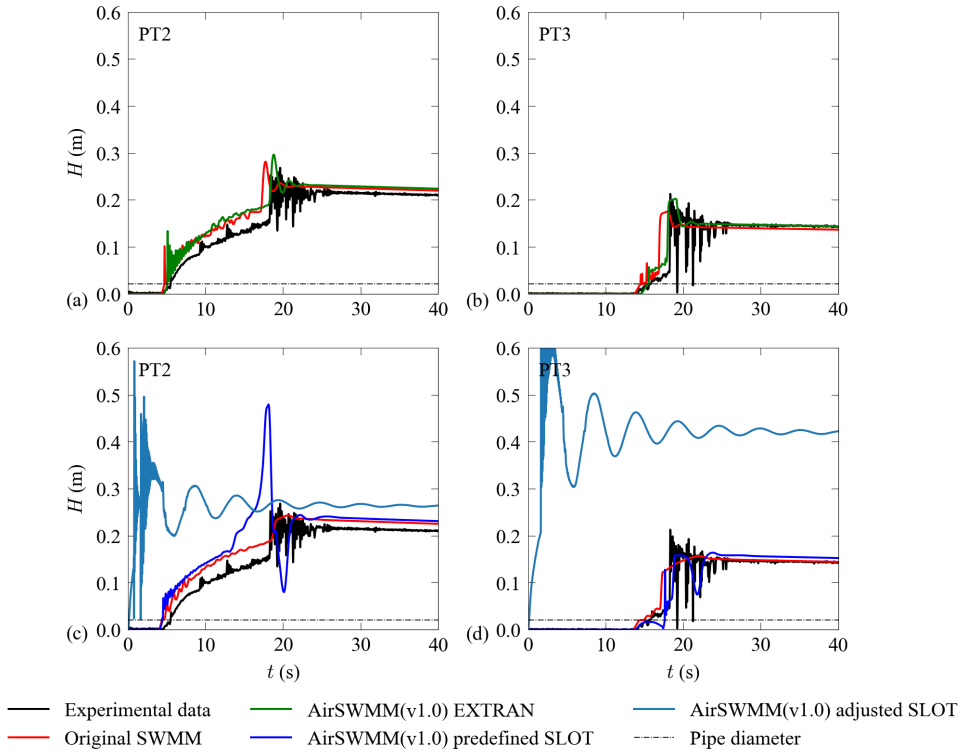

Figure 4.7: Comparison between experimental data and numerical pressure-head results for H_{ini} = 0.35 m and unrestricted air release configuration at PT2 and PT3: (a and b) with EXTRAN model; and (c and d) with SLOT method considering SWMM predefined and adjusted slot width.

Both original SWMM and AirSWMM(v1.0) with EXTRAN surcharge method can describe the pipe-filling behaviour in terms of pressure heads. The pressure-head slightly increases after the valve opening (t = 0 s) because the water inflow and the air release predictions are decoupled. The calculated wavefront arrives at the pressure transducers at the same time as observed in the experimental data.

On the one hand, results from the original SWMM, using the SLOT surcharge method, are numerically stable and agree, to a certain extent, with the experimental data. The arrival time is correctly estimated, but the arrival at the downstream end is anticipated. On the other hand, results from AirSWMM(v1.0) are not numerically stable and, hence, this model is not capable of simulating well the pipe-filling process. Therefore, once again, SLOT method is not suitable for describing the filling event when used with AirSWMM(v1.0) model.

4.4.5. AIRSWMM(V1.0) VALIDATION

Previous sections have demonstrated the predictive performance of AirSWMM(v1.0) for the data set used for calibration. This section assesses the performance of this model with the validation dataset (i.e., not used in the calibration process), which includes collected data for the initial water tank level of H_{ini} = 1.50 m. Figure 4.8 shows the comparison of predictions obtained using the AirSWMM(v1.0) models with EXTRAN surcharge method with the corresponding experimental data, all for the three analysed configurations.

Figures 4.8a and b show the numerical results with experimental data for the dead-end configuration. AirSWMM(v1.0) is still capable of describing well the air behaviour during the pipe pressurisation. The pressure-head amplitude is still correctly estimated but the wave period is slightly delayed. A different polytropic coefficient value is needed to address this, as a faster pipe-filling event makes the thermodynamic process more adiabatic. As a result, the polytropic coefficient of 1.0 is found more appropriate for this specific case. Even though the polytropic coefficient k may vary, the overall behaviour is not deeply affected. Hence, a value of k = 1.2 is recommended.

The numerical results and experimental data for the restricted air release configuration are shown in Figures 4.8c and d. Again, AirSWMM(v1.0) is able to describe the air behaviour during the pipe pressurisation. In the AirSWMM(v1.0) results, the pressure amplitude is correctly estimated after the valve opening. However, the pipe fully pressurises sooner than observed in the experimental data. Such a time difference is due to the calibrated polytropic coefficient k for H_{ini} = 0.35 m: the value of this coefficient not only influences the air pressurisation and the air density but also affects the air release estimated by Eq. (4.2). Hence, k value influences the pipe-filling in two different ways. Still, the observed pressure-heads and the time of arrival have clear improvements using AirSWMM(v1.0) model when compared to the original SWMM results.

Figures 4.8e and f compares the numerical results and experimental data for the unrestricted air release configuration. AirSWMM(v1.0) still has some air pressurisation during pipe-filling, but both the arrival time and the pressurisation time agree with experimental data. The model estimates the correct steady-state pressure-head, but does not reproduce the pressure peak when the wavefront reaches the downstream end.

The RMSE between experimental and numerical data for the simulations with EXTRAN surcharge method are included in Table 4.3. Calibration parameter values show a worse agreement for the restricted air release configuration in general but that is due to the hydraulic transient generated when the waterfront wave reaches the orifice, which the original SWMM is not capable of accurately reproducing. Nevertheless, validation numerical results still present a good agreement with experimental data.

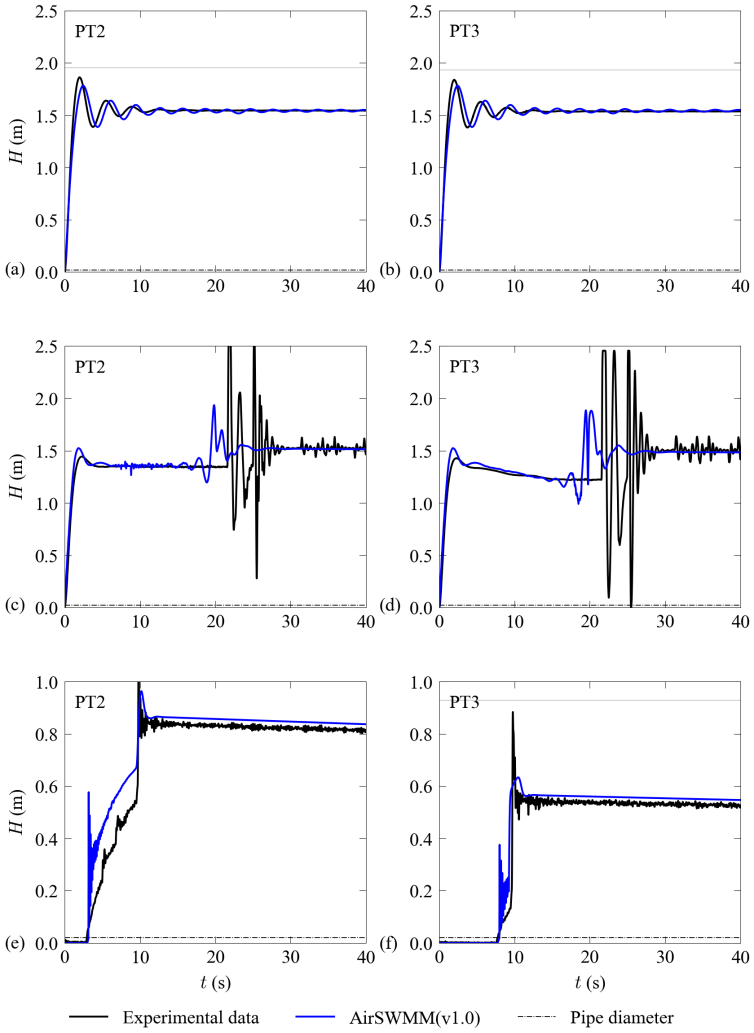

Figure 4.8: Comparison between experimental data and numerical results for H_{ini} = 1.50 m using EXTRAN surcharge model at PT2 and PT3: (a and b) for no air release conditions; (c and d) for the restricted air release conditions (d = 1.1 mm) and (e and f) for unrestricted air release conditions (d = 10 mm).

Experimental results could have been compared with those obtained from analytical solutions where the considered assumptions were applicable to the experimental tests. One of the main assumptions of these solutions (eg. Tijsseling et al. (2019)) is that the waterfront is perpendicular to the pipe axis. The same conclusion has been drawn when simulating pipe-filling events in restricted air release conditions with a rigid water column (Ferreira et al., 2023), which has the same core assumption. The fact was that the observed waterfront had a low slope in most tests, even in the fast filling events with the downstream end fully open to the atmosphere, reason why these where not compared

with analytical solutions.

Table 4.3: RMSE values from calibration and validation comparison between collected experimental data and numerical results using AirSWMM(v1.0).

	RMSE (m)				
	No air release	Restricted air release		Unrestricted air release	
H_{ini} (m)	d = 0 mm	d = 1.1 mm	d = 2.2 mm	d = 10 mm	d = 21 mm
0.35	1.8×10^{-4}	2.0×10^{-3}	1.5×10^{-2}	2.7×10^{-4}	4.9×10^{-4}
1.50	1.6×10^{-3}	2.8×10^{-2}	6.0×10^{-2}	2.0×10^{-3}	2.9×10^{-4}

4.5. DISCUSSION

SWMM has been used by researchers as a solver for the modelling of IWS systems, especially for the description of the pipe-filling stage (Cabrera-Bejar and Tzatchkov, 2009, Campisano et al., 2019). Previous contributions using SWMM assume air is released at each calculation node, which is not always the case in intermittent water supply systems, leading to inaccurate results. Even though the present work addresses only water filling in a single pipe (or several pipes in series), this methodology could be extended to pipe networks by creating multiple air pockets, tracking the flow path into multiple branches and adjusting the flow rate accordingly.

Incorporating air behaviour in SWMM will allow a better simulation of pipe-filling events for three reasons. Firstly, air in pipes is one of the main causes for pipe operation disruptions and pipe failures (Fuertes-Miquel et al., 2019), which were shown to increase from 30% to 70% for water mains and household connections in IWS operation (Christodoulou and Agathokleous, 2012). Incorporating the air behaviour will allow to better estimate the air pressure in the pipes and the definition of measures to prevent unusually high pressures that lead to pipe failures. Secondly, entrapped air pockets also create additional head losses in the system which only aggravate the already low pressures in IWS systems, since head losses can be 20% - 35% higher than in air-free pipes (Stephenson, 1997, Pothof and Clemens, 2010). Such losses could be obtained by estimating the air volume in the pipes using AirSWMM(v1.0). This estimation allows for a better quantification of pressures at each service connection and, hence, a better determination of the supplied water volume. Finally, IWS creates great social equity problems between service connections closer to storage tanks and those at the network outskirts (Sharma and Vairavamoorthy, 2009). AirSWMM(v1.0) allows a more accurate estimation of the system filling time due to the air release, thus providing better means to define measures to improve IWS equity.

Thus, AirSWMM(v1.0) is an improved modelling tool for intermittent water supply system designers, consultants and utilities. This applies to both: i) the redesign of existing WDS that were originally designed for continuous water supply but had to be converted into IWS for various reasons (Andey and Kelkar, 2007) and ii) the design of new IWS systems when subjected to other constraints like water shortage, power instabilities and unreliable water treatment reagents supply chain (Simukonda et al., 2018b).

Based on the presented experimental and numerical analyses, the authors advocate the use of AirSWMM(v1.0), including compressible flow theory for the air behaviour de-

scription and the EXTRAN surcharge method for the description of pressurisation transitions, as a most convenient trade-off between theory and practice when undertaking numerically pipe-filling analyses and air volume quantification.

4.6. CONCLUSIONS

Air behaviour is of great relevance in pipe-filling events and simulations are required to estimate maximum and minimum pressure variations generated by the air presence. So far, there are no available modelling tools to simulate the pipe-filling operations of IWS systems considering the air-water behaviour. This chapter experimentally describes the effect of air during the pipe-filling process, confirming its relevance based on three scenarios: no, restricted and unrestricted air release conditions. An explanation of the phenomenon is provided by the development of an improved SWMM code that includes compressible flow theory for air release. After experimental verification, the model has proven to have good predictive potential in estimating pressure variations and the time arrival of the filling and pressurisation of the system. Based on the results obtained the following conclusions are drawn:

- AirSWMM(v1.0) model with the EXTRAN surcharge method can reproduce well the observed experimental data for the three analysed pipe-filling cases. This applies to predicted pressure-heads, wavefront arrival times and pressurisation time.
- When compared to the original SWMM model, AirSWMM(v1.0) model shows a significant performance improvement in terms of all aforementioned predictions, which is important for the modelling of pipe-filling in real IWS systems, as elaborated in the discussion section.
- AirSWMM(v1.0) model with the SLOT surcharge method cannot accurately describe the pipe-filling event in any of the analysed configurations. When compared to experimental data, either the numerical pressure-heads were overestimated or the solver had numerical instabilities that turned it virtually unusable. Attention should be given to the SWMM's Preissmann slot to account for the potential calculated pipe wave celerity change due to air existence in the flow.

Further research is required to assess whether an adjusted Preissmann slot width could be valid by using higher time steps for larger systems (i.e., higher than the minimum required to ensure numerical stability). More importantly, the AirSWMM(v1.0) model needs to be further developed to simulate the pressure and flow rate conditions in the presence of air in more complex IWS systems, like pipe networks, and also for pipe emptying events, as air entrainment might also play an important role during such processes.

5

AIR POCKET ENTRAPMENT MODELLING BASED ON SWMM FOR A PIPELINE

This chapter is an adapted version of:

Ferreira, J. P., Ferràs, D., Covas, D. I. C., van der Werf, J. A., Kapelan, Z. (2024). Air entrapment modelling during pipe-filling events based on SWMM. Journal of Hydraulic Research, 62 (1). DOI: https://doi.org/10.1080/00221686.2024.2305354.

5.1. INTRODUCTION

The presence of air severely affects water supply, urban drainage and stormwater systems (Fuertes-Miquel et al., 2019). IWS systems are particularly affected by air since they are not always pressurised, i.e., they continuously go through a cycle of filling, supplying and emptying stages. The filling stage is characterised by water abruptly entering the system, forcing the air inside to be released. Conversely, the air release rate influences the flow rate going into the system. The air release delays the pipe-filling and affects the water supply time to end consumers. During the filling stage (and also due to possible inadequate air valve design and maintenance), air pockets can get entrapped in the pipes. These pockets can cause pipe malfunctioning and local head losses (Ramezani et al., 2016) and can induce high-pressure variations during transient events (Martins et al., 2015, Martins et al., 2017, Ferreira et al., 2021, Gonzalez et al., 2020). This behaviour has also been observed in water supply systems after the implementation of IWS: increased pipe failures and higher leakage levels are observed after a water supply system starts operating intermittently (Christodoulou and Agathokleous, 2012, Charalambous and Laspidou, 2017).

Despite all the associated problems with air pockets, the present state of engineering practice does not offer a numerical methodology to detect, locate and quantify air pockets using more traditional one-dimensional models. Work has been developed to locate and quantify entrapped air pocket volumes in a bridging pipe using a 3D CFD model (Kaur et al., 2023). However, using such models for network assessment and engineering practice is not a viable solution due to the computational effort and specialist knowledge required to set up and use these models.

Stormwater Management Model (SWMM) is a 1D model developed for urban drainage and stormwater design and management that has been used as a computationally inexpensive tool to simulate IWS systems (Cabrera-Bejar and Tzatchkov, 2009). Campisano et al. (2019) investigated pipe-filling using SWMM and obtained a satisfactory agreement between field data and numerical results. However, the model does not incorporate the air phase during the filling stage. Gullotta et al. (2021) expanded the use of SWMM to determine the optimal location of pressure-reducing valves to equitably distribute water under IWS conditions. Still, this work did not consider the air phase. A method has been developed to identify possible entrapped air pockets locations using SWMM, but it overestimated the entrapped air pocket volumes (Ferreira et al., 2022). An air accumulator model has been incorporated in SWMM to simulate the air pressure and density with a piston equation to track the waterfront's position (as observed in 4); this model allows to simulate the air pressurisation in pipes but is not able to detect or quantify air pockets due to the assumption of a perpendicular waterfront to the pipe axis.

This chapter presents and proves a novel methodology for improved one-dimensional modelling of air pockets during pipe-filling events in IWS systems. This methodology incorporates a more robust waterfront tracking method and two-phase flow dynamics mechanisms, i.e., pocket creation, dragging and entrainment than the one presented in Chapter 4. This new methodology enables locating air pockets and quantifying their respective volumes, which was not possible in the previously referred method. Novel experimental tests are conducted in the pipe system layout #2 (Section 3.2.2) to understand the process of air pocket creation and volume variation at a high

point in the system. Pressure and flow rate measurements as well as video recordings are carried out. Image processing is used to estimate the actual entrapped air pocket volumes and air travelling in the pipe. Collected data are used to calibrate and validate the new air entrapment model, AirSWMM(v2.0).

The outline of the chapter is as follows. Section 5.2 describes the experimental data collection and corresponding analysis. Section 5.3 gives a summary of the original SWMM model and proposes the methodology to locate and quantify entrapped air pockets. Section 5.4 presents the model assumptions, describes the calibration process and shows the validation results by using the proposed methodology. The application of the outputs from this chapter is discussed in Section 5.5 and a summary of the results and conclusions are presented in Section 5.6.

5.2. EXPERIMENTAL TESTS AND DATA ANALYSES

Twenty pipe-filling tests are carried out in the pipe layout #2 in Section 3.2.2 for each downstream orifice size to ensure reproducibility and observe the stochastic nature of the pipe-filling and the respective air pocket sizes. The pipe is empty at the beginning of the experiments and all tests start with a constant water head H_{ini} = 0.5 m in the upstream tank. The valve is opened to start the test with an effective opening time of 0.0021 s (Ferreira et al., 2018), allowing water to flow into the pipe. After the pipe-filling is completed and a steady state flow is reached, the test is considered to have finished. After each test, the pipe is emptied with compressed air and the upstream tank level is reset to 0.5 m, so that the system is ready for the next test. Water temperature varied less than 0.5° C during all conducted tests.

5.2.1. AIR POCKET FORMATION AND DEVELOPMENT

Three types of air pockets are observed during the pipe-filling process: travelling air pockets, dynamic entrapped air pockets and steady-state entrapped air pockets. Travelling air pockets are formed during the filling process and are carried with the flow due to the velocity profile's shape, pipe layout and diameter. These often collide and merge with other entrapped air pockets of the other two categories. Dynamic entrapped air pockets are created or dragged into high points during the pipe-filling process but are unable to be dragged by the flow. These pockets can have their air-water interface disrupted from the collision with other pockets or bubbles. Air entrainment is also observed in these pockets' tail during the pipe-filling. Steady-state entrapped air pockets are formed by the coalescence of all dynamic and travelling air pockets converging to higher elevation points due to the lack of flow momentum to drag them or to compensate for the air buoyancy after reaching steady-state flow. Steady-state entrapped air pockets show clearer and more static boundaries than dynamic entrapped air pockets.

An example of collected pressure-head signal and air pocket images is shown in Figure 5.1a for each air pocket type for a test with a downstream orifice diameter d = 3.0 mm. Figure 5.1a shows the pressure-head time series for the sampled pipe-filling test at each transducer and Figure 5.1b shows the corresponding images of the high point.

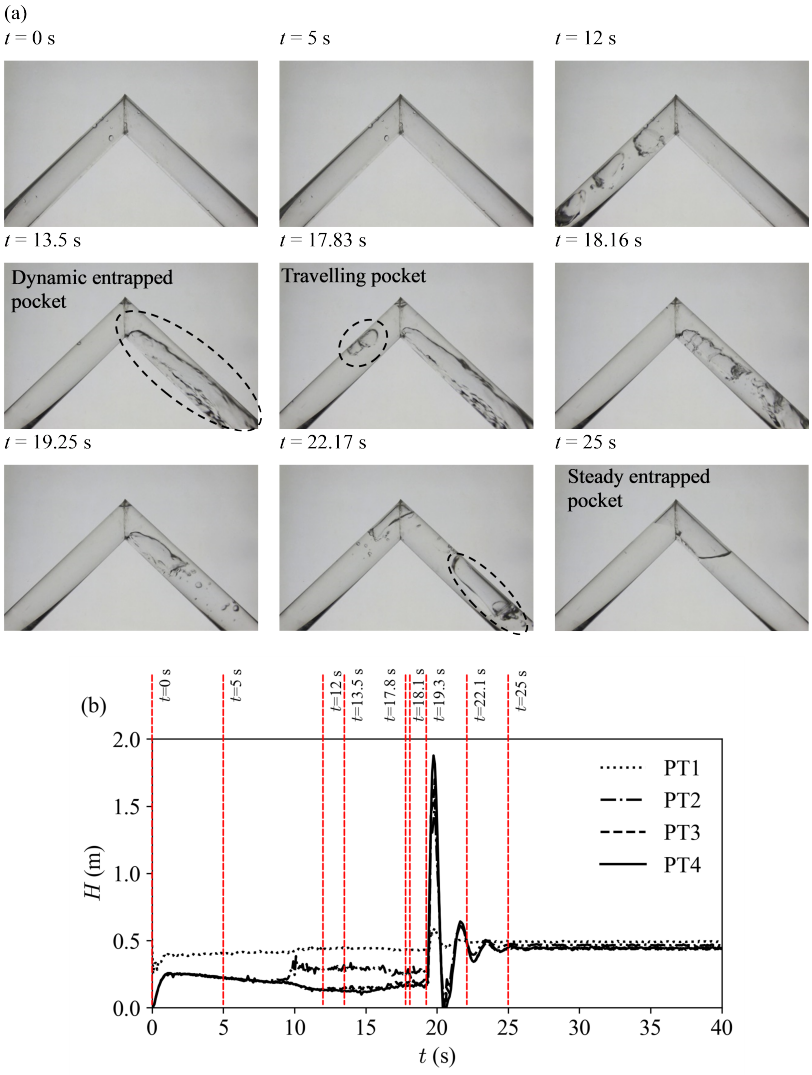

Figure 5.1: Test with d = 3.0 mm: a) images at different pipe-filling moments and b) pressure-head signal at each pressure transducer.

The images shown in Figure 5.1a come from the video recordings for the same test. The timestamps of each image are shown in Figure 5.1b. The high point of the rising pipe is empty until t = 10 s, i.e., the moment when a waterfront reaches this location. Air pockets are observed on the waterfront due to the turbulence of the filling behaviour. At t = 13 s, an air pocket is created after the high point and does not get dragged due to the high pipe's downward slope, the low flow velocity and the large air pocket size. The filling continues and an unexpected behaviour is observed at t = 17.83 s. The highlighted air bubble coming from upstream collides with the entrapped air pocket and splits into

two smaller-sized ones as observed at t = 18.16 s. The air entrainment process keeps occurring at the downstream bottom side of the air pocket in the form of air bubbles until the waterfront reaches the downstream end at t = 19.25 s. The air pockets rise to higher points due to the lack of drag force from the steady-state flow and, consequently, take a more stable shape. Air pockets close to the slope change (from the downstream sloped pipe to the horizontal pipe) rise to the high point. The air pocket that stays at the high point (dynamic entrapped air pocket) and the one rising from the downwards sloped pipe coalesce and reach an equilibrium when a steady state flow is achieved, t = 25 s. A small local head loss is observed in the pressure-head signal from the difference between PT2 and PT3 due to the air pocket in the high point.

Figure 5.1b shows pressure-head time variations in four transducers. A pressure-head drop from 0.50 to 0.30 m is observed at t = 0 s in PT1, corresponding to the valve opening. As the water enters the pipe, the air becomes pressurised, as observed in the pressure head rise at PT2 - PT4. The latter transducers measure the same pressure-head until t = 7.5 s since these values correspond to the air pressure ahead of the waterfront. The waterfront arrival to each transducer is identified by the pressure-head stabilization or increase. Pressure-head signals diverge when the waterfront reaches each transducer: PT2 is reached around t = 7.5 s, PT3 at t = 13 s and PT4 at t = 16 s, since air pressure decreases as is released and water pressure depends on the upstream water tank head and head losses. Two more pressure-head features are identified. The pressure-head rise at PT2 at t = 10 s corresponds to the waterfront rise towards the high point between PT2 and PT3 by building up pressure to the upstream section of the pipe. The sharp pressure variations following t = 19.5 s correspond to the moment the waterfront hits the downstream acrylic plate and generates a pressure wave (water hammer), thus concluding the filling process. The pressure wave goes back and forth along the pipe until the flow energy is dissipated by friction, heat transfer by air compression and expansion and pipe wall viscoelastic behaviour, reaching a new steady state. From this moment onwards, the flow becomes steady and all entrapped air pockets are formed and attain their final volume.

In this chapter, all the comparisons between experimental and numerical entrapped air pocket volumes refer to steady-state air pockets. Initial and evolving air volumes were not quantified because of the lack of a second camera while running the tests. The air pocket splitting and eventual further coalescent phenomena (seen at t = 18.16 and t = 22.17 s in Figure 5.1b) have been disregarded for the following reasons. Firstly, air pocket splitting does not occur in all tests, as it only occurs in ca. 35% of the tests, very much depending on the tested air release conditions. When this behaviour occurs, most air pockets with a disrupted interface are dragged downstream. Thus, no substantial difference is expected between split and non-split air volumes at the final steady-state air pocket volume. Secondly, dynamic air pockets seem to depend on the air bubble size that causes the split, the split air pocket size, its shape and the angle of incidence when both collide. The numerical modelling of this behaviour is not possible using a one-dimensional (1D) model and, therefore, it is out of the proposed work scope. More complex modelling, such as 3D CFD models, is needed to simulate these phenomena.

5.2.2. FLOW RATE VARIATION

Maximum and steady-state flow rates are higher for larger downstream orifice sizes (Figures 5.2a, b). Large orifice cross sections allow higher initial air flows and, consequently, higher initial (maximum) water flows. Also, larger orifice sizes lead to lower the local head losses are and, thus, higher (final) steady-state flow rates.

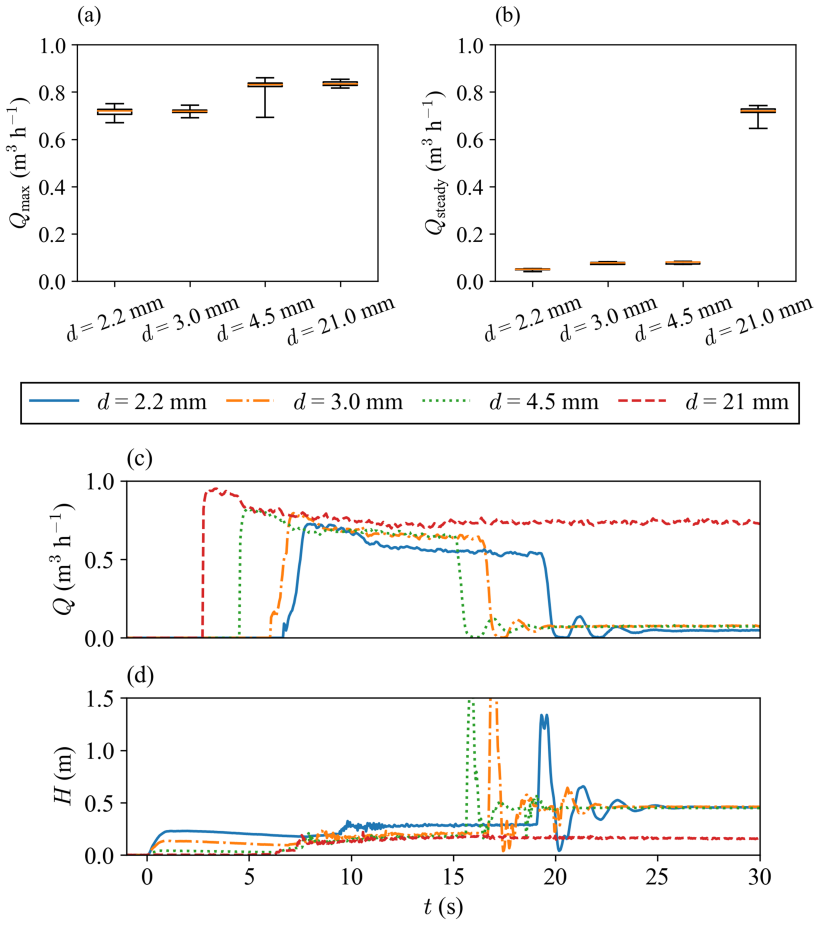

Figure 5.2: Distribution of the a) maximum and b) final steady-state flow rates during the pipe-filling process for each downstream orifice size considering all tests; and c) examples of flow rate time series and d) corresponding pressure-head signal for each downstream orifice size.

Figure 5.2c shows the flow rate time series for each of the four orifice sizes' tests. As the valve is opened (at t = 0 s), the waterfront takes some time to reach the ultrasonic flowmeter which is located 5 m from the upstream valve, reason why flow rate rise occurs at different times. The flow rate is high during the pipe-filling, and sharply decreases to the smallest three orifice sizes (d = 2.2, 3.0 and 4.5 mm). There is a short period when the flow rate fluctuates at the end of the filling due to the pressure wave going back and

forth until steady state is reached. No sharp flow rate variation is observed for $d = 21$ mm because no orifice is at the downstream end (i.e., the downstream end is fully open into the atmosphere). Figure 5.2d shows the corresponding pressure signal for each orifice size presented in Figure 5.2c. The pressure in the air increases for smaller orifice sizes. A higher pressure at the initial stage of opening also indicates a slower filling, hence a delayed arrival to the downstream end of the system where the waterfront hits the orifice and creates a pressure peak.

5.2.3. ENTRAPPED AIR POCKET VOLUME

The air pocket volumes at the high point are determined based on the processing of the video-recorded images. Air pockets are assumed to be axisymmetric (i.e., of cylindrical shape) around the air pocket axis. The air pocket height, l_{AP}, and diameter, D_{AP}, are obtained once the pixels corresponding to the air pockets are identified by cropping (done using Gaussian filters and binarizing the images). Each air pocket pixel dimension is obtained and the air pocket pixels are converted into lateral air pocket area. This area allows to obtain the final entrapped air pocket volume, V_{AP}, when the air pocket resembles a cylinder by:

$$V_{\mathrm{AP}} = \frac{\pi D_{\mathrm{AP}}^2}{4} l_{\mathrm{AP}} = \frac{\pi D_{\mathrm{AP}}}{2} S_{\mathrm{AP}} \tag{5.1}$$

where S_{AP} is the air pocket area in the image given by $S_{\mathrm{AP}} = D_{\mathrm{AP}} l_{\mathrm{AP}}$. Air pockets that more resemble a cone (see Figure 5.3a) have their volume calculated by:

$$V_{\mathrm{AP}} = (\pi r_{\mathrm{AP}} S_{\mathrm{AP}})/3 \tag{5.2}$$

where r_{AP} becomes the radius of the cone base.

Figure 5.3a presents an example of the original image with the analysed region of interest (ROI) and Figure 5.3b the final cropped, filtered, binarised and filled air pocket area. The area of each air pocket is calculated by counting the number of white pixels in Figure 5.3b and converting such value into the air pocket cross-section area and volume according to Eqs. (5.1) and (5.2).

Steady-state entrapped air pocket volumes show a considerable variation between tests, as depicted in Figure 5.4a. Maximum and median volumes of final entrapped air pocket decrease with the increase of downstream orifice size (Figure 5.4a). As the orifice size increases, the less steep the waterfront becomes, originating lower air pocket volumes (Guizani et al., 2006). This is reinforced by the progressively higher maximum filling flow rate, Q_{max}, in the flow rate time series for a sampled tested for each downstream orifice diameter. The maximum filling flow rate decreases as the downstream orifice size decreases, taking longer time the waterfront to reach the downstream orifice (note the sharp maximum flow rate drop from $d = 2.2$ to 4.5 mm in Figure 5.2a. For the case of the fully open downstream end ($d = 21$ mm), the average is 280 mm^3 and median air pocket volumes is 0 mm^3. The maximum and minimum entrapped air pockets for $d = 2.2$ mm are shown in Figures 5.4b and c.

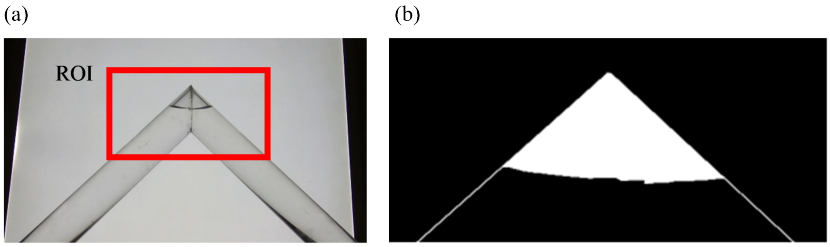

Figure 5.3: Example of image treatment from video recordings to determine the air volume of air pockets: a) original image with ROI and b) detail of processed and binarised image.

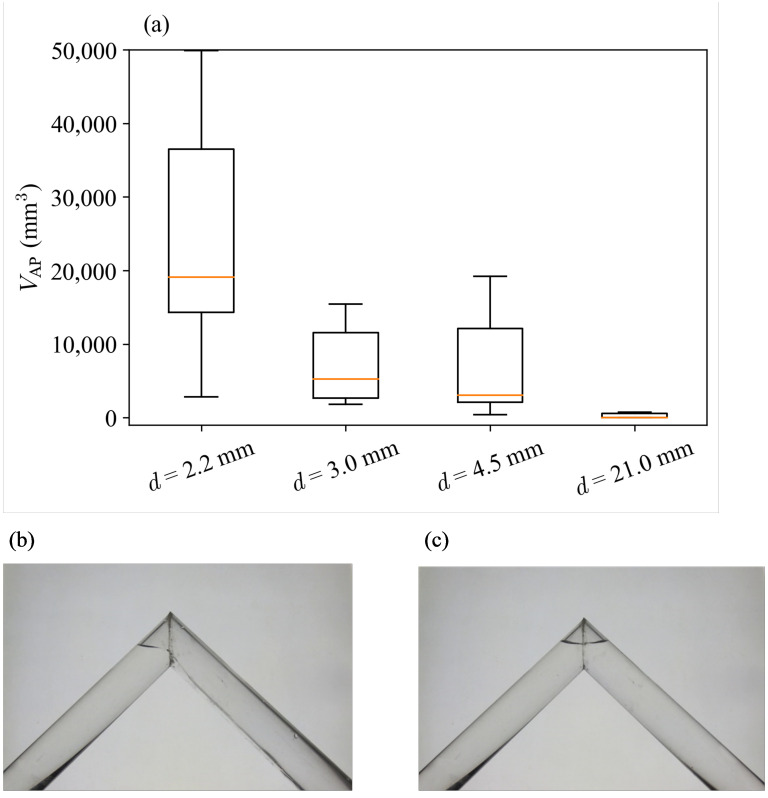

Figure 5.4: a) Air pocket volume boxplots for each orifice size and b) maximum air pocket for d = 2.2 mm and c) minimum air pockets for d = 2.2 mm.

5.2.4. AIR POCKET DRAGGING

An additional category of air pockets is identified during the experimental tests. Small air pockets are created in the horizontal pipe section during the pipe-filling. Their formation is not directly observed in the video recordings but their dragging in the flow over time allows for their identification. Image processing like carried out to steady-state air pockets is carried out to quantify their volume. Each test's recordings are analysed to understand the influence of the air release conditions on the small air pocket creation in the horizontal pipe section.

The distribution of the volumes of travelling air pockets for each downstream orifice is presented in Figure 5.5 in non-dimensional terms as a ratio of the dragged air volume and the upstream pipe volume. Maximum and average dragged air volumes decrease with the downstream orifice diameter increase, whilst the minimum is within the same order of magnitude. This decrease in the volumes can be explained by the waterfront wave becoming gradually steeper and, consequently, fewer air pockets being created on the pipe crown to be later dragged. Maximum and average values of dragged air volumes increase after d = 4.5 mm, caused by the considerably higher flow rate during the filling process and when the steady state is reached. This means all the air pockets created in the upstream pipe section are effectively dragged, pass by the ROI and are released at the downstream end, whilst that is not possible for the d = 4.5 mm and below. Staggered air pockets are visually observed at the upstream section of the pipe at the end of each test for d = 2.2 - 4.5 mm but not for d = 21 mm. No videos were recorded other than from the high point.

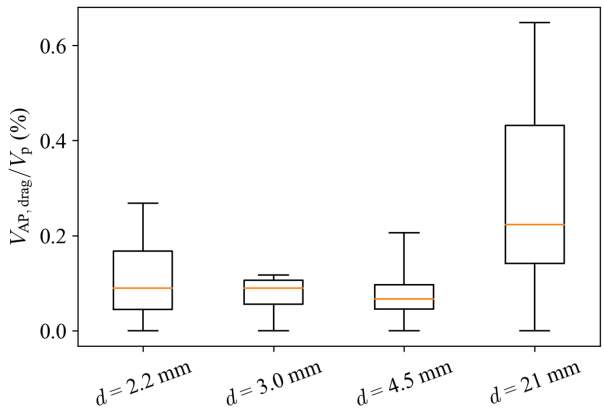

Figure 5.5: Normalised travelling air pocket volume for each downstream orifice.

Travelling air pockets can, partially or fully, coalesce with air pockets created at the high points or further down. Ultimately, the travelling air volume is dragged until the high point where it can coalesce with the air pocket. Image processing was carried out to quantify the coalescence ratio between the dragged volume and the volume that overcomes the high point air volume and goes downstream. However, no conclusive results could be obtained. The air-water mixing behaviour at the air pocket tail and the rela-

tively low contrast image did not allow to establish a clear delimitation between the air and the water in that region. The same reasoning applies to the air entrainment observed at the entrapped air pocket tail, where small air bubbles are observed to detach from the original air pocket and are dragged downstream (see Figure 5.1b, t = 19.25 s). Other researchers managed to quantify the air entrainment in pressurised flows but for steady-state flows and the air volume was artificially injected in the pipe rather than as a consequence of a pipe-filling event (Kalinske and Bliss, 1943, Wisner et al., 1975, Escarameia, 2007), leading to lower air-water mixtures and more observable pockets.

5.3. NUMERICAL MODEL

5.3.1. AIRSWMM(V2.0)

The original SWMM described in section 4.3.2 is modified by adding post-processing calculations that are performed at each time step, to account for different aspects of air pockets formation and fate during the simulation. Figure 5.6 presents a flowchart of these additional calculations composed of four main steps. Step 1 corresponds to the tracking and quantification of the initial air pocket volume at the moment the pipe-filling is completed (i.e., waterfront reaches the downstream pipe end). In Step 2, air release and accumulator calculations are carried out to correct the air pocket volume according to the surrounding pressure. This step changes the hydraulic conditions (pressure and water flow rate) that will influence the air pocket creation and its initial volume. Step 3 consists of the verification if the air pocket is being dragged and if any air entrainment is occurring. In Step 4, it is identified if any air volume has arrived at the air pocket section and, if yes, merges both volumes.

This methodology builds upon the one presented in Chapter 4 by modifying Step 1 to a more robust method that simulates waterfronts not perpendicular to the pipe axis and by adding Steps 3 and 4.

The final entrapped air pocket volume at time t is estimated based on the balance between the initial air pocket volume calculated in Steps 1 and 2, the air volume that is lost by the entrained air volume in Step 3 and the incoming bubbly flow to the air pocket from Step 4, as follows:

$$V_{\mathrm{AP,\,f}} = V_{\mathrm{AP,\,i}} - \sum a(F-1)^b + \sum \frac{V_{\mathrm{AP,\,drag}}}{V_p} Q_{\mathrm{w};t} \tag{5.3}$$

where: $V_{\mathrm{AP,\,f}}$ and $V_{\mathrm{AP,\,i}}$ are the final and initial entrapped air pocket volumes, respectively, a and b are entrainment function parameters, F is the Froude number, $V_{\mathrm{AP,\,drag}}/V_p$ is the air-pipe volume ratio from the small air pocket creation from Figure 5.5. Details of the calculations in each of the four steps are detailed in the following sections.

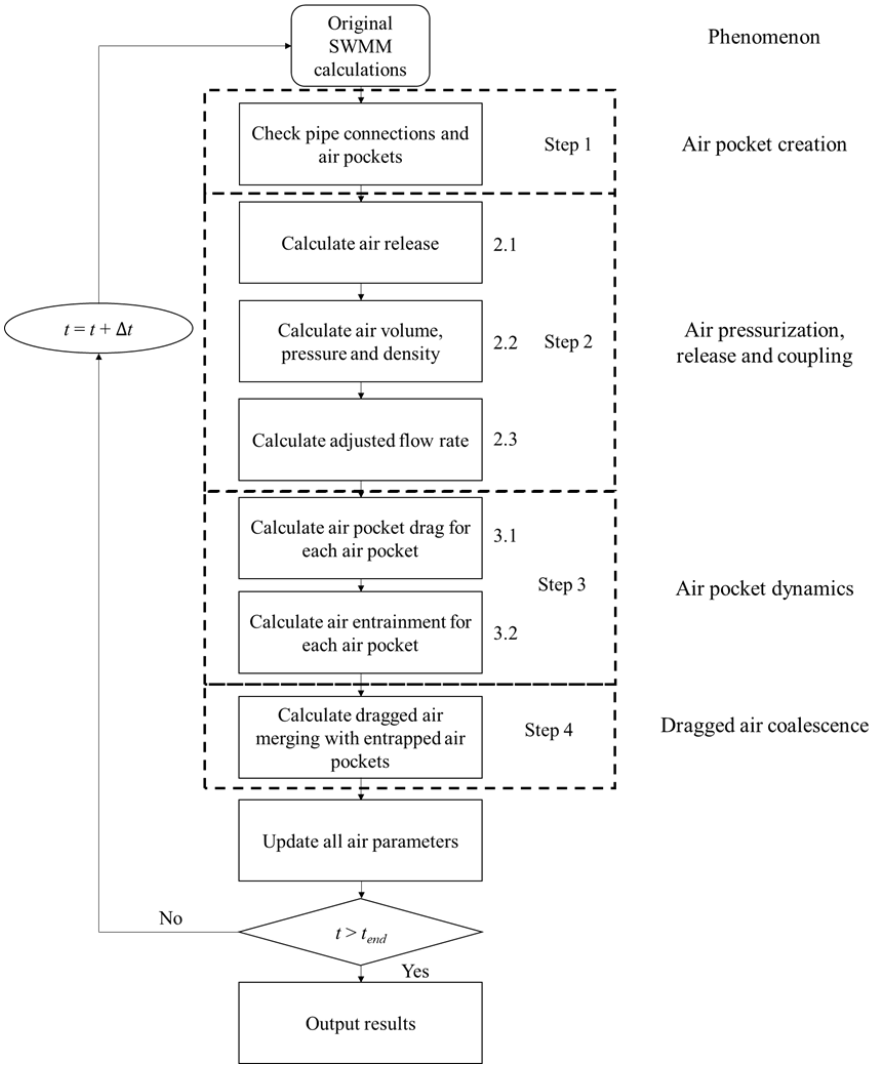

Figure 5.6: Flowchart of the proposed air pocket creation, transport and entrainment methodology implemented in AirSWMM(v2.0).

5.3.2. STEP 1: AIR POCKET VOLUME TRACKING AND QUANTIFICATION METHOD

Step 1 aims to identify which pipes may contain entrapped air pockets and quantify their volume. The method is initialized by going through each pipe to check if its upstream or downstream nodes' water depths are lower than the pipe diameter (i.e. if water has a free surface flow). Pipes with free surface flow are added to a "pool" of non-pressurised pipes. pressurised pipes are assumed to continue to be pressurised in the subsequent time steps (pipe filling up) and, thus, no longer requiring to be checked. The method

proceeds to iteratively connect identified non-pressurised pipes and to add them to a "pool" of connected pipes. Each "pool" corresponds to an air pocket. When no pipes remain to be added to the "pool", the air pocket tracking process is interrupted, and air release conditions are assessed for each air pocket. If any pipe pool is connected to an orifice, that air pocket features air release. Alternatively, an air pocket is considered an entrapped air pocket, if the pipe-set is between two pressurised nodes and not in contact with a non-pressurised orifice. The above process is repeated until no pipes are left in the "pool", from where the tracking finishes and Step 2 starts.

The formation of entrapped air pockets occurs as follows (see Figure 5.7): a) the pipe is filling with a free surface flow, b) until a hydraulic jump is identified due to a slope change or an obstacle; an air pocket is created, once the jump creates a void upstream the slope change; c) the "void" pipe section between those nodes (marked using different colour) corresponds to an entrapped air pocket. Once an air pocket is formed, several variables are initialized: the air pocket's centre of mass, the water depth in the pipes where the air pocket is contained (pipe diameter minus the average depth the air pocket occupies in the pipe), the air pocket pressure and density, and the entrapped air pocket volume. The entrapped air pocket volume is computed by running the average water depth in the air pocket's pipe using linear interpolation between nodes and discounting it to the total volume of where the air pocket is contained. This is schematized in Figure 5.7d.

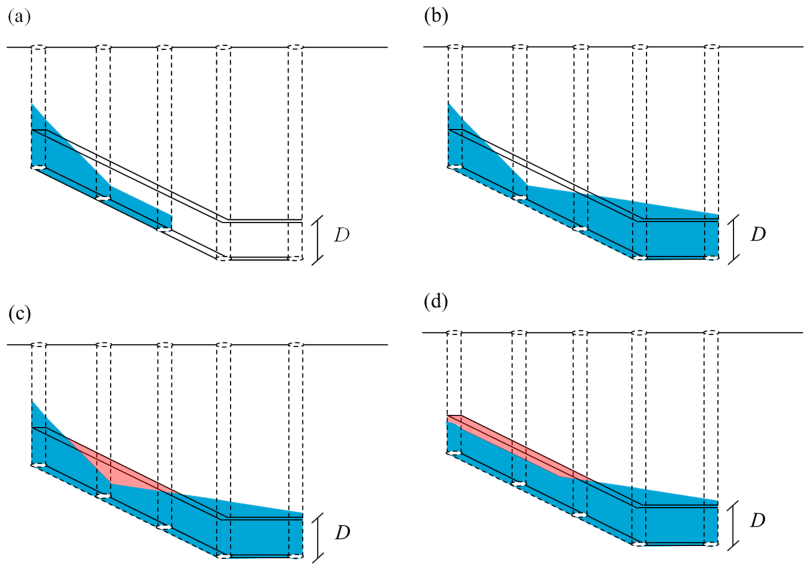

Figure 5.7: Air pocket creation conceptual representation: a) pipe-filling with free surface flow, b) sudden pressurisation of the pipe with an empty volume in the sloped pipe, c) filled pipe with an entrapped air pocket and d) numerical implementation of entrapped air pockets.

Three relevant assumptions are: i) entrapped air pockets can increase and reduce volume over time; ii) an entrapped air pocket has the volume equally distributed between the pipes where the air pocket is identified; iii) an air pocket can move between pipes but keep its initial shape. An important remark is that air pocket location and volume are obtained simply by using flow rate and water depths that the original SWMM already calculates.

5.3.3. STEP 2: AIR PRESSURISATION, RELEASE AND COUPLING

STEP 2.1: AIR RELEASE MODEL:

This step calculates the air release from each orifice from the system. Air release depends on the downstream boundary conditions and the air pressure inside the pipes. The air inside the pipes is initialized at atmospheric pressure p_{atm}. Once the valve is opened, the pipe-filling starts and the air inside the pipe compresses depending on the system boundary conditions. When the air pressure of the air pocket inside the pipe p_{a} is such that $p < p_{\text{atm}} < 1.89$, the air release from an orifice occurs under subsonic conditions (Binder, 1955). The airflow rate is then described as follows (Zhou et al., 2002):

$$Q_{\text{AP};t} = \sum_{j=0}^{\text{AP}_{\text{exits}}} C_{\text{d};j} A_{0;j} Y_{j,t} \sqrt{2g \frac{\rho_{\text{w};t-\Delta t}}{\rho_{\text{AP};t-\Delta t}} \frac{(p_{\text{AP};t-\Delta t} - p_{\text{atm}})}{\gamma_{\text{w};t-\Delta t}}} \tag{5.4}$$

where Y is described by Eq. (4.3). Conversely, whenever $p_{\text{AP}}/p_{\text{atm}} \geq 1.89$, the flow through the orifice becomes supersonic and the flow becomes chocked with a maximum airflow rate being released as follows (Binder, 1955):

$$Q_{\text{AP};t} = \sum_{j=0}^{\text{AP}_{exits}} C_{\text{d};j} A_{0;j} \sqrt{g \frac{\rho_{\text{w};t-\Delta t}}{\rho_{\text{AP},t-\Delta t}} p_{\text{AP};t-\Delta t}} \sqrt{k \left(\frac{2}{k+1}\right)^{(k+1)/(k-1)}} \tag{5.5}$$

The air pocket pressure p_{AP} is obtained from the air accumulator model described in the next subsection.

STEP 2.2: AIR ACCUMULATOR

This subsection complements the air release model by calculating the air pressure and density of the air mass downstream of the waterfront. Air masses in between a waterfront and any kind of boundary or another waterfront, are described by the following equations (which differ from the ones from the previous chapter due to generalisations) assuming the air behaves as an ideal gas (Vasconcelos and Leite, 2012):

$$\frac{dp_{\text{AP};t}}{dt} = \frac{p_{\text{AP};t-\Delta t} k}{V_{\text{AP};t}} \left(\sum Q_{\text{w};t-\Delta t} - \sum Q_{\text{AP};t}\right) \tag{5.6}$$

$$\frac{d\rho_{\text{AP};t}}{dt} = \frac{\rho_{\text{AP};t-\Delta t}}{V_{\text{AP};t}} \left(\sum Q_{\text{w};t-\Delta t} - \sum Q_{\text{AP};t}\right) \tag{5.7}$$

$$p_{\text{AP};t} = p_{\text{AP};t-\Delta t} + dp_{\text{AP};t}\Delta t \tag{5.8}$$

$$\rho_{\text{AP};t} = \rho_{\text{AP};t-\Delta t} + d\rho_{\text{AP};t}\Delta t \tag{5.9}$$

where V_{AP} is the air pocket volume, Q_{w} is the water flow rate filling and compressing the air pocket, Q_{AP} is the released air flow rate obtained according to the equations in the previous subsection.

Air pocket in no air release conditions are described by Eqs. (5.4) to (5.9) with Q_{AP} being zero. Thus, the air pocket volume and density of no air release and entrapped air pockets will vary over time but follow the ideal gas law for assumes near constant ambient temperature: $p_t(V_t)^k = p_{t+\Delta t}(V_{t+\Delta t})^k$. A polytropic coefficient of $k = 1.2$ is used here since the polytropic coefficient does not considerably influence pipe-filling when there is air release as observed in the previous chapter.

STEP 2.3: AIR-WATER INTERACTION IN FLOW RATE CALCULATIONS

This step presents the coupling between the air release and accumulator models from the previous subsections and the original SWMM. The original SWMM model calculates the water flow rate in each pipe as follows:

$$Q_{\text{w};t+1,p} = \frac{Q_{\text{w};t,p} + \Delta Q^{\text{inertia}}_{\text{w};t,p} + \Delta Q^{\text{pressure}}_{\text{w};t,p}}{1 + \Delta Q^{\text{friction}}_{\text{w};t,p}} \tag{5.10}$$

where $Q_{\text{w};t}$ is the water flow rate in a specific pipe p at a given time step, $\Delta Q^{\text{inertia}}_{\text{w};t}$ is the flow rate change during the analysed time step corresponding to inertial forces, $\Delta Q^{\text{pressure}}_{\text{w};t}$ is the corresponding water flow rate change based on pressure forces and $\Delta Q^{\text{friction}}_{\text{w};t}$ is the water flow rate change based on the friction forces. More information on each of these terms can be found in Rossman (2017).

Two changes to the above flow variation terms are required to account for the air compression during pipe-filling events and entrapped air pockets. Firstly, the flow rate variation associated with the pressure component needs to be adjusted as proposed in the previous chapter:

$$\Delta Q^{pressure}_{\text{w};t} = -g\overline{A}\frac{H_2 - H_1}{L}\Delta t \text{ to } \Delta Q^{pressure}_{\text{w};t} = -g\overline{A}\frac{(H_2 + H_{\text{AP}}) - (H_1 + H_{\text{AP}})}{L}\Delta t \tag{5.11}$$

where $\overline{A}$ is the change in average flow area between time steps and H_{AP} is the pressure-head of the air pocket in gauge pressures. H_{AP} is null when H is higher than the pipe diameter. Secondly, the original SWMM model calculates the flow rate considering the total water flow cross-section area when using the EXTRAN surcharging method. By introducing the entrapped air pockets and bubbly flow in the model, the pipe flow cross section area must be reduced by the cross-section area occupied by the air volume in the pipe where the flow rate is being calculated. Thus, the flow cross-section area becomes $A_p = A_{p,0} - V_{AP}/L$. Flow rate inertial and friction terms in Eq. (5.10) remain unchanged (other than the influence of reduced flow cross-section area).

5.3.4. STEP 3: AIR POCKET DYNAMICS

STEP 3.1: AIR POCKET DRAG MODEL

A minimum critical flow velocity is required to overcome the surface tension near the pipe wall to induce movement to a static air pocket in the pipe. Previous literature contributions propose different values or ranges of critical flow velocities depending on the

pipe's slope and diameter. Theoretical approaches determined the critical velocity for horizontal pipes (Dumitrescu, 1943, Davies and Taylor, 1950, Benjamin, 1968) and experimental approaches of the critical velocity determined the ranges if critical velocity for varying pipe slopes (Goldring, 1979, Walski et al., 1994, Liou and Hunt, 1996). Gandenberger (1957) also proposed different critical flow velocities that are based on the air pocket volume. Most studies present formulations to obtain the air pocket critical flow velocity $U_{\mathrm{AP};c}$, as in Escarameia (2004), the formulation that is used herein:

$$U_{\mathrm{AP};c} = (0.55\sqrt{sin\theta} + 0.53)\sqrt{gD_p} \tag{5.12}$$

where θ is the pipe slope. Once the flow velocity at the upstream pipe of the air pocket is higher than the critical flow velocity, the corresponding air pocket starts moving at a given velocity.

Conversely, little information is available in the literature about air pocket velocity. Escarameia (2004) experimental data show the air pocket velocity increases with the critical flow velocity, but this is very limited for pipe angles higher than 6° and it does not consider the water flow velocity as a variable. Given this lack of experimental data, a model based on air pockets' drag coefficients, the water flow velocity, the pipe diameter and the pipe slope are used here instead. Once critical flow velocity shown in Eq.(5.12) is reached, the relative velocity of the air pocket, $U_{\mathrm{AP},r}$ is calculated by Archimedes' law accounting for buoyancy as follows:

$$U_{\mathrm{AP};r} = \sqrt{\frac{4}{3}\frac{gD_p sin\theta}{C_{\mathrm{drag}}}} \tag{5.13}$$

where C_{drag} is the drag coefficient of the air pocket. A spherical shape is assumed for co-current air pockets when they are contained in two pipes, thus originating a C_{drag} = 0.47 (Idel'čik and Steinberg, 2005). Once the air pocket relative velocity is calculated, the final air pocket velocity, U_{AP}, is obtained as:

$$U_{\mathrm{AP};r} = \sqrt{\frac{4}{3}\frac{gD_p sin\theta}{C_{\mathrm{drag}}}} \tag{5.14}$$

where U_{w} is the mean water velocity.

When using the above equations, it is assumed that air pocket velocity is null until the critical flow rate is reached from Eq. (5.12). In addition, it is assumed that when the air pocket centre of mass exceeds the pipe boundaries, the air pocket moves to the next pipe or set of pipes and the air pocket centre of mass is reset to zero.

STEP 3.2: AIR ENTRAINMENT MODEL

Air entrainment from entrapped air pockets is a complex two-phase flow behaviour. The water flow has enough momentum to emulsify part of the air pocket in the form of air bubbles at its tail but not enough to fully drag the air pocket. Several literature contributions were made in this direction based on different experimental setups used. In all these approaches, no air entrainment is observed for $F < 1$ (i.e., for sub-critical flow) and the higher the Froude number in supercritical flow the higher the air/water flow ratio entrained by the water flow. Previous studies on free-surface flow setups (Kent, 1952,

Rajaratnam, 1967, USACE, 1980) and pressurised flows (Kalinske and Bliss, 1943, Wisner et al., 1975, Rabben et al., 1983, Escarameia, 2007, Mortensen et al., 2011b) agree that the air entrainment ratio, $Q_{a,\,\mathrm{ent}}$, can be obtained as follows:

$$\frac{Q_{a,\,\mathrm{ent}}}{Q_{\mathrm{w}}} = a(F-1)^b \tag{5.15}$$

However, authors disagree on the a and b values, originating a considerable uncertainty range (Schulz et al., 2020). For this reason, these parameters will be calibrated in the next section to estimate the entrapped air pocket volumes in this work.

Further considerations are required for this model's implementation. The air entrainment starts as soon as an entrapped air pocket is created, and no entrainment is assumed if the F is below the unit. Air volume due to air entrainment is not included in the model as an entrapped air pocket but as a bubbly flow. This is done because they do not have a clear boundary at the pipe crown but rather travel within the flow as a mixture. These two types of two-phase flow are tracked and analysed separately in our model because they move at different velocities (although these two are still subjected to volume changes according to the ideal gas law $pV = kRT$). The assumption presented in the previous section on entrapped air pocket drag is applied to the bubbly flow as well: a centre of mass is assigned to this bubbly flow that travels inside the pipe and moves from pipe to pipe according to its centre of mass.

STEP 3.3: SIMULATING ENTRAPPED AIR POCKET STOCHASTIC NATURE

The previous section presented the deterministic model to simulate the air pocket entrapment. This section presents how the stochastic nature of the air pocket entrapment observed in the experimental tests is introduced.

A single final air pocket is obtained by running a single simulation with Steps 1-4 because the model is deterministic. The stochastic nature of the phenomenon is introduced by varying the air entrainment coefficients from Steps 3.1 and 3.2, obtaining a range of entrapped air pocket volume after a predetermined amount of model runs rather than a single volume. Thus, the user should specify the number of simulations, run the model each time with a different combination of a and b values (according to with a predetermined distribution and interval) and obtain the range of volumes.

It is recommended to modify only one of these two parameters in simulations within the defined interval since different pairs of a and b might lead to the same final entrapped air pocket volumes. Varying both parameters at the same time would only increase the required computational time and result in the same air pocket volume range.

5.3.5. STEP 4: AIR COALESCENCE

The air volume is calculated after each time step in each pipe, distinguishing whether the volume is originally entrapped or entrained. Entrapped air pockets are added to other pockets fully if they happen to be in the same pipe due to air pocket transport. Their volumes are added and equally distributed between the previously defined air pocket limits, keeping their previous centre of mass. Entrained air coming from an upstream section is fully added to entrapped air pockets as an assumption. A coalescence percentage could be adopted but, given the limitations of the experimental setup, that topic has not been analysed.

5.4. RESULTS AND DISCUSSION

5.4.1. AIRSWMM(V2.0) CALIBRATION

The calibration of the newly proposed model is done in two stages. First, a spatial discretisation analysis is carried out to assess the influence of pipe length on the entrapped air pocket volume throughout the pipe. Pressure-head results are then compared between the proposed methodology with the predetermined spatial discretisation and results from the previous air model incorporation in SWMM in the previous chapter to determine if any major changes are observed. Secondly, entrapped air pocket volumes are calibrated adjusting the air entrainment parameters in Eq. (5.15). pressure-head and air pocket volume from tests with orifices d = 2.2, 3.0 and 21 mm are used as calibration data for all the above stages. Data from d = 4.5 mm are used only for validation.

SPATIAL DISCRETISATION ANALYSIS

The analysed pipeline system implemented in the experimental rig is modelled using the AirSWMM(v2.0) proposed in this chapter. The "surcharge depth" of every node is set to 100 m for the nodes not to pond. The required spatial discretisation is obtained by a mesh analysis. The pipe length is progressively decreasing and the corresponding time step ratio is obtained for pipe-filling events according to $\Delta t = 0.1L/\sqrt{gD_p}$ using the EXTRAN surcharge method (Vasconcelos et al., 2018). Simulations are run with no air dragging or air entrainment (thus only following steps 1 and 2 of the methodology) to obtain the initial air pocket volumes in the pipe from Eq. (6.1). The initial air pocket volumes are obtained for d = 2.2, 3.0 and 21 mm and for different pipe lengths (Figure 5.8).

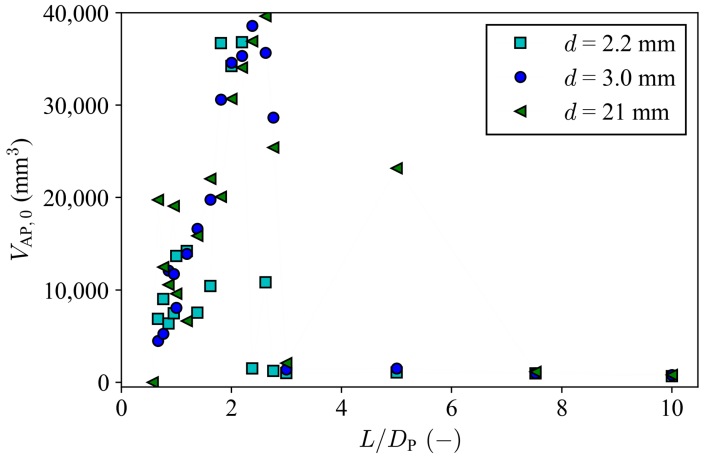

Figure 5.8: Initial air pocket volume for different normalised pipe lengths.

This analysis has shown that only pipe lengths L/D_p between 1.7 and 2.3 (see grey rectangle in Figure 5.4a) return the air pocket volumes within the same order of magnitude of those experimentally observed. The average value of L/D_p = 2 is considered

for further simulations. This length-diameter ratio corresponds to 300 pipes in the numerical model, each with $L = 0.042$ m. The time step is obtained using the following Eq. (4.12), $\Delta t = 0.1L/\sqrt{gD_p} = 0.00924$ s, proposed by Vasconcelos et al. (2018).

Experimental pressure-head for a sampled test from $d = 3.0$ mm is compared with the results obtained by the new proposed model and by the previous model (Figure 5.9). The new model provides a better fit with experimental data than that from the previous chapter since the model no longer relies on the assumption of perpendicular waterfront to the pipe which was inherent in the piston equation previously used. A lower air pressure is obtained during the filling process because the air volume is better quantified in the proposed version of the model (Eqs. (5.6) and (5.7)). This allows for a better estimate of the arrival of the waterfront to the downstream end time because the downstream node of the system can pressurise sooner. The presented model still identifies the existence of a pressure peak but is not capable of describing it due to the limitations presented in the Discussion section 5.5. The previously developed model used a piston equation to simulate the pipe-filling behaviour with air pressurisation. However, the assumption that the waterfront is perpendicular to the pipe axis is very restricted, since most pipe systems are undulated. The model presented herein does not require such an assumption, making the model more robust and applicable to rising, horizontal and descending pipes. Thus, this new model is more accurate than the previously proposed one except for continuously rising pipes with a considerable slope for which results from both models are equivalent. This is because the waterfront's tail length (i.e., the length of water further than the corresponding pipe axis location) is negligible and can be considered perpendicular to the pipe axis. This is numerically demonstrated by the obtained RMSE values which are 0.0395 m for AirSWMM(v1.0) and 0.0158 m for AirSWMM(v2.0). The main drawback of the new model is that it requires a more detailed spatial discretisation resulting in increased computational time (i.e., 10 times slower).

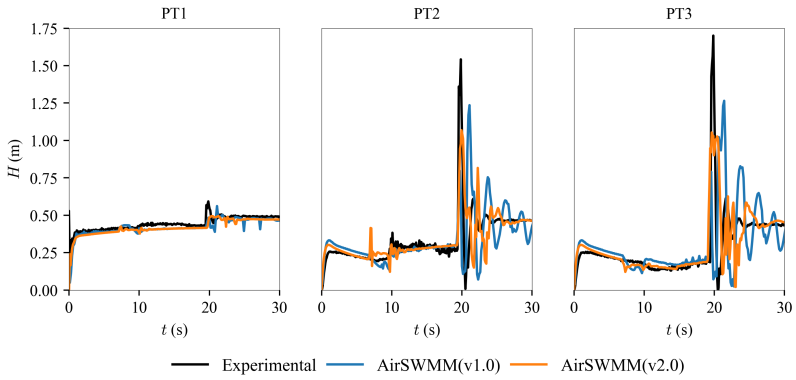

Figure 5.9: Experimental data and numerical results pressure-head time series for $d = 3.0$ mm from AirSWMM(v1.0) and the AirSWMM(v2.0) at pressure transducers PT1, PT2 and PT3.

AIR POCKET VOLUMES

Entrainment factors, a, are calibrated to obtain maximum, average and minimum entrapped air pocket volumes by running the deterministic model 200 times. Tested entrainment factor values varied between 0 and 30 (i.e., parameter a of Eq. (5.15)). Thus, a predicted entrapped air pocket volume range is obtained and should be compared to that experimentally obtained. Entrainment rate parameter b is considered constant, equal to 1.3 (i.e., the average value between different contributions in literature), in all simulations. A total of 200 model runs is carried out because no air pocket volume change over 100 mm^3 is observed in each quartile of predicted air volumes. The same number of runs is used in the validation process.

The values of a that lead to absolute errors of air volumes higher than 100 mm^3 are discarded. By determining the range of the entrainment factors a for each calibration diameter, regression laws are calculated to estimate values of a for validation. The obtained calibrated parameter values are shown in Figure 5.10. The minimum value of parameter a obtained for d = 2.2 mm is not used for calibration purposes since the model is not able to reproduce the initial entrapped volume and, thus, is considered an outlier. This is a limitation of the model and will be discussed in the discussion section. The calibration datasets are expressed in the cross-section area of the orifice with the pipe is, s/S. Figure 5.10 shows the higher the orifice size ratio, the lower the entrainment factor range. Also, note that values higher than observed in literature parameter a values are required to attain the observed volumes (0.03 in literature and 0.05 here).

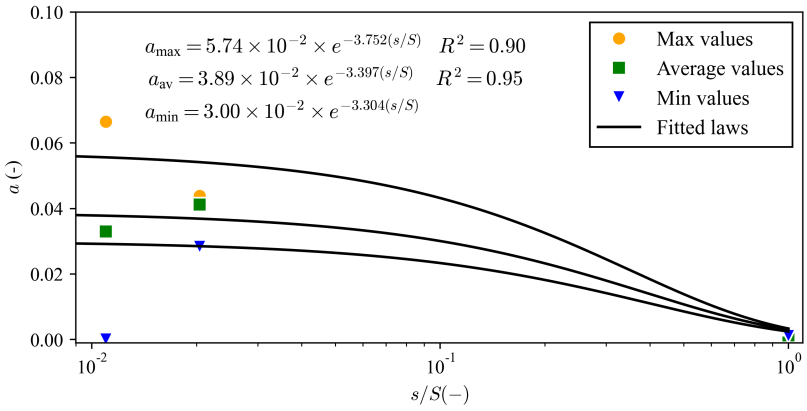

Figure 5.10: Calibration curves for maximum, average and minimum entrainment factors for d = 2.2, 3.0 and 21 mm cross-section area ratios s/S.

Orifices d = 2.2 mm and d = 3.0 mm were used to obtain the sharper flow rate variations and their influence on air entrainment. Orifice d = 21 mm was used as the opposite extreme to obtain the minimum a air entrainment coefficients. These orifices allow covering the full range of flow rates possible to be analysed in this system. Orifice d = 4.5 mm, which is an intermediate one in terms of size given the range used here, is used for validation using an entrainment coefficient according to the fitted laws. More diameters could have been tested and used to calibrate and validate the model. However, as seen in Figure 5.2a, the air pressurisation effect on the entrapped air pocket decreases for larger orifice diameters and, ultimately (for orifices d > 10 mm), tends to the air entrainment behaviour for d = 21 mm. The reader can also observe the air pressure variation during the filling is progressively decreasing with the orifice size increase in Figure 5.2d. There are three main reasons for the observed discrepancies in parameters a and b values. Firstly, as shown in the literature, a and b values strongly depend on the experimental setup size, configuration and being pressurised or free surface. Even though the highest a value found is 0.03, the authors mention that downstream boundary conditions are relevant. Higher entrainment factor values are necessary for d = 2.2 mm, where the air release is severely constrained, and the air cushioning effect actively delays the pipe-filling. Secondly, the air pressure might influence the entrainment rate, a phenomenon not accounted for in previous studies (Pothof and Clemens, 2011, Pozos et al., 2010). Literature experiments were carried out under steady-state flows and with air being injected artificially and not entrapped by hydraulic means. More experimental research is required to validate this hypothesis. Thirdly, incorporating a turbulent and complex 3D phenomenon into a 1D model carries uncertainties and might not be able to fully reproduce behaviours observed experimentally.

5.4.2. AIRSWMM(V2.0) VALIDATION

The entrapped air pocket volumes obtained from AirSWMM(v2.0) are validated using a different dataset for the orifice size of d = 4.5 mm. The fixed value of b = 1.3 is used in all 200 model runs with uncertain parameter a value represented using a triangular probability density function with the same minimum to the maximum a values and with the mean value of the distribution being the entrainment factor that corresponds to the average air volume. The comparison of experimental air pocket distributions (based on 20 repeated experiments) with the corresponding distributions of model-predicted air pocket volumes (based on the 200 simulation runs) are shown in Figure 5.11. The respective maximum, average and minimum air pocket volumes are presented in Table 5.1 together with absolute and relative errors.

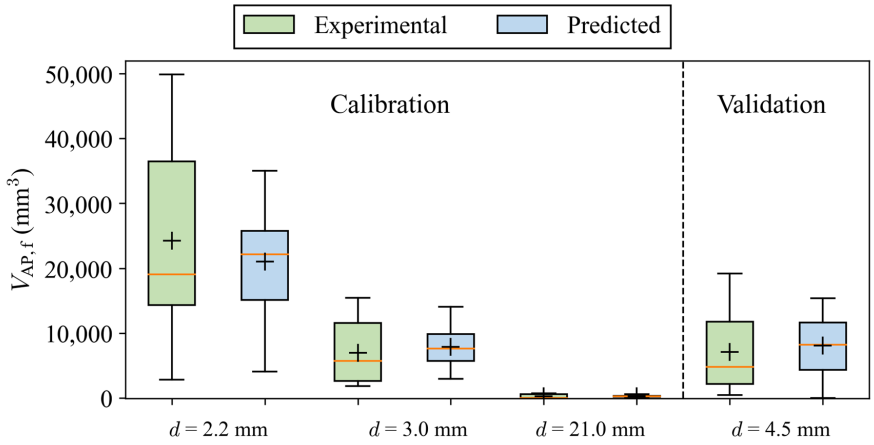

Figure 5.11: Comparison between experimental and predicted entrapped air pocket volumes for calibration and validation.

5

Table 5.1: Maximum, average and minimum experimental and AirSWMM(v2.0) numerical entrapped air pocket volumes and their respective errors for all orifice sizes.

		Calibration			Validation
d (mm)		2.2	3.0	21	4.5
Experimental air pocket volume (mm^3)	Min	2,835	1,832	0	422
	Average	24,270	6,773	280	6,939
	Max	49,868	15,455	732	19,207
Predicted air pocket volume (mm^3)	Min	2,893	1,820	0	0
	Average	24,278	6,775	350	7,739
	Max	36,810	15,495	700	13,673
Relative error (%)	Min	-2.0	0.7	0.0	-
	Average	0.0	0.0	-25.0	-11.5
	Max	26.2	-0.3	4.4	28.8
Absolute error (mm^3)	Min	-58	12	0	422
	Average	-8	-2	-70	-800
	Max	13,058	-40	32	5,534

Small differences are observed between the experimental and predicted air pocket volumes for three calibration cases. The only exception is the case of orifice size of d = 2.2 mm. The original SWMM engine is not able to reproduce the maximum volumes for d = 2.2 mm. Nevertheless, these limitations are only observed for the most extreme scenario and constrained air release, which is not expected to be observed in water networks. Additionally, high relative errors are observed for minimum air volumes, though these are not as relevant as average and maximum because of safety purposes. The remaining air pocket volumes for calibration orifice sizes show good agreements between predicted and observed, that is small errors are obtained for maximum, average and minimum volumes.

The results obtained for the validation dataset of d = 4.5 mm present relatively small errors for minimum and average air pocket volumes (11-29%). Some larger errors are obtained for the maximum air pocket volume which can be caused by higher uncertainties from: i) the influence of the flow cross-section reduction for the flow rate calculation in the air pocket cross-section, which can be much more complex than a simple and linear interface as needed to consider in a 1D model and ii) the air entrainment being considered independent, which is a simplification, Schulz et al. (2020), on the pressure at the air pocket location since the flow cross-section reduction has a higher impact on the overall Froude number at the upstream section of the air pocket. Nevertheless, final air pocket volumes and errors are within the order of magnitude of the experimentally observed and errors from the calibration stage, respectively.

Thus, the modified SWMM model incorporating air detection, location, dragging and entrainment allows making reasonably accurate predictions of entrapped air pocket volumes in a system analysed here, despite that complex related phenomena are modelled in a simplified way based on a one-dimensional modelling approach.

5

5.5. DISCUSSION

5.5.1. AIRSWMM(V2.0) LIMITATIONS

The proposed AirSWMM(v2.0) model has limitations originating from two different sources: the SWMM engine and the new AirSWMM(v2.0) model. There are two limitations associated with the original SWMM model (i.e. SWMM numerical engine). The first is that SWMM cannot simulate sub-atmospheric pressures. SWMM assumes a free-surface flow and uses the Saint-Venant equations to solve the flow under such a regime. When the flow is pressurised, it either uses the EXTRAN surcharge method (assuming fully pressurised flow, solving the flow through another set of equations) or uses the Preissmann SLOT method (that uses an artificial slot to solve the Saint-Venant equations). However, neither of these can simulate sub-atmospheric pressures which other pressurised flow models can. Secondly, intermittent water supply systems are also susceptible to hydraulic transients (Erickson et al., 2022) which cannot be correctly reproduced in the SWMM. The EXTRAN surcharge method considers a wave celerity equal to $\sqrt{gD_p}$ = 0.45 m s^{-1} and the SLOT method considers a celerity varying with the slot width, B, equal to $\sqrt{gS/B}$ = 12.59 m s^{-1}. None of these formulations reproduces a realistic pipe wave celerity (around 300 m s^{-1} for acrylic pipes) obtained by $c_p = \sqrt{(K/\rho_w)/c_1(1+[(K/E)(D_p/e)])}$ the pipe wave celerity, in which K is the water bulk modulus, c_1 is a constant dependent on the pipe support conditions and the pipe material, E is the Young modulus of elasticity of the pipe and e is the pipe wall thickness. Water compressibility would need to be several times lower for the celerities in the model to be representative of reality To the authors' knowledge, only the SLOT surcharge method can describe the elastic column behaviour by changing the slot width as proposed by Pachaly, Vasconcelos, Allasia, and Bocchi (2021), making the slot width equal to $B = gS/C^2$. However, this modification has only been verified in conceptual conditions and is to be compared with measurements.

Additional limitations come from the surcharge method and air pocket shape used in the implementation of AirSWMM(v2.0). First, this model only provides good results

when using the EXTRAN surcharge method, as observed in Chapter 4. This limits the AirSWMM(v2.0) model to this surcharge method even though the SLOT method provides better results for fast unsteady events as demonstrated by Pachaly et al. (2019). Secondly, the air pocket shape is imprecise because the 1D nature of SWMM does not allow the introduction of the round shape of air pockets, caused by the surface tension equilibrium laterally and longitudinally, and therefore inhibits the correct air-pocket length estimation in horizontal pipes. As a consequence, no additional local head losses are taken into account where air pockets are estimated due to the shape's imprecision. The only modification that reduces the flow rate around the air pocket is the flow cross-section area reduction corresponding to the existing air pocket depth.

5.5.2. AIRSWMM(V2.0) APPLICATIONS AND DEVELOPMENTS

The proposed model can be extended to incorporate urban drainage system features, such as manholes or pipe shafts. That will require further developments, namely: i) including the air volume in storage components to the overall air being pressurised, ii) including air release devices possibly connected to such components and iii) implementing a local air movement model so that air in the pipes would rise in the manhole or shaft rather than being dragged in the pipes. Another element that could be included is the air valve which can also be found in urban water networks.

5.6. CONCLUSIONS

A methodology for simulating the creation, location and entrainment of air pockets during filling conditions in a pipeline system is proposed. Novel experimental pipe-filling tests are carried out in a laboratory setup to understand the expected pressure heads of the entrapped air pocket formation at high points and to quantify their volumes. The new model AirSWMM(v2.0) is implemented as an extension of the existing SWMM model. This is an upgrade of the previously published model in Chapter 4, allowing the waterfront tracking based on the hydraulics (SWMM) as well as locating and replicating the drag and entrainment of air pockets. The new model AirSWMM(v2.0) was calibrated and validated using the collected experimental data. The main conclusions are as follows:

- The new AirSWMM(v2.0) model captures reasonably well different aspects of air pocket creation and its fate during the pipe-filling conditions. It is able to predict the location and final volume of an entrapped air pocket with an average relative error of 20% which is deemed good given the complex nature of the analysed phenomena and the use of a 1D model. Still, some dynamic behaviours such as air pocket interface disruption could not be simulated due to the complexities involved and limitations of a 1D model.
- The obtained experimental observations provided evidence of a stochastic nature of air pocket creation and its dependency on air release conditions. Since the proposed AirSWMM(v2.0) model is deterministic in nature, a set of simulations should be run with different entrainment rates to obtain a realistic range of entrapped air volumes. In this study, 200 samples were used for this resulting in aforementioned prediction accuracy.

- The obtained experimental observations also provide evidence that lower filling flow rates (which are commonly recommended in practice) tend to create larger entrapped air pocket volumes whilst delaying the pipe-filling time. Therefore, this advice should be revisited in future work.

The AirSWMM(v2.0) methodology presents considerable scientific advances since no previous 1D model allowed for locating and correct quantification of entrapped air pockets. Still, the proposed model has some limitations. The air accumulator model assumes the air inside the pipe pressurises all at once and does not take into consideration the compressibility rate of the air. This methodology no longer requires the piston equation to track the waterfront, thus allowing to analyse each air pocket separately.

Additional pipe systems should be tested to further validate this methodology in larger setups to account for scale effects in pipe filling and air drag and entrainment events. The validation of this methodology in a real system would require to have several see-through unburied cross-sections, located at high points (to assess the air entrainment) and at intermediate sections of high slope rising pipes (to assess the air volume) and of horizontal pipes (to assess the drag). This methodology has been implemented in SWMM but could be implemented in other free-surface flow models, provided a stable algorithm coupling between the air and the water phase is obtained. Further research should focus on testing this methodology in other linear and branched pipe layouts.

6

AIR POCKET ENTRAPMENT MODELLING FOR A PIPE NETWORK

This chapter is an adapted version of:

Ferreira, J. P., Ferràs, D., Covas, D. I. C., Kapelan, Z. (2024). Air entrapment modelling in networks in pipe-filling events. Urban Water Journal, 21 (6). DOI: https://doi.org/10.1080/1573062X.2024.2342785.

6.1. INTRODUCTION

Intermittent water supply systems operate under three operational stages: pipe-filling, supply and pipe emptying (Walter et al., 2017). When a utility starts the pipe-filling process, the water going into the pipes generates a two-phase flow, entrapped air pockets, and hydraulic transients. Observed transient pressure variations with entrapped air pockets tend to be higher than those estimated by classic water hammer theory (Ferreira et al., 2021, Martins et al., 2017). Such higher-pressure variations are a possible cause for the increasing leakage levels and pipe burst frequency after the implementation of IWS operation (Christodoulou and Agathokleous, 2012, Christodoulou et al., 2017). Several experimental and numerical efforts have been made to address the two-phase flow, but there are still gaps in knowledge to be addressed, as outlined below.

Researchers started by experimentally analysing two-phase flows by determining air pockets' critical velocity in pipes, the minimum velocity to ensure their drag and consequent release. Dumitrescu (1943), Davies and Taylor (1950) and Benjamin (1968) focused on determining theoretical critical velocities for horizontal pipes. Gandenberger (1957), Goldring (1979), Walski et al. (1994) and Liou and Hunt (1996) continued this research by experimentally determining the critical velocities that vary with the pipe slope and diameter. Escarameia (2004) also analysed the air pocket velocity once the critical velocity is reached. Lubbers and Clemens (2007) and Pothof and Clemens (2010, 2011) further determined local head losses caused by air pockets and their breakdown time. However, according to our best knowledge, there has been no experimental research so far on entrapped air pocket formation and location during pipe-filling events, even though these events can create several types of disruptions in pressurised pipe systems (Lauchlan et al., 2005, Simukonda et al., 2018a).

Past numerical developments on two-phase flows have focused on the usage of three main types of models: a lumped inertial model or RWC, a free surface model based on Saint-Venant equations solved using the Preissmann slot method and an elastic column model solved by using the method of characteristics (MOC). Such developments cover empty and partially filled pipes that would be subject to a filling wave or full pressurisation. Martin (1976) first analysed pipe-filling events with an RWC model and the ideal gas law to simulate entrapped air pockets' expansion and compression cycles. Several contributions followed to analyse the effect of air release on the pressure (Zhou et al., 2002), and the effect of two air pockets on the pressure-head signal (Zhou, Liu, and Karney, 2013). Saint-Venant equations' models have been used to bridge the gap of pipe-filling models, not accounting for the free-surface section of the flow and forcing a perpendicular waterfront to the pipes. Vasconcelos et al. (2006) and Vasconcelos and Marwell (2011) proposed a two-component pressure approach to solve such a scheme and obtained relatively good results for pipe-filling. However, instabilities were observed in the pipe length where the air pocket would be, since those elements were not accounted for in the model development (Vasconcelos and Leite, 2012). Further modelling attempts used an elastic column model using the MOC for pipe-filling events. A piston equation to track the waterfront position was used to simulate pipe-filling events, being able to accurately reproduce the measurements from a system filling (Freni et al., 2014, Marchis et al., 2010) but still neglecting free surface flows. Regardless of the focus and the used model, none of these contributions aimed at simulating the dynamics of air pocket cre-

ation, movement, and entrainment previously observed in pipe-filling events.

Results from above and other studies on air-water behaviour led to the establishment of current guidelines for the design and location of air-release devices proposed by the American Water Works Association (2001) and by Deltares (2016). However, these recommendations are mostly based on empirical knowledge gathered over time. Current numerical models are not able to support or complement these guidelines, since these models do not estimate the location of entrapped air pockets in a network.

Cabrera-Bejar and Tzatchkov (2009) proposed using the Stormwater Management Model (SWMM) as an inexpensive tool to simulate IWS since it is freely available and open-source software that simulates both free surface and pressurised flows using the Preissmann slot method. Campisano et al. (2019) continued Cabrera's work, further validating SWMM for an IWS context and proposed a pressure-driven demand implementation adapted to water supply applications. However, none of the previously mentioned contributions introduced the air phase in a free surface flow model, nor aimed to detect, locate and quantify entrapped air pockets.

The ideal gas law model was incorporated into SWMM as a proof of concept in Chapter 4, concluding that SWMM's enhanced version AirSWMM(v1.0) results can accurately describe the air phase. A methodology to detect and locate entrapped air pockets using SWMM model without modifying the subroutine for flow rate calculations was proposed in Chapter 5. The application of the AirSWWM model has major benefits over the original SWWM. The first is the detection and quantification of air pockets created at high points and along pipes during pipe-filling events, a functionality that the original SWWM did not have. For instance, this enables the improved determination of the location and size of air valves. Secondly, a better description of air-water interaction during the filling process allows more accurate predictions of pressure variations and of the waterfront arrival time along the network, improving for instance the assessment of the water supply equity when existing water demands, by including the filling stage. Moreover, the use of this model provides additional knowledge for better zoning intermittent water supply systems. Such methodology was further improved with entrapped air pocket dynamics, namely movement, entrainment and compression/expansion. Even though the methodology is transferable to pipe networks, it was only experimentally validated for a single pipe with an intermediate high point.

This chapter presents the application of the second version of the model AirSWMM(v2.0) proposed in Chapter 5 to a pipe network. Different pipe-filling conditions and network configurations are tested. Pressure-head measurements and video recordings are carried out at different network locations to assess AirSWMM(v2.0) model performance when applied to a pipe network with air entrapment conditions. The obtained results are analysed and compared with collected data, in terms of different air pockets' locations and sizes, resulting in new insights on how these pockets are created in a pipe network. The corresponding AirSWMM(v2.0) model limitations are discussed too.

The outline of this chapter is as follows. Section 6.2 describes the experimental data collection and corresponding analysis. Section 6.3 provides a summary of the original SWMM and the AirSWMM(v2.0) model. Section 6.4 presents the input parameters, shows the validation results by using the proposed model and discusses the positions of the final entrapped air pockets in comparison to the experimentally observed. A brief

discussion of the model's applicability is presented in Section 6.5 and the conclusions are presented in Section 6.6.

6.2. EXPERIMENTAL ANALYSIS

This section analyses the collected data on pressure-head measurements and entrapped air pocket volumes from the pipe layout #3 in Section 3.2.3 in detail in sections 6.2.1 and 6.2.2, respectively.

6.2.1. PRESSURE-HEAD SIGNALS

A series of experimental tests have been conducted for six pipe configurations (C1 - C6) and four orifice sizes (d = 2.2, 3.0, 4.5 and 21 mm) and each configuration-orifice size test has been repeated four times. This was done due to the somewhat uncertain nature of air entrapment and the creation of air pockets. Four repetitions demonstrated that measured air pocket volumes did not vary significantly, unlike what was observed in the single pipe system in Chapter 5.

Experimental pressure-head signals are present in Figure 6.1 for the two orifice diameters (d = 2.2 and 21 mm) and for Configurations C1 and C2. The main differences in the pressure-head signals of Configurations C1 and C2 include the pressurisation times at each pressure transducer and the magnitude and timing of the pressure surge associated with the waterfront arrival at the downstream end. All tests start with the upstream valve opening at t = 0 s (Node 1).

For Configuration C1 with orifice d = 2.2 mm (Figure 6.1a), the air inside the pipe pressurises simultaneously in all transducers. When the waterfront reaches PT2 at t = 11 s, the pressure-head increases due to a backward pressurisation from the high point to the main pipe. Subsequent pressure-head signals steadily decrease as air is being released. pressurisation extends also to the side pipe, with water reaching PT3 at t = 23 s and PT4 at t = 32 s. A water hammer event is observed at t = 36 s when the waterfront reaches the downstream end orifice, nearly reaching a maximum value H = 1.5 m.

For Configuration C1 with d = 21 mm, Figure 6.1b shows that the pressure-head signals do not increase when the upstream valve is opened (t = 0 s). The pressure-head at PT2 increases at t = 7 s since the waterfront reaches the high point in the main pipe and backwards pressurises the pipe, filling the side pipe. The water reaches PT3 at t = 17 s and PT4 at t = 20 s, considerably sooner than in C1 since the waterfront elevation does not exceed the high point during the pipe-filling (unlike the case for C1 and d = 2.2 mm) and the side pipe pressurisation occurs before it is completely filled. A pressure-head increase is observed around t = 22 s due to the shock between the two waterfronts (from the main pipe and side pipe), which decreases when the waterfront reaches the downstream end. No significant pressure transient is observed since there is no orifice at the downstream end.

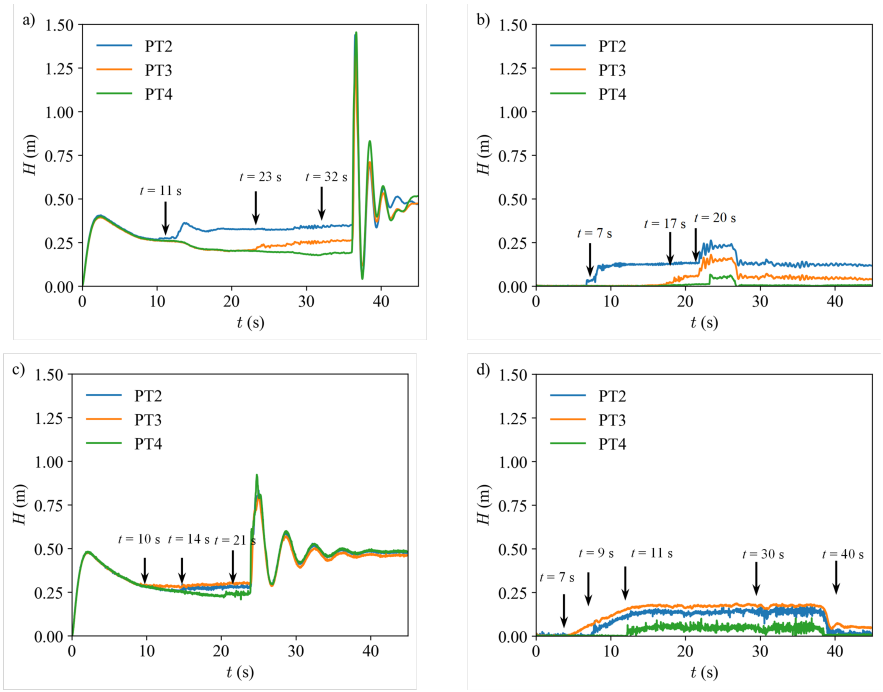

Figure 6.1: Comparison between experimental and predicted entrapped air pocket volumes for calibration and validation.

For Configuration C2 with $d = 2.2$ mm (Figure 6.1c), air pressurisation is observed as the pressure-head increases in all pressure transducers, stabilising when the waterfront reaches their location (PT2 at $t = 10$ s, PT3 at $t = 14$ s and PT4 at $t = 21$ s). The waterfront reaches PT2 before PT3 and Node 6 pressurises before the waterfront overtops the high point in the side pipe. Similar to configuration C1 with $d = 2.2$ mm (Figure 6.1a), the pressure-head increases as the waterfront reaches each transducer. The filling process continues until the waterfront reaches the downstream end at $t = 24$ s, 13 s sooner than in configuration C1. The generated water hammer wave amplitude and frequency are lower than in the case of configuration C1 because of the higher damping effect from a larger entrapped air pocket volume.

For Configuration C2 with $d = 21$ mm (Figure 6.1d), the observed pressure-head has a similar behaviour as for $d = 2.2$ mm. The waterfront advances until it reaches PT2 and PT3, at $t = 7$ s and $t = 9$ s, respectively. The waterfront reaches the downstream end at $t = 17$ s, 6 s sooner than in configuration C1 due to the high point location. It is worth noting that the pressure-head drops at $t = 30$ s and $t = 40$ s, corresponding to the release of entrapped air pockets, creating small pressure-head perturbation. Once these air pockets are released, no additional local head losses exist due to the air pocket blockage and the final pressure-head decreases.

6.2.2. ENTRAPPED AIR POCKET VOLUMES

The quantification of the entrapped air pocket volumes observed in the experimental tests is carried out by using two methods depending on the air pocket location and size. The volume of the air pockets located at the high point is quantified by cropping the images, running these through Gaussian filters to reduce image noise and binarising to quantify the air volume of the air pocket (see Figure 6.2), like in the air-water interface measurements carried out in literature (Kong et al., 2019, Peddu et al., 2018). The volume of elongated air pockets outside the high point is quantified by measuring the length and the cord of each air pocket cross-section with accuracies of 1.0 and 0.1 mm, respectively. Each air volume is estimated using the cross-sectional area of the air and the length of each air pocket. Since several air pockets are entrapped for each experimental test, the total air volume is obtained by the summation of individual volumes in each area, and the respective value for each configuration and orifice size is represented in Section 6.3.

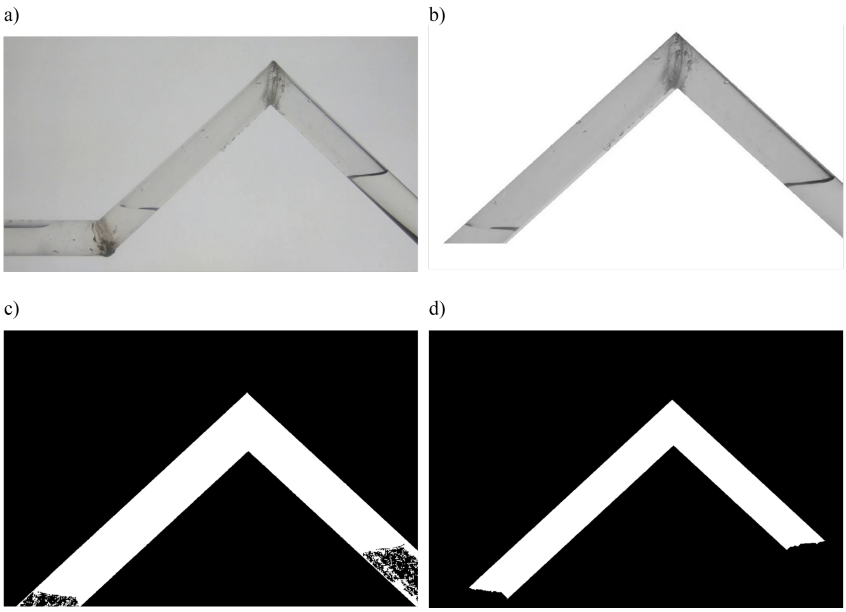

Figure 6.2: Image treatment example of air pocket volume for Configuration C1 and d = 3.0 mm: a) Original image, b) Cropped image, c) Image after edge detection and binarised and d) Smoothed out image to reduce image noise.

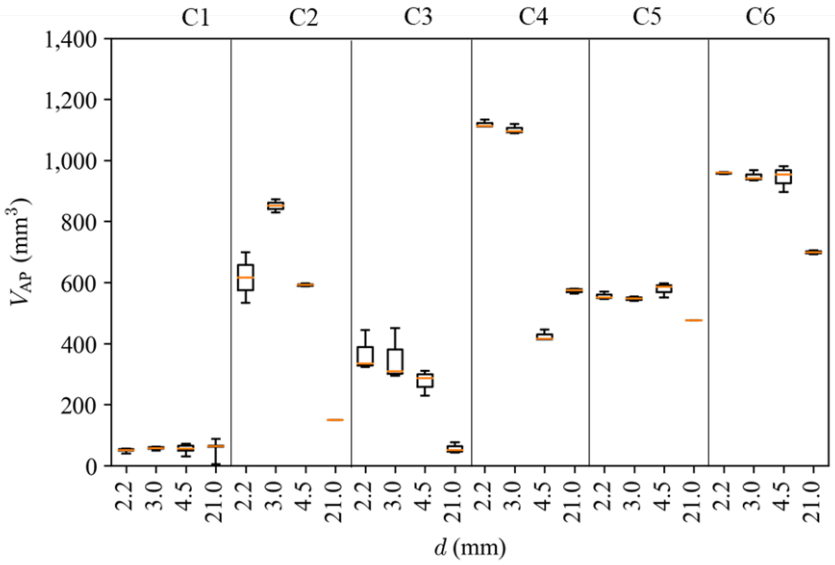

Figure 6.3: Comparison between experimental and predicted entrapped air pocket volumes for calibration and validation.

Most volumes observed in this study are higher than those previously reported. In Chapter 5, air pocket formation was primarily due to flow pressurisation from the high point until the downstream section of the downwards-sloped pipe. In contrast, in this chapter, air pocket creation results from the simultaneous pressurisation of an empty section of the pipe by two different waterfronts approaching from opposing sides, creating an entrapped air pocket. Consequently, air pockets are entrapped at the high point and spread along the system.

Configuration C1 demonstrates considerably lower entrapped air volumes than other configurations. This is due to the relatively short length of the air pocket creation zone downstream of the high point in the main pipe (Nodes 1-2-4-6-8). In this case, the air pocket is formed between the high point (Node 4) and Node 6, due to the travelling of the waterfront in the side pipe (Nodes 2-3-5-7-6) until pressurising Node 6.

In contrast to C1, Configuration C2 shows significantly higher volumes for d = 2.2, 3.0 and 4.5 mm. This is primarily because the waterfronts are not perpendicular to the pipe axis, causing the entrapment of larger air volumes. This behaviour has already been observed in single pipes in Chapter 5.

Configuration C3 exhibits an overall lower air volume than C2. This is attributed to the main pipe-filling more rapidly than the side pipe. During the filling process, when Node 6 becomes pressurised, the side pipe entraps more air despite having lower elevations.

Configuration C4 shows higher air volumes than C2 and C3 for similar orifice sizes, mainly due to the side pipe being located higher than the main pipe and air entrapped in the side pipe tends to remain there.

Configuration C5 shows larger entrapped air volumes than C3, despite both configurations having decreasing elevations in the side pipe from Node 2 to Node 3. This is because, in configuration C5, the side pipe between Node 3 to 7 rises (except in the high point zone) and, consequently, the filling process is comparatively slower than in C3 in which this pipe is horizontal and lower than the main pipe.

Configuration C6 shows lower volumes than C4 for d = 2.2 mm and 3.0 mm orifice sizes, despite higher volumes entrapped for d = 4.5 and 21 mm. This is due to the waterfront ascending from Node 2 to 3 in C6, which delays the filling process of the side pipe and does not allow air release due to the downwards-sloped pipe, unlike the horizontal side pipe in configuration C4.

6.3. NUMERICAL MODEL

6.3.1. ORIGINAL SWMM

SWMM, typically used to simulate urban drainage and stormwater systems, is based on an implicit numerical method to solve the simplified Saint-Venant equations in a one-dimensional format. Whenever a node is pressurised, the model uses one of two methods to simulate pressurised flow (defined by the user). The first is the Extended Transport (EXTRAN) method that solves mass and momentum equations typical for pressurised pipe flows and is used in EPANET software (the US-EPA's model for pressurised pipe networks) but using SWMM's implicit scheme and considering the flow occupies the total pipe cross-section. The second is the SLOT method, which features an artificial slot at the pipe crown with a width of $0.01D$ (being D the pipe diameter) and allows the model to keep simulating the flow with Saint-Venant equations. This slot increases the storage of each section since the flow cross-section is higher than the pipe's (Sharior et al., 2023). Only the EXTRAN method is used herein since the SLOT method did not show good results when applying an air accumulator in SWMM (Chapter 4). Further information on the general SWMM engine and its numerical implementation can be found in Rossman (2017); more details on each surcharge method can be found in Roesner et al. (1988) and in Rossman (2022). SWMM software version v5.1.015 is used since no further developments have been made regarding pipe flow rates or water depths.

6.3.2. AIRSWMM(V2.0)

The numerical model used to simulate the pipe-filling process, AirSWMM(v2.0), is an improvement of SWMM developed in Chapter 5. AirSWMM(v2.0) is an add-on to SWMM's source code and does not require changes in the input file. No object (e.g. pipe, node, tank) from the original SWMM was modified nor was a new object created. The modifications are carried out at the hydraulic engine by means of the implementation of an algorithm to detect entrapped air pockets to calculate their volume and pressure, and to incorporate this air pressure in the flow rate and water depth calculations. Hence, the AirSWMM(v2.0) add-on does not require any additional input data from the user rather than building the model with some space-time discretisation constraints, i.e. a finer spatial discretisation (e.g. L/D_P = 2, in this case, L = 0.042 m), to attain more accurate air pocket volume and location. This model uses the original SWMM as a baseline incorporating three main steps that require additional calculations in each time step, allowing

the estimation of the air pocket location and volume. The first step checks which pipes are pressurised and updates the air pockets' volumes being released from the system. This step also detects air volumes between two waterfronts, flagging them as entrapped air pockets. The second step incorporates the ideal gas model, relevant during the air pressurisation, and the air release when orifices exist at the entrapped air location. The third step incorporates the dynamics of entrapped air pockets, namely the dragging due to the water flow rate and the air entrainment within the water flow. Some features of the last step are only activated for specific hydraulic conditions, namely: the air drag occurs when the water velocity is higher than the critical flow velocity and the air entrainment occurs when the water Froude number is above 1. In summary, the entrapped air pocket volume is obtained by the following mass balance equation:

$$V_{AP,f} = V_{AP,i} - \sum a(F-1)^b + \sum \frac{V_{AP,drag}}{V_p} Q_{w,t} \tag{6.1}$$

where $V_{AP,f}$ and $V_{AP,i}$ are the final and initial entrapped air pocket volumes, respectively, a and b are entrainment function parameters, F is the Froude number, $V_{AP,drag}/V_p$ is the air-pipe volume ration from the small air pocket creation and Q_w is the water flow rate.

The AirSWMM(v2.0) input file from the previous chapter, which includes pipes, tank and model parameters, is modified to account for the side pipe and different pipe elevations. All remaining input parameters are the same: the inertial damping is not considered, normal flow conditions are Froude-dominated, no variable time step is used and a and b coefficients are as previously calibrated. The pipes are discretised with a $\Delta x/D = 2$ ratio, being Δx the spatial discretisation of the pipes, to maximize the entrapped air pocket volume, as calibrated in Chapter 5. The used time step is obtained by $\Delta t = 0.1\Delta x/\sqrt{gD}$ being the gravity acceleration, to have a Courant number ($C_r = c/(\Delta x/\Delta t)$) below 1, being c the pipe wave celerity. Such a Courant number leads to the best compromise between numerical accuracy and computational time Vasconcelos et al. (2018).

6.4. RESULTS

This section compares the experimental and predicted pressure-head signals intending to validate further the AirSWMM(v2.0) model in the pipe network context (section 6.4.1). Insights on the pipe-filling process and the air entrapment not described in previous studies are presented in section 6.4.2 and the comparison between experimental and predicted entrapped air pocket volumes and the results discussion are presented in section 6.4.3.

6.4.1. PRESSURE-HEAD SIGNALS

The model is evaluated using the collected pressure-head from PT2, PT3 and PT4 for the configurations and orifice sizes presented in Figure 6.1 (configurations C1 and C2 for d = 2.2 and 21 mm). While the model captures the overall filling behaviour, certain numerical instabilities are noticeable when comparing numerical results to experimental data, as illustrated in Figure 6.4.

As it can be seen from Figure 6.4, in configuration C1 and orifice size of d = 2.2 mm, after the initial pressurisation, the predicted pressure-head decreases until the water reaches the pressure transducers since the air release rate is low enough to create air pressurisation in the pipe. However, when the waterfront reaches each transducer (at t = 13.5 s for PT2, t = 22.5 s for PT3, and t = 27 s for PT4), numerical instabilities are observed, likely due to backward pressurisation within the main pipe. Further insights on the dynamics of the filling process are provided in subsection 4.2. The pressure-head variation observed after 36 s is a consequence of the waterfront reaching the downstream end and colliding with the orifice. Although the time of waterfront arrival at the downstream end is accurately estimated, AirSWMM(v2.0) is not able to describe accurately the pressure transient event created. SWMM considers pipe rigid walls, and the water compressibility is simulated by the EXTRAN surcharge method. However, the pipe wave celerity (c) in the EXTRAN surcharge method, obtained by $c = \Delta x/\sqrt{gD} = 0.45 ms^{-1}$ (Roesner et al. 1988), is considerably lower than in plastic pipes ($c \approx 300 ms^{-1}$). Thus, SWMM and AirSWMM(v2.0) using the EXTRAN surcharge method are not prepared to simulate water hammer events. SWMM's Preissmann slot width can be adjusted to replicate the pipe wave celerity but such modification has been shown not to provide good results while simultaneously using the air model like in Chapter 4.

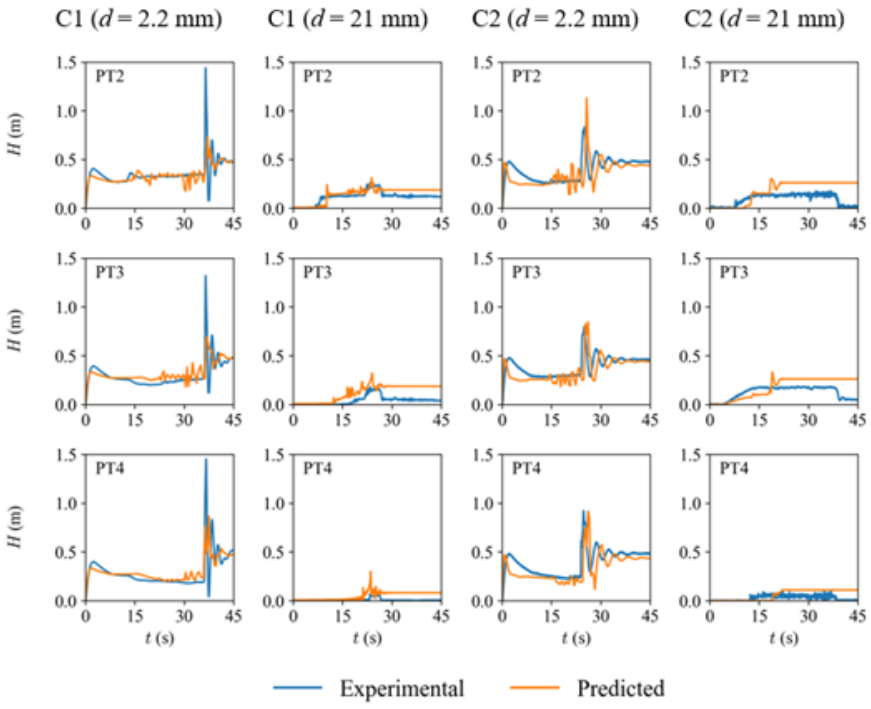

Figure 6.4: Experimental and predicted pressure-head signals in pressure transducers PT2, PT3 and PT4 for C1 with downstream orifice with d = 2.2 mm, and d = 21 mm and for C2 with downstream orifice with d = 2.2 mm, and d = 21 mm.

In Configuration C1 with d = 21 mm (see Figure 6.4), the orifice with the same diameter as the pipe does not restrict air release during the pipe-filling. As a consequence, the air inside the pipe does not pressurise immediately after the valve opening. The estimated waterfront arrival time at each transducer is accurately predicted by the model but the predicted pressure-heads tend to be slightly overestimated for PT3 and PT4. This is consistent with the previous observations when using the original SWMM. The air pressurisation feature of the AirSWMM(v2.0) model is not activated and hence the pressure-head and flow rate values are calculated as in the original SWMM, only tracking the location where air pockets are likely to exist.

For Configuration C2 and d = 2.2 and 21 mm, similar instabilities are observed as in C1 when the waterfront reaches the transducers' locations (see Figure 6.4). The waterfront arrival time at each transducer is correctly predicted and the filling process is generally well described. However, the waterfront arrives sooner at the downstream end of the system (Node 8) than in configuration C1 since the main pipe is filled sooner. Additional insights on the pipe-filling process for each configuration analysed and the explanation for why the waterfront reaches the orifice sooner in C2 than in C1 are provided in the next section.

6.4.2. PIPE-FILLING PROCESS

This subsection provides insights into how the network topography can influence the creation of air pockets. It is evident from the results shown above for different configurations that the dynamics of the pipe-filling process, as well as the entrapped air pockets formation and location, are strongly influenced by the network layout and elevation. The water flows into the pipe when the upstream valve is opened at t = 0 s, primarily advancing in a pressurised flow until it reaches the junction Node 2. At this node, the waterfront divides in two fronts progressing as free surface flow in both the main and the side pipes. This is observed for all configurations with d = 2.2 mm (exemplified in Figures 6.5 and 6.6 for C1 and C2) until t = 9.4 s when the specific pipe layout begins to influence the pipe-filling process.

The progression of waterfronts during the filling process for configuration C1 and orifice d = 2.2 mm is schematically illustrated in Figure 6.5 for five snapshots in time. As seen from this figure, as the waterfront reaches the rising pipe immediately upstream Node 4, considerable changes occur in the system. At t = 14 s, the flow in the main pipe generates a backward pressurisation process in the main pipe which propagates into the side pipe. Subsequently, at t = 26 s, the side pipe fills with water until the waterfront reaches Node 5. The side pipe becomes fully pressurised and the developing free surface flow, predicted after the high point within the main pipe, gives rise to an entrapped air pocket. At t = 29.2 s, the waterfront continues its progression towards the downstream end, ultimately reaching the orifice at Node 8 at t = 35.6 s. At this time, the pipe-filling process has concluded, culminating in a water hammer event created by the waterfront collision with the orifice at the downstream pipe end. Entrapped air pockets remain in the pipe even after the filling process has finished, making it necessary to have the pipe pressurised for a long period and with high pressure for the air to dissolve or mix in the water and be ultimately drained out. As it can be seen from Figure 6.5 for t = 36.5 s, the predicted location of the air pocket corresponds to the experimentally observed one.

Additional entrapped air pockets are predicted in the side pipe by the model but are not observed in the experiments. However, the predicted additional pockets, originating from the numerical instabilities during the pipe-filling process, are very small (4 mm^3), i.e. negligible when compared to the volume of the actual air pocket (50 cm^3).

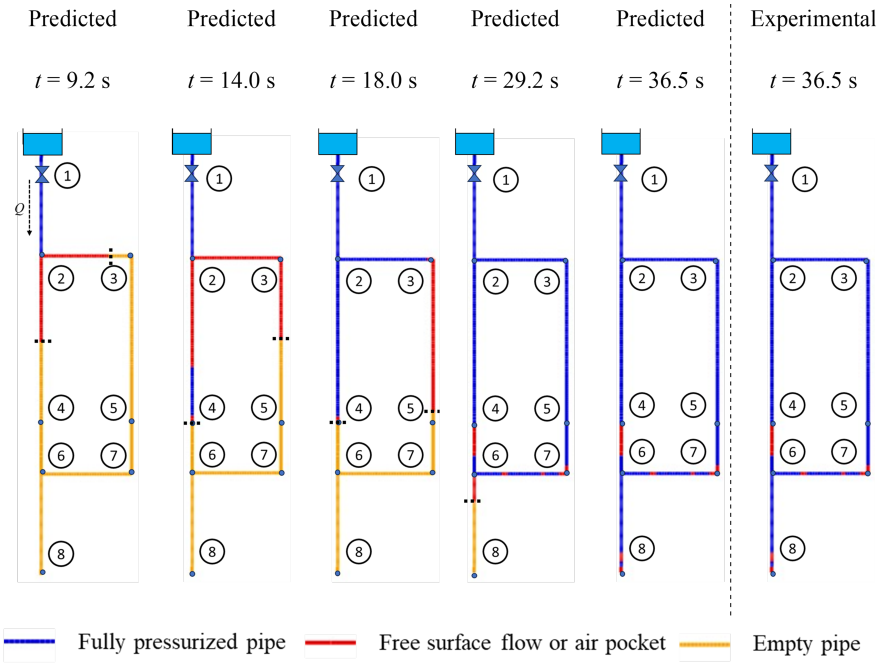

Figure 6.5: Snapshots of the predicted pipe-filling process in Configuration C1 with d = 2.2 mm at different filling times and the final steady state when the air pocket is fully formed.

The filling process in Configuration C2 with d = 2.2 mm (Figure 6.6) is different from the one observed in C1 after t = 9.4 s. At t = 14 s, the water does not ascend in the rising pipe of the high point but continues to advance along the main pipe. When reaching the junction at Node 6, the waterfront divides into two: one front progresses towards the downstream end (Node 8), while the other front fills the side pipe in the opposite direction than in C1 (from Node 6 to 7). At t = 18 s, the waterfront coming from Node 3 in the side pipe reaches the rising pipe of the high point. This pressurises the water column upstream, which was initially a free-surface flow, resulting in the formation of the observed entrapped air pocket. Subsequently, the waterfront ascends the high point and overcomes, appearing as a continuous free surface flow from the high point until the junction Node 6. At t = 18 s, i.e. the moment just before the pipe between Nodes 6 and 7 pressurises, an air pocket is created from Node 5 to Node 6. At t = 29.2 s, the water column pressurises in a reverse direction, moving towards Node 7 in a downstream direction (since Node 7 has not yet pressurised). At the final steady state condition in the system (t = 35.6 s), major differences between predicted and observed can be seen, as opposed to configuration C1 where the waterfront had already reached the downstream

end at this point.

Despite the predicted and the experimentally measured air pockets being located in the same areas of the pipe system, two main differences should be highlighted. Firstly, the experimental total air pocket volume (840 cm^3) exceeds the predicted one (300 cm^3). The lack of air entrainment was also observed during the experimental testing, explaining the relatively minor variation in air pocket volumes as depicted in Figure 6.4.

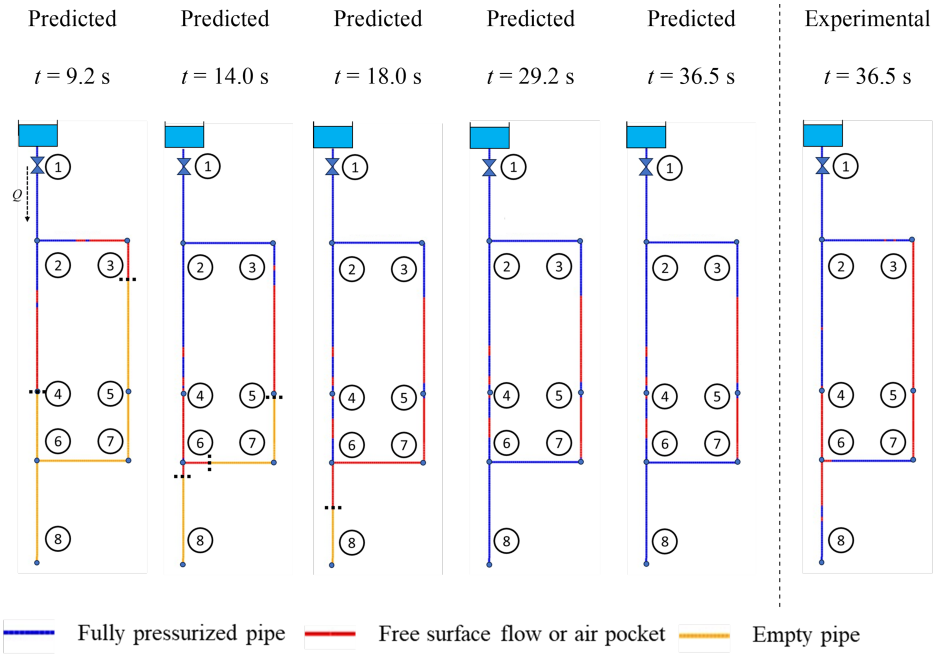

Figure 6.6: Snapshots of the predicted pipe-filling process in Configuration C2 with d = 2.2 mm at different filling times and the final steady state when the air pocket is fully formed.

6.4.3. AIR POCKET VOLUMES

Figure 6.7 presents the experimental and predicted air pocket volumes obtained at the final steady state in the analysed pipe network for 6 different configurations and 4 orifice sizes, with each experiment repeated four times.

Two main observations can be drawn from these results. Firstly, experimental air volumes show some variability for the same Configuration-orifice size test due to the randomness of the filling process, whereas only one predicted air volume is obtained given the deterministic nature of the AirSWMM(v2.0) model. Secondly, the results obtained are somewhat mixed in terms of prediction accuracy. The model predicted reasonably well air pocket volumes for configurations C1 and C6 for most orifice sizes but underestimated air pocket volumes for configurations C2, C3, C4 and C5 for most (in some cases) orifice sizes, in some cases quite substantially.

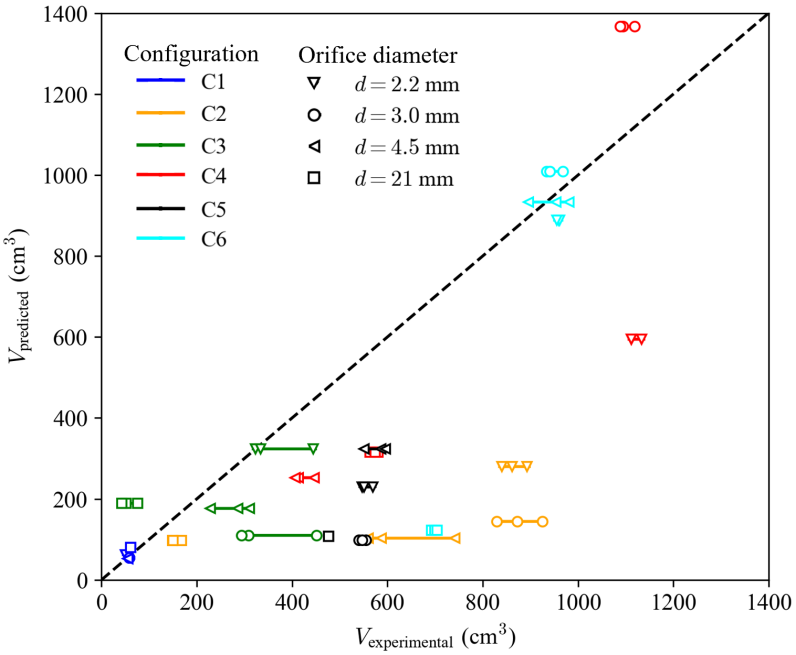

Figure 6.7: Comparison between experimental and predicted air pocket volumes across configurations and orifice diameters.

For Configuration C1, air pockets are comparatively smaller than the remaining configurations, with volumes lower than 100 cm^3, and restricted to the high point location. The AirSWMM(v2.0) model is capable of predicting air pocket volume with a maximum relative error ϵ^r_{max}, of 25%, which is of the same order of magnitude as results obtained in the single pipe presented in Chapter 5.

For Configuration C2, experimental pocket air volumes range between 180 and 950 cm^3, decreasing with the orifice size increase, and the model significantly underpredicts these volumes, not leading to volumes higher than 300 cm^3, i.e. an error of ϵ^r_{max} = 83%. This is because the model more easily creates air pockets in the high points due to the considerable elevation differences whilst their creation is generally more difficult in horizontal or low-slopped pipes because of the steeper wavefront. Nevertheless, as exemplified in Figures 6.6 and 6.7, estimated air pockets are created at the high point and along the pipe in the same locations as observed in experimental tests.

For Configuration C3, experimental air volumes are lower than those for Configuration C2, ranging from 80 to 420 cm^3 since the side pipe is positioned 3 cm below the main pipe. The air pocket volume is underestimated by the numerical model for smaller orifice diameters (d = 2.2, 3.0 and 4.5 mm) with ϵ^r_{max} = 65%, whereas, for the system without the orifice (d = 21 mm), ϵ^r_{max} increases to 280%; this is because the actual air pocket volume for d = 21 mm is quite small (42-50 cm^3) in comparison with those from other tests for C3 (220-450 cm^3), suggesting that the numerical model is more sensitive to the network elevation than to the filling rate conditions.

For Configuration C4, with the side pipe raised 3 cm above the main pipe, the experimental air volumes reach their highest values, ranging from 410 to 1080 cm^3. Air volumes are better estimated (ϵ^r_{max} = 45%) than for the previous two configurations (C2, C3) since the waterfront principally progresses in the main pipe and the side pipe remains mostly empty during the filling process, both in the experimental tests and in the numerical model, leading to good air volume estimates.

The air pocket volumes for Configuration C5 present a narrow range from 475 to 600 cm^3, despite being relatively high volumes in absolute terms. Predicted values range from 100 to 320 cm^3, with ϵ^r_{max} = 80%. This underprediction is likely due to the same reasons as in C3, that is the numerical model being more sensitive to the network elevation than to the filling rate. However, the experimental air volume for d = 21 mm hardly varies since air is only entrapped at the high point.

For Configuration C6, air volumes show a wide variation, ranging from 720 to 1050 cm^3. Unlike other configurations, the model is capable of accurately predicting air pocket volumes (900-1000 cm^3) for smaller orifices sizes (d = 2.2 - 4.5 mm) with ϵ^r_{max} = 9%. However, for d = 21 mm, the experimental and predicted volumes differ significantly, with values of 720 cm^3 and 160 cm^3, respectively (ϵ^r_{max} = 82%). Higher estimate accuracies for smaller orifices are associated with lower flow rates, being entrapped air volume mainly conditioned by the slope of the pipe. The numerical model seems to simulate better downwards-sloped pipes than rising pipes (like in C5) for these flow rates. The worst estimate is associated with the highest flow rate, where the pipe slope is not as relevant in the creation of entrapped air pockets.

Overall, smaller air pockets are more accurately predicted, especially when the air pocket is confined to the high point location. Opposite of this, air pocket volumes are considerably overestimated when the air pockets are elongated and spread along the pipes. Conversely, larger air pocket volumes tend to be mostly underestimated. There are several reasons for AirSWMM(v2.0) to consistently underpredict entrapped air pocket volumes and to have different air pocket lengths.

Firstly, the model predicts steeper waterfront slopes in comparison with those observed in experimental conditions. As waterfronts push air to the downstream end of the pipe system, this results in less predicted air volume than the actually entrapped. The objective of this research is to detect and quantify entrapped air pocket volumes using a set of valid assumptions for 1D solvers rather than targeting more accurate but complex 3D analyses, which are impractical in standard water distribution problems. Thus, minor modifications were incorporated in the original SWMM code to account for the air phase in water flow rate and depth calculations and these are not sufficient to describe the observed waterfront propagation and, consequently, the accurate estimate of the final volumes.

Secondly, the AirSWMM(v2.0) model cannot reproduce the exact air pocket length and depth at the final steady state. This is mainly due to simplifications associated with the 1D model used (e.g., air pocket geometrical representation, surface tension, etc.) which do not allow to describe the 3D nature of the observed phenomena. In fact, the shape and length of air pockets vary with pressure, volume and incoming flow (Perron et al., 2006). However, this behaviour cannot be incorporated into the AirSWMM(v2.0) model, which was deliberately kept simple, as a 1D model. Therefore, AirSWMM(v2.0) is

not able to reproduce the angle of the air pockets with the pipe wall resulting in different air pocket lengths than the actual ones. Still, despite the underestimation of air pocket volume and length, the AirSWMM(v2.0) model is a step ahead in the determination of the approximate locations and sizes of the air pockets.

6.5. DISCUSSION

AirSWMM(v2.0) allows determining the accurate location of the air pockets, though the air pocket volumes are not accurately predicted for all configurations-orifice sizes. The air pocket volume is well estimated when it is limited to a small length of the pipe, it is overestimated when the volume is small and spread along the pipe and underestimated for larger air volumes, also spread along the pipe. AirSWMM(v2.0) uses the SWMM engine for calculating flow rates and pressure-heads and has additional features to compute, in a simply coupled way, the air-phase interaction at each time step. Entrapped air pocket volumes strongly depend on the water depths calculated by the SWMM engine at each node, during the pipe-filling process. A more accurate air pocket volume estimation would require modifying the core components of the SWMM engine, which was not the purpose of this research. Thus, users should be aware of the limitations of the AirSWMM(v2.0) model, when estimating the air pocket volumes. Additionally, the model prediction of the air pocket shape does not correspond to that of the experimental observations with shorter air pocket lengths predicted than observed. Nevertheless, AirSWMM(v2.0) can be used to identify the likely locations of air pockets hence, in turn, the best locations for air release devices. It can also be used to determine locations where the pipe layout could be optimised to improve the operation during IWS.

AirSWMM(v2.0) can also be useful for improving the operation of IWS systems. Firstly, AirSWMM(v2.0) allows a better estimation of pipe-filling times in comparison with the original SWMM. This is because the presence of air in the system delays the pipe-filling process and the incorporation of the air-water interaction in AirSWMM(v2.0) allows a better description of existing phenomena. Secondly, SWMM provides an overestimate of the pressure-heads because it does not incorporate entrapped air pockets' local head losses, whereas AirSWMM(v2.0) provides a more realistic estimate of pressure-heads along the pipes. This is because the head losses created by entrapped air pockets are partially accounted for in the AirSWMM(v2.0) through higher friction in wet perimeters, along the air pocket lengths as observed in Chapter 5. Thirdly, a better description of pressure distribution along the pipe network during IWS operation will help to identify with higher accuracy the pipe locations with lower pressure, providing, therefore, a better assessment of potential intrusion or cross-contamination risk assessment. Finally, AirSWMM(v2.0) allows quantifying the flow rate of air being released at each system orifice which cannot be done by the SWMM. Such quantification can help utilities to assess which domestic flowmeters should be more frequently replaced, since running dry wears the meters faster than under continuous water supply (Ferrante et al., 2022).

6.6. CONCLUSIONS

New experimental tests have been conducted to better understand the entrapped air pocket formation at high points in the pipe network, including the influence of network topography and the filling rate on the air pocket location and volume. AirSWMM(v2.0) model, developed and validated for a single pipe, configuration is tested herein in a single loop network at a laboratory scale with varying pipe elevations and filling rates.

Based on the experimental and modelling results obtained the following conclusions are made:

- Experiments have revealed that air pocket volumes and shapes strongly depend on the location of the high point in the network, the pipe slopes and the water filling rate. It was observed that entrapped air volumes can be up to 100 times higher when the high point is located in the side pipe than when it is located on the main pipe. It was also observed that air pocket volumes tend to decrease with the increasing water filling rate, which is determined by downstream orifice size, a finding consistent with the observations from 5. Finally, experimental observations provide evidence that air pocket creation and final volumes are dominated by the waterfront division and merging at network node junctions and the waterfront progression along the multiple pipes, despite the processes also having a stochastic nature.

- AirSWMM(v2.0) has shown a good prediction capability for the water filling behaviour, with and without air pressurisation, for the tested pipe network. Some numerical instabilities were observed when the waterfront reaches each node but this does not affect the prediction of the overall filling process nor the arrival time at the downstream end of the system.

- AirSWMM(v2.0) model also predicts well the air pocket network location in all cases allowing the use of such predictions to support or complement the recommendations from the American Water Works Association (2007) and Deltares (2016) on where air release devices should be installed.

- AirSWMM(v2.0) model tends to over-predict the volume of smaller and elongated air pockets whereas smaller and concentrated air pockets are predicted reasonably well, with a 25% relative error. AirSWMM(v2.0) can both correctly predict (with ϵ^r_{max} = 10%) or under-predict larger air pocket volumes (with ϵ^r_{max} = 90% of the observed values) depending on the pipe configuration and elevations. The inaccuracies in predictions arise mainly from the simplified single-phase 1D flow modelled by the AirSWMM(v2.0) whereas the real flow is multi-phase 3D.

Collected experimental data can be used as a benchmark data set for further numerical developments. Additional experimental tests, with a broader range of pipe diameters, similar to those conducted by Guizani et al. (2006) on waterfront slopes during pipe-filling events, are recommended to better numerically describe pipe-filling processes. Future research should focus on using 3D CFD models for the simulation of pipe-filling stages considering the geometrical shape of the pipe and water surface tension to better describe the waterfront propagation and the entrapped air pocket's volumes, shape and

length. Combining 1D and 3D CFD models should also be focused on considering the local diagnosis of systems and post-accident analyses. This work did not consider the existence of water demand throughout the pipe system, which is likely to influence the overall filling process dynamics. Water demand could be implemented with already existing SWMM elements as proposed by Campisano et al. (2019) or directly in the source code. Experimental tests with water demand at different nodes should be carried out in the future (supported by the corresponding numerical tests) as these may influence the formation of air pockets. In addition, the influence of user's private tanks on the formation of entrapped air pockets should also be carried out.

7

APPLICATION TO A REAL-LIFE PIPE NETWORK

This chapter is the initial work of:

Ferreira, J. P., Ferràs, D., Covas, D.I.C., Kapelan, K. (In preparation). Air pocket modelling and air valve positions in a water network filling events.

7.1. INTRODUCTION

The entrapment of air pockets is one of the possible causes of pipe bursts, equipment malfunctioning and operational constraints upon the occurrence of hydraulic transients (Fuertes-Miquel et al., 2019, Ramezani et al., 2016). Many studies have been developed to analyse the effects of entrapped air pockets in unsteady events (Bergant et al., 2018, Ferreira et al., 2021, Alexander et al., 2019). Observations have demonstrated that the maximum pressure variations may attained for certain air pocket volumes and locations and that air pockets introduce a delay in the pressure wave propagation and a sudden drop in the first pressure wave. However, very limited research has been carried out to assess the mechanisms of air entrapment in the pipes and which are the most prone air pocket locations during pipe-filling events. Additionally, air pockets' simulation in pipe systems requires considerable computational power since small space and time steps are required to capture the in-analysis phenomena, such as the compression and expansion cycles of the air.

International engineering guidelines have been established for installing air release devices at different locations to prevent operation disruptions and mitigate entrapped air (Tukker et al., 2016, Ballun, 2016). However, these guidelines are based on experimental tests at a laboratory scale and empirical evidence collected throughout the years from real-life systems' operations. There is still no numerical study research on where air pockets can get entrapped and air valves should be installed, nor the discussion and comparison of those results with the international guidelines.

This chapter provides a first assessment of the location of air pockets in a case study from the literature by using the developed AirSWMM. A pressure-driven analysis is implemented in the source code of AirSWMM(v2.0) to better simulate the nodal demand, since this feature was not originally included in SWMM. AirSWMM(v2.0) is used instead of a MoC model to allow simulating the pipe filling event and the air pocket entrapment which is not possible with pressurized flow equations. Pressure-head results for different spatial discretisations are compared with collected field data to assess the best compromise between spatial discretisation and the results' accuracy. The recommendations from international guidelines for the location of air release devices are compared to the predicted air pocket locations to assess if the numerical estimates are in agreement with the empirical evidence.

7.2. CASE STUDY

The case study from the literature used herein to analyse the air pocket entrapment during pipe-filling events in a real-life system is depicted in Figure 7.1 (Campisano et al., 2019). This system is composed of 58 pipes with slopes varying from 1% to 23%, 56 junction nodes, most with water demand, and one storage tank with an initial water depth of 2.8 m. The storage tank is considered large enough for the water level not to vary, behaving like a constant-head reservoir. Pressure-head data are collected at Nodes 13 and 46, highlighted in Figure 7.1. Collected pressure-head data will be compared with numerical results obtained by the SWMM model, as used in that study to simulate the pipe-filling event.

Since the original SWMM was used and this model has been developed for urban

drainage systems, further assumptions and model settings are established to describe the pipe-filling process in water supply systems, namely:

- the tank is modelled as a storage node, neglecting water level variations during the filling;
- nodal surcharge depths (water depths for which nodes would flood) are set to 100 m above the nodes' elevation to prevent any artificial flooding;
- a negligible minimum nodal surface area is considered to use the surface area of the node-link assembly in SWMM to determine the water depth;
- specific controls for pipes connected to the storage tank are implemented to simulate the instantaneous opening of the gate valve in the network that determines the start of the filling process;
- flow supplied at each node with water demand is implemented with a pressure-driven analysis given the low pressures in the system; this adaptation is carried out by using the available elements in the original SWMM, like outlet links and outfalls, with a costing rating curve to better describe the flow rate;
- diurnal variations of the nodal demands are implemented in the control rules of the outlet links.

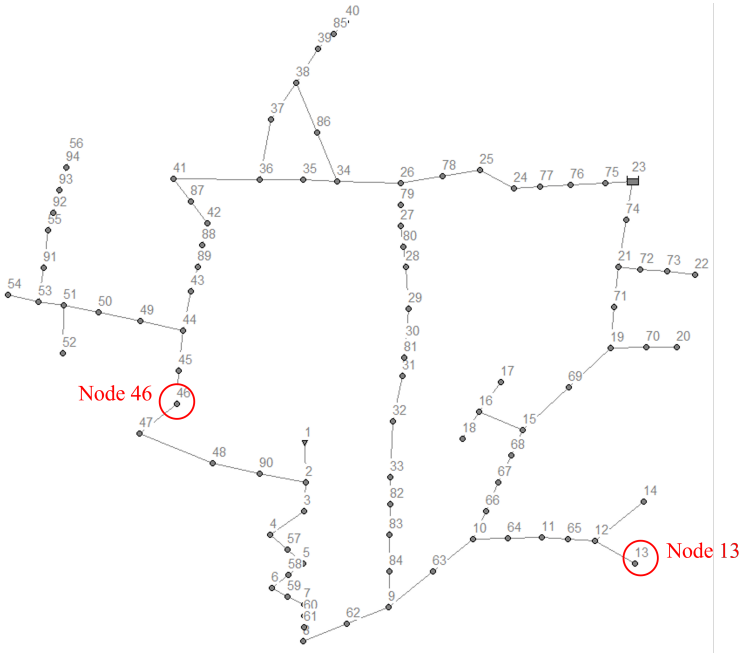

Figure 7.1: Case study network layout with node ID labels.

Pipe lengths are adjusted to have pipes with a maximum length of 100 m to obtain more accurate results and ensure numerical stability. The time-step was determined by using Eq. (4.11) proposed by Roesner et al. (1988), having been obtained Δt = 11.3 s, for a maximum space-step Δx = 100 m. Only the EXTRAN surcharge method is used because, at the time of the original study was developed in 2019, SWMM (before version 5.1.013), there was no SLOT method option to simulate the pressurisation in the pipes.

A pressure-driven analysis (PDA) is further implemented to simulate more realistically the behaviour of domestic tanks as described in Chapter 2. Eq. (2.2) is used to simulate the demand at each node considering h_{min} = 5 m, h_{req} = 30 m and β = 0.5. This implementation is developed with existing SWMM elements, namely the outlets that can control the flow rate going out of the system and the rules for defining a no outlet flow condition when the pressure-head is below the minimum required. This implementation is illustrated in Figure 7.2. Numerical pressure-head results show a good agreement with field data in terms of arrival time and pressure-head at the measurement nodes, thus demonstrating that SWMM is able to simulate network pipe-filling events in a downwards-sloped pipe network.

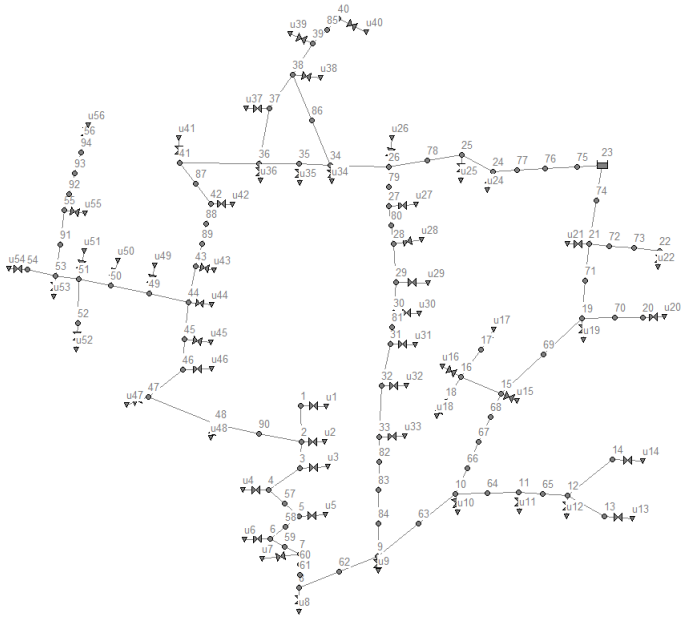

Figure 7.2: Network layout with Campisano PDA model implementation.

7.3. AIRSWMM(V2.1) IMPLEMENTATION

7.3.1. PRESSURE-DRIVEN ANALYSIS IN AIRSWMM

AirSWMM's(v2.0) source code is improved to include the pressure-driven analysis in the function **addExternalInflows**. The same pressure-driven analysis parameters (p_{min} = 5.0 m, p_{req} = 30.0 m, β = 0.5) are used and demands are introduced in AirSWMM as usually carried out in EPANET but with negative values. That is because the original SWMM considers water going into the pipe system as a reference (typical of urban drainage and stormwater systems) instead of water going out.

Simulations are run with the same assumptions and parameters as those considered in Campisano et al. (2019) not to introduce any modifications other than how demand is modelled. Figure 7.3 shows the demand variations as a function of the pressure-head at Nodes 2, 13, 14 and 54 in the case-study network. As seen from this figure, the final supplied flow rate is the same as obtained using Campisano's PDA and AirSWMM's PDA implementations. Still, despite the numerical results of both PDA implementations showing good agreement at nodes 2 and 41, some discrepancies are observed in the flow rates at Nodes 13 and 54. For Node 13, the Campisano's PDA implementation starts delivering water before the minimum required pressure-head of 5 m. This can be attributed to the time-step used in SWMM. Likewise, the results from the source code PDA implementation do not have any intermediate calculation step with a pressure-head between 0 and 10 m. Node 54 starts delivering water slightly before reaching the minimum required pressure in both implementations due to the iterative calculation process of SWMM. That is SWMM first calculates the flow rates (in the pipes, lateral inflows and outflows) and only then calculates the pressure-head at each node. Nevertheless, this should only be observable in the very first pressurisation instances of a node, being its relevance negligible during the filling process. Note that implementation in AirSWMM(v2.1) does not require the calculation of the outlet links nor the need to design rules from the previous implementation.

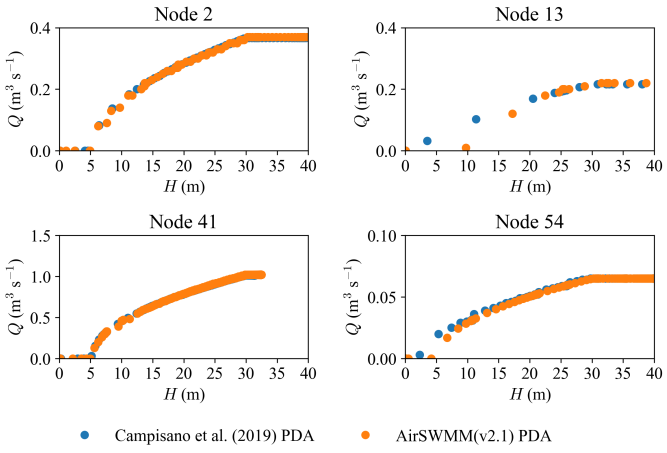

Figure 7.3: Comparison between output flow rate at nodes with pressure-head using Campisano's PDA and AirSWMM(v2.1)PDA implementations in Nodes 2, 13, 14 and 54.

7.3.2. PRESSURE-HEAD RESULTS

Since the pressure-driven analysis implementation has been validated, the pressure-head results using Campisano's PDA and AirSWMM PDA implementations are compared in Figure 7.4. Both models correctly describe the water arrival times at each node with an overall match between field data and the predicted pressure-head data. The AirSWMM PDA implementation better describes the filling process when analysing Node 13 pressure-head where Campisano's PDA leads to a faster increase than AirSWMM's PDA, diverging from the field data. This can be attributed to the small differences in the demand during the filling process observed in Figure 7.3. Nevertheless, the differences are negligible in the whole pipe-filling process and the AirSWMM's PDA is considered to be validated in terms of demand and pressure-head for the literature case study network and model. The AirSWMM's PDA implementation is considered to be calibrated and the pressure-head results can be analysed. Only the AirSWMM's PDA implementation results are presented from here onwards.

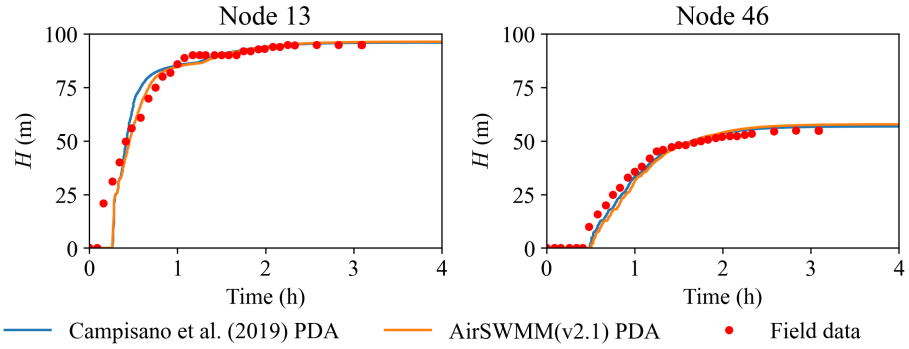

Figure 7.4: Comparison between field and numerical pressure-head obtained using Campisano's PDA and AirSWMM PDA implementations.

The AirSWMM PDA implementation is further tested by changing the time step since it has been previously demonstrated to lead to better results in pipe-filling events than when simply using SWMM. Figure 7.5 shows the comparison between the estimated pressure-head using $\Delta t = 11.3$ s and $\Delta t = 1.13$ s, corresponding to $C_r = 1.0$ (Eq. (4.9)) and 0.1 (Eq. (4.10)), respectively. The arrival time at each of the analysed nodes is well estimated, though the pressure-head increase shows a different behaviour. The pressure-head increase in both nodes is much sharper than in the field data when using a larger time step. Since nothing else has been changed in the model parametrisation, this is attributed to SWMM's implicit calculating scheme. However, this raises questions on when and under which circumstances SWMM is applicable to water supply filling conditions. A possible explanation for this is the pipes being only partially filled with the original discretisation while some are fully pressurised while others remain empty. These differences in pipe-filling processes make the friction formulation different between the cases.

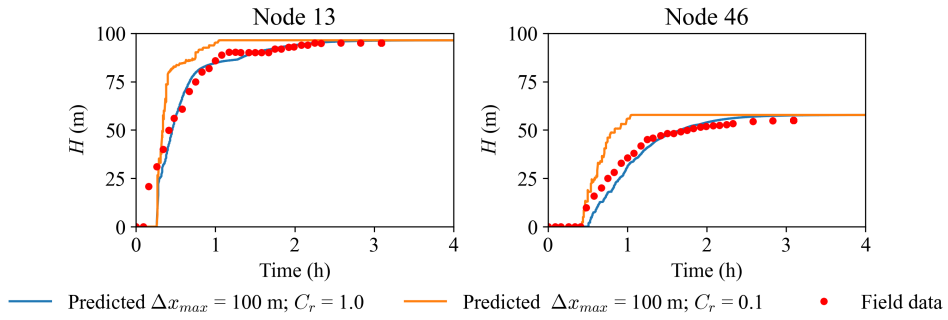

Figure 7.5: Comparison between field and numerical pressure-head with different time-steps Δt = 11.3 and 1.13 s, leading to Courant numbers of C_r = 1.0 and 0.1, respectively.

7.4. AIRSWMM(V2.1) VALIDATION

7.4.1. PRESSURE-HEAD RESULTS

The developed numerical model AirSWMM(v2.1) is applied to identify the potential locations of air pockets created during pipe-filling events in the case-study network. The network system is further spatially discretised (Δx lower than 100 m) to more accurately estimate the air pocket volumes and positions. Two fixed spatial discretisations are used: i) Δx = 5 m and ii) Δx = 2 m. The last pipe stretch in each pipe discretisation can be higher than these Δx so that the sum of the partial lengths of pipes stretches equals the total length of the pipe. Different time steps are also analysed to assess which is the Courant number that leads to better results when discretising the pipe network since several pressure-head differences have been previously observed (see 7.5).

Figure 7.6 shows the comparison of the pressure-head results at Nodes 13 and 46 obtained considering Courant numbers between 0.1 and 0.5 for Δx = 5 m with those from Campisano et al. (2019) and with field data. The water reaches Nodes 13 and 46 later than observed in the field measurements. Also, the pressure-head variations show increasing discrepancies from field data as the Courant number increases (i.e. for $C_r > 0.2$), unlike what was observed in Campisano et al. (2019). Nevertheless, when the system is discretised with a fixed space step, the C_r = 0.15 leads to pressure-head results close to the field data. This Courant number is close to that recommended by Pachaly et al. (2019) (C_r = 0.1) to describe pipe-filling events.

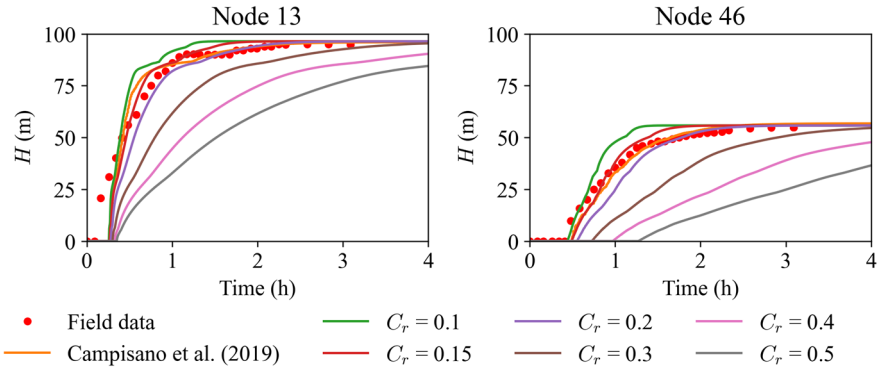

Figure 7.6: Comparison between field and numerical pressure-heads at Nodes 13 and 46 for different Courant numbers with fixed $\Delta x = 5$ m.

A smaller spatial discretisation ($\Delta x = 2$ m) is analysed to assess whether the pressure head results also change with varying Courant numbers. Figure 7.7 shows the comparison of the pressure-head results for Courant numbers varying between 0.1 and 0.5, for $\Delta x = 2$ m with Campisano et al. (2019) pressure-head results and with the field data. The pressure-head results for this finer spatial discretisation and different Courant numbers are consistent with the results observed for $\Delta x = 5$ m presented in Figure 7.6. The $C_r = 0.15$ provides a good fit between predicted and field data and higher Courant numbers lead to pressure-head damping and propagation delay and the final value steady state value is significantly lower than the physically observed. Overall, the obtained results for the two space steps demonstrate that pressure-head time variation is not much affected by the spatial discretisation, as long as it is small enough (much less than pipe length). However, the Courant number much influences pressure-head variation, being the discrepancies with field data larger for higher C_r values.

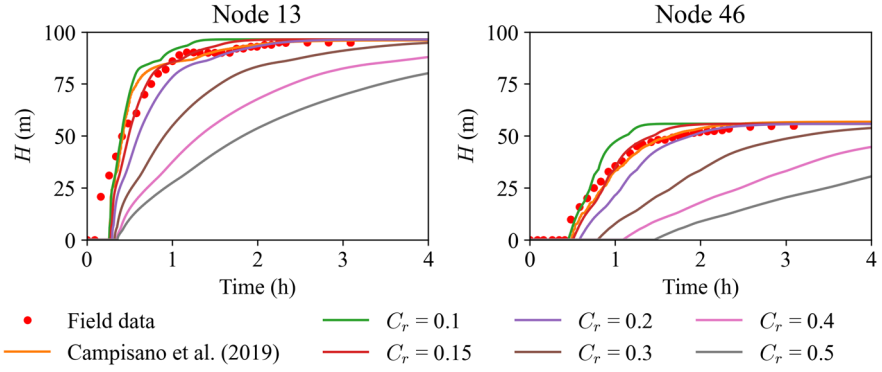

Figure 7.7: Comparison between field and predicted pressure-heads at Nodes 13 and 46 for different Courant numbers with fixed $\Delta x = 2$ m.

Tests have also been carried out with the recommended spatial discretisation in Chapter 5 ($\Delta x = 2D$), but major numerical damping and dispersion have been observed, not being presented herein. These results should be further analysed in future research.

These initial tests demonstrated that, for this case study, C_r = 0.15 leads to consistently good estimates of pressure head in pipe-filling events for the two tested spatial discretisations. The spatial discretisation of Δx = 2 m and a C_r = 0.15 have been used in the simulations in the next section to estimate the air pocket volumes and locations since these have been shown to lead to the best fitting results.

7.4.2. COMPARISON BETWEEN AIR POCKET LOCATIONS AND RECOMMENDED AIR RELEASE DEVICES' LOCATION

Since no air pocket measurements are possible in real-life pipe systems as pipes and fittings are mostly buried, and the air pocket locations resulting from AirSWMM(v2.1) are compared with engineering recommendations for the location of air valves. As referred, there are two international guidelines for defining the location of air release valves in pressurised water transmission and distribution systems to promote air release at those locations and, thus, mitigate operational problems and eventual pipe failures. Numerical results of air pocket locations from AirSWMM(v2.1) are compared with the recommended air valve locations as a proxy for the potential location of entrapped air pockets.

Following the guidelines from the American Water Works Association (Ballun, 2016) and Deltares (Tukker et al., 2016), the recommended air release valve (AV) locations are presented in Figure 7.8. Most correspond to pipe slope increases or localised high points at the network. Air valves are categorised into three main groups: AV1 to be installed at high points, AV2 to be installed in considerable slope changes and AV3 to be installed in lengthy pipes. A total of 16 air valves should be installed.

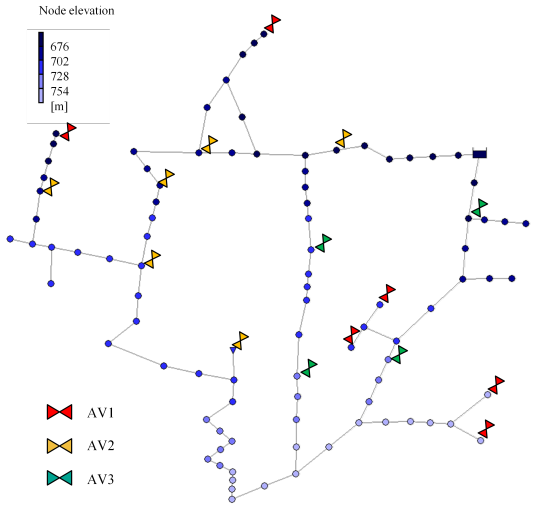

Figure 7.8: Air release valve locations according to the international guidelines from the American Water Works Association (Ballun, 2016) and Deltares (Tukker et al., 2016).

When using AirSWMM(v2.1) to locate air pockets, results have shown the location of air pockets only in the single pipes at the network outskirts. To better understand these results, the filling process is analysed step-by-step depicted in Figure 7.9. Considering the network is composed of a left, a middle and a right branch (see dashed-black lines in Figure 7.9a), the right branch has a considerably higher slope than the left one. Thus, the flow rate goes mostly to the right branch (Figure 7.9a), filling it until the lowest elevation point (Figure 7.9b). Once that point is pressurised, the filling continues from the right branch but also from the bottom up, forcing the filling to develop as a pressurised waterfront from the lowest elevation point of the network towards the storage tank, but from the left and middle branches (Figure 7.9c). Once the water reaches the elevation of the left and middle branches near the storage tank, the system keeps being filled from the bottom-up (Figure 7.9d).

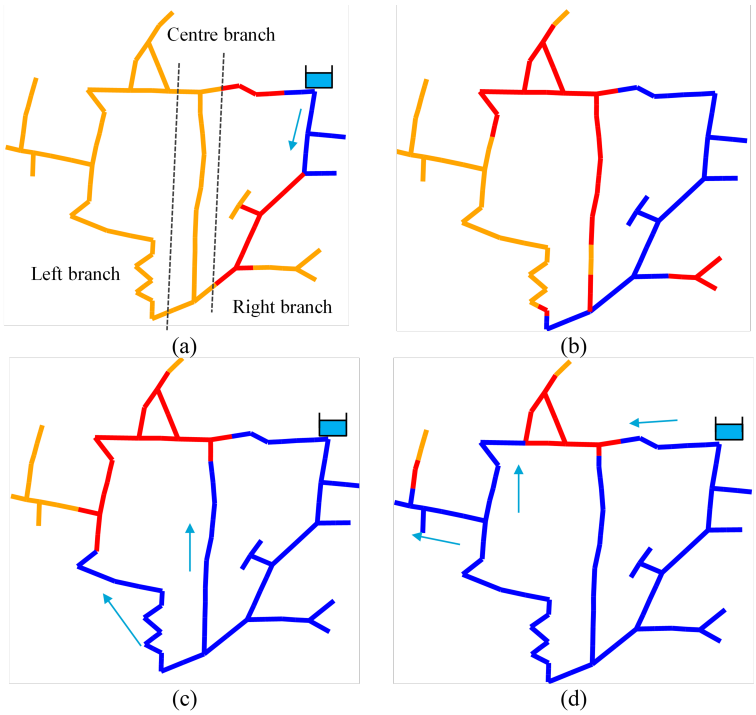

Figure 7.9: Network filling process at different times: (a) 7.5 min, (b) 16.7 min, (c) 31.5 mins and (d) 59.0 min. Filled pipes are represented in blue, partially filled pipes or air pockets are represented in red and empty pipes are represented in orange.

Despite the developed model being able to detect and quantify entrapped air pockets, this network configuration and topography do not entrap air pockets during its filling process. Since the model and the respective simulation parameters have been calibrated with the field data for this network, the network configuration can be modified to pre-

vent the system from filling from the bottom up and to analyse results in terms of air pocket locations and volumes. Thus, the pipe with the lowest elevation is closed and the pipe-filling of the new system configuration is simulated again.

Figure 7.10 shows the filling process of the network when the lowest elevation pipe is closed by closing an isolation valve. The system is initially filled in the right branch just like in the previous configuration (Figure 7.10a), creating some air pockets at the highest points. The middle branch fills just afterwards from the bottom up with a pressurised wavefront, not creating any air pockets (Figure 7.10b). When the waterfront reaches the upper pipe connected to the left branch, the left branch starts filling with a free surface flow and pressurising from the points of lower elevation to the ones at higher elevations (Figure 7.10c), creating some entrapped air pockets. Once the system is fully pressurised, several air pockets are observed in the system, mostly at the highest elevation points of the network (Figure 7.10d).

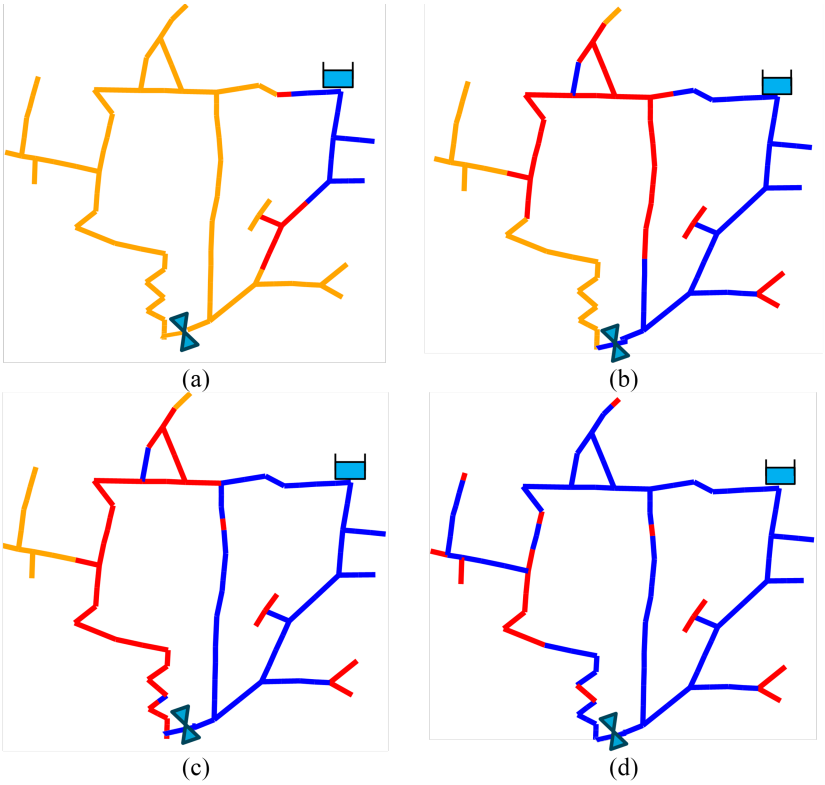

Figure 7.10: Modified network filling process at times (a) 4.2 mins, (b) 18.2 mins, (c) 35.0 mins and (d) 54.6 mins. Filled pipes are represented in blue, partially-filled pipes or air pockets are represented in red and empty pipes are represented in orange.

An estimation of the air pocket volumes and lengths inside the pipes is presented in Figure 7.11. The air pockets are long and assumed to be continuous air bodies. As mentioned in Chapter 6, the air pocket can take a more elongated shape due to pressure and flow rate conditions, features that are not possible to be described in 1D models. Thus, the estimated air pocket lengths are possibly longer in real life with a lower thickness than estimated from the model.

Figure 7.12 shows the predicted air pocket locations and the location of the air valves according to international guidelines. Results show a considerable overlap between those two locations. Pipes with air pockets are represented in orange and pipes without air are shown in blue. The right branch of the network does not show any air pockets which is caused by the considerable slope and upstream head, forcing the waterfront to be close to perpendicular to the pipe axis.

The numerical predictions of the entrapped air pocket locations are larger than the ones from the guidelines since the air is expected to rise in the pipe and, ultimately, be released from the air valve at the top of high points. The predicted air pockets extend further downstream the pipes in lower elevation areas, being the air release devices suggested to be installed at the highest elevation points of the numerical estimates. The location of air valves of category AV1 is adequately estimated, having mixed results for category AV2. Air valve locations for category AV3 are not represented since those are only recommended in the guidelines due to long pipe lengths without any air release device requirement as a conservative design approach.

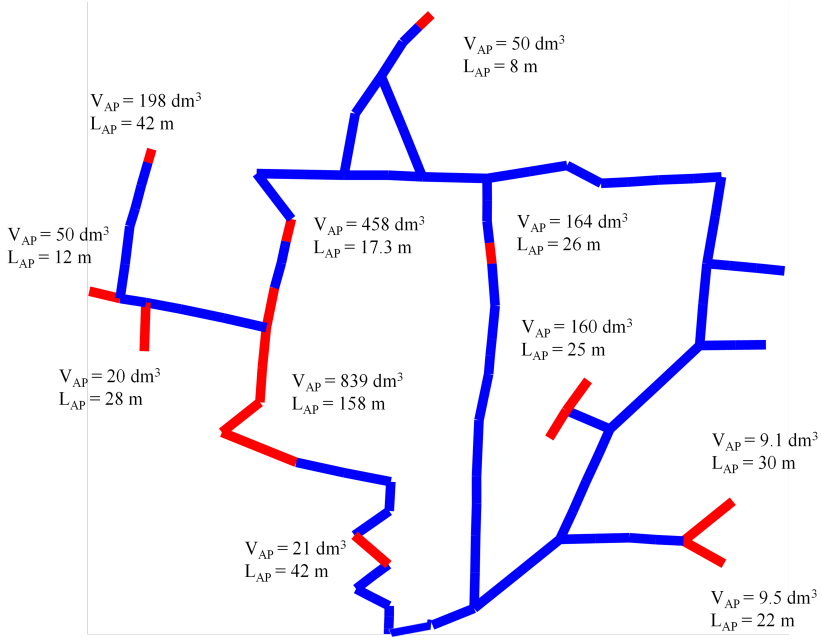

Figure 7.11: Air pocket volume and length of each entrapped air pocket in the modified network, with red pipes corresponding to pipes with entrapped air pockets and the blue pipes without any air pockets.

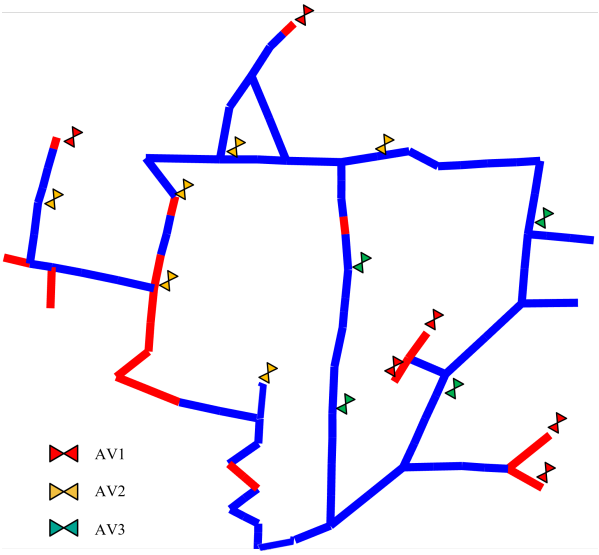

Figure 7.12: Comparison of air release devices' location from international guidelines (Ballun, 2016, Tukker et al., 2016) and the predicted air pocket locations. The red pipes correspond to pipes with entrapped air pockets and the blue ones without air pockets.

7.5. CONCLUSIONS

This chapter presents exploratory testing of AirSWMM(v2.1) in a real-life case study to analyse whether the model provides correct air pocket locations when compared to the air release device locations suggested by the international guidelines. Campisano et al. (2019) case-study network is used to test and validate the model and to predict the air pocket locations. A new implementation of the pressure-driven analysis is carried out in the AirSWMM source code, to better simulate the demand given the existence of domestic tanks.

The main conclusions from using the AirSWMM(v2.1) model in Campisano's network are:

- pressure-head results show that the AirSWMM PDA implementation reproduces the field data, thus validating the PDA implementation in the source code;
- spatial discretisation ($\Delta x = 2D$) and initial simulation parameters recommendations in the previous chapters do not allow for obtaining accurate pressure-head results in real-life networks; possible explanations are different friction loss quantification and numerical dispersion due to changing pipe lengths and diameters;
- a fixed spatial discretisation provides more accurate results than a diameter-dependent spatial discretisation; the space step is considered constant in Chapters 4-6 since the diameter is constant; here, with different diameters, the rule of fixed spatial discretisations may be necessary to provide accurate results;

- a sensitivity analysis of the time step needs to be developed for a fixed spatial discretisation in pipe-filling events given the pressure-head differences observed;
- assuming the international guidelines (Ballun, 2016, Tukker et al., 2016) recommendations for air release devices are considered as a proxy for air pocket locations, AirSWMM(v2.1) can predict where air pockets get entrapped despite the differences in pressure-heads during the network-filling.

Results from this exploratory analysis are promising, but further work needs to be carried out. Previous recommendations regarding spatial discretisation and initial simulation parameters to use in AirSWMM(v2.1) need to be further analysed in large-scale systems, with special attention to spatial discretisation. Air pocket volumes in real systems should also be estimated to determine the air pocket volume accuracy of AirSWMM(v2.1) when simulating real-life systems.

8

Conclusions

8.1. FOREWORD

This chapter summarises the main conclusions from the work previously presented. The practical implications are laid out and further research directions are proposed.

This thesis focused on the air-water interaction of the pipe-filling process to better describe the phenomena occurring in IWS. Two methodologies were developed to include the air-water interaction in a 1D Saint-Venant Equation (SV-E) based model. The first methodology aimed to couple a classic air accumulator model with the SV-E hydraulic model to better describe the pressurisation and the waterfront advance in the pipe system. The second methodology aimed at determining where entrapped air pockets would be created, how and where they are transported and how much of the air pockets' volume is entrained. These methodologies were implemented in the SWMM source code and validated with experimental tests. The methodologies were tested for a laboratory single-loop pipe network to determine the accuracy of the entrapped air pocket volumes in a looped network when compared with experimental measurements. At last, a real-life case study from the literature was used to determine whether the recommendations from international guidelines for air valve positioning correspond to where the model estimates air pockets to be created and to provide an order of magnitude of those air pocket volumes.

8.2. SUMMARY OF CONCLUSIONS

Besides the conclusions presented in each chapter, the main conclusions of this research work are:

1. **The air pressurisation model can be incorporated in a generalised 1D Saint-Venant based model, like SWMM, using an air accumulator formulation and assuming a piston-equation to define the waterfront position**

   SWMM can reproduce well the observed air pressurisation for pipe-filling in IWS systems when incorporating an air-accumulator formulation in the hydraulic model. The improved model is named AirSWMM(v1.0). As demonstrated in this work, predicted piezometric heads, wavefront arrival times and pressurisation time are better estimated by AirSWMM(v1.0) than by the original SWMM. These modifications considerably improve the modelling of the phenomena in real IWS systems. AirSWMM(v1.0) provides good results when using the EXTRAN surcharge method, but it is still not understood why the SLOT surcharge method is unable to reproduce the air pressurisation dynamics. The piezometric heads numerically calculated were slightly overestimated or the solver had numerical instabilities that did not allow the solution calculation. A possible cause for this difference is the local additional storage at each node when using the SLOT surcharge method.

2. **Entrapped air pocket creation, movement and entrainment are the most relevant air pocket dynamic phenomena in pipe-filling events and should be considered in numerical simulations for the correct definition of air pockets location and size.**

   An improved version of the model was developed, AirSWMM(v2.0), incorporating the most relevant mechanisms associated with air pockets creation, transport and entrainment. According to the results from the experimental tests, air pocket creation and volume vary considerably depending on the filling conditions and the pipe layout. The higher the filling flow rate is, the steeper the filling waterfront becomes, leading to fewer and smaller air pockets in the system. This contradicts existing knowledge that pipes should be slowly filled after a maintenance intervention to minimise pressure variations and pipe disruptions in the future. However, such recommendations assume the system purging is effective and releases all the air in the system. Additional experimental tests at a larger scale should be carried out to verify this claim and revisit the pipe-filling guidelines after maintenance interventions. Air entrainment is shown to be relevant when simulating the air pocket volume when the water flows $F > 1$, since it introduces a stochastic nature to the process. Experimental observations also show that air pocket creation and final volumes are dominated by the waterfront division and merging at network node junctions and the waterfront progression along the multiple pipes, despite the variability of the air pocket volumes.

3. **The mechanisms of air pocket entrapment, transport and entrainment can be described in hydraulic solvers by further spatially discretising the initial model and analysing each air pocket with a Lagrangian approach.**

   The waterfront tracking based on the water depths in each pipe allows for a more versatile and robust air volume quantification and the application of the developed methodology for entrapped air pockets' creation. AirSWMM(v2.0) can predict the entrapped air pocket location and their final volume with an average relative error of 20% in the tested conditions, considered good given the complex nature of the analysed phenomena and the use of a 1D model. Some dynamic behaviours, such as air pocket interface disruption due to the collision of flowing air pockets in the water flow, could not be simulated due to the complexities involved and limitations of a 1D model.

4. **AirSWMM(v2.0) can reproduce the air pockets creation, location and volume in a single-loop network under laboratory conditions. Air pockets' locations are correctly estimated but the corresponding air volumes are often underpredicted.**

   The AirSWMM(v2.0) model is able to correctly estimate the air pockets' location, but the air pockets' length is inaccurately calculated due to the model assumptions. The air pocket shape is not adjusted within the pipe cross-section to reach a stable shape, thus making the predicted pocket length shorter than the observed one. The model tends to over-predict the volume of smaller and elongated air

pockets, whereas smaller and concentrated air pockets are reasonably well predicted, with a 25% relative error. AirSWMM(v2.0) can both correctly predict (with ϵ^r_{max} = 10%) or under-predict larger air pocket volumes (with ϵ^r_{max} = 90% of the observed values) depending on the pipe configuration and elevations. The inaccuracies in predictions arise mainly from the simplified single-phase 1D flow modelled by the AirSWMM(v2.0) when the real flow is multi-phase and 3D.

5. **In real-life networks, AirSWMM(v2.1) model can correctly estimate the locations of entrapped air pockets in pipe-filling events, but these locations do not correspond fully to the locations of air release valves determined by the conservative design of international guidelines.**

   The air pocket locations estimated by AirSWMM(v2.1) are in agreement with those suggested by international guidelines for installing air release devices. A fixed spatial discretisation provides more accurate results than a diameter-dependent spatial discretisation. However, it is not clear if a fixed spatial discretisation provides accurate results in systems with severely different diameters.

8.3. THESIS SCIENTIFIC CONTRIBUTIONS

This thesis work has the following scientific contributions to literature:

1. Defining how the air phase should be incorporated in 1D Saint-Venant equations models and the definition of their applicability for pipe filling events.
2. Determining the relevant phenomena to be accounted for in two-phase flow modelling in the pipe-filling stage of IWS to better understand entrapped air pockets.
3. Developing a methodology to create, drag and entrain air pockets in a finite element 1D model with Saint-Venant equations during pipe-filling events to detect, locate, and quantify entrapped air pockets in pipe systems.
4. Quantifying the uncertainties of the developed models regarding the locations of air pockets and their volumes.
5. Determining if the model is capable of providing the locations where air valves should be installed when considering the recommendations of the international guidelines as a proxy for the air pocket locations.

8.4. FURTHER RESEARCH

This thesis has contributed to a better understanding of the effect of air pressurisation and air pocket creation, dragging and entrainment during pipe-filling events. However, further research is recommended, particularly on research topics that would improve IWS modelling and the air phase in the pipe-filling stage as follows.

1. **The assessment of the spatial discretisation and Courant number required to better simulate pipe-filling events in real-life networks.**

   Despite the good fit with experimental data, a more detailed analysis should be carried out to define the spatial discretisation and Courant numbers that have the best compromise in AirSWMM in terms of computational effort to determine the creation of air pockets and describe their dynamics.

2. **Assessing the usage of the Preissmann SLOT method with AirSWMM.**

   Initial tests showed the SLOT method does not correctly describe the air pressurisation and leads to severe numerical instabilities during pipe-filling events. A more in-depth analysis should be carried out on its applicability in the current circumstances given that the SLOT method is more computationally efficient and has been shown to provide better results (Pachaly et al., 2020).

3. **Additional experimental studies concerning air pockets creation and entrainment rate quantification.**

   As observed in Chapter 5, the final air pocket volume has a stochastic nature due to air entrainment. However, the air pocket creation and its entrainment rate quantification are still imprecise, with a broad margin of uncertainty. More experimental tests should be carried out, supported by numerical 3D CFD research. These should feature different hydraulic conditions and larger pipe diameters to better describe the air pocket dynamics in pipes and account for scale effects.

4. **Assessment of leaks in IWS concerning aeration conditions and influence of two-phase flow on leakage.**

   This thesis does not cover the existence of leaks, inevitable in water supply systems. However, these can influence the air release conditions during pipe-filling events since there is a higher air release potential. Additionally, the influence of a water and air flow mixture on the leak flow rate is still uncertain. A better quantification of such dynamics should be analysed for a more correct management of water supply systems.

5. **Adapting the current version of AirSWMM (v2.0) to simulate geysering in urban drainage systems.**

   Water supply systems with intermittent operation are not the only urban pipe systems with strong air-water interactions. The creation of geysers in stormwater systems, caused by the lack of air release devices, could be more efficiently simulated with a model like AirSWMM (v2.0). Nevertheless, the model should be adapted to the circumstances of these systems.

6. **Further validation of AirSWMM and similar methods on real-life IWS systems.**

   More pipe-filling case studies from IWS should be reported and analysed with AirSWMM or other methods to detect and quantify entrapped air pockets. As in other types of analyses, pressure measurements should be carried out with a high frequency of acquisition to fully describe these phenomena. Additionally, non-numerical techniques should be developed to estimate the air pocket volume in pipes to further validate these tools.

About the Author

João Paulo Borges Coury Cavaleiro de Ferreira was born on 25th of August 1993 in Lisbon, Portugal. He did his basic education there at *Colégio de Santa Doroteia* and *Escola Secundária Vergílio Ferreira*. He started studying Civil Engineering at *Instituto Superior Técnico* in Lisbon, where his interest in hydraulics prevented him from pursuing a mechanical engineering degree. His interest in waterhammer events sparked early on in the Masters course when he started carrying out consultancy projects within the university. He also became an "adopted Italian" in his own city during that period, which he is very grateful for to his Italian friends from *Napoli*, *Caserta*, *Perugia* and *Milano*. After graduating, João started carrying out research at the same time he was working at EPAL, Lisbon water utility, where he was greatly inspired to do further research on intermittent water supply. That led him to apply for an individual fellowship to do his PhD in the Netherlands on one of the stages of this type of water supply. After 4 years, he is sold on riding a bicycle everywhere and is keen on doing research and working with the industry.

LIST OF PUBLICATIONS

Peer-reviewed journal publications

- **Ferreira, J. P.**, Ferràs, D., Covas, D. I. C., Kapelan, K. (2024). Air entrapment modelling in networks during pipe filling events. *Urban Water Journal*, 21(6): 685-697. DOI: http://doi.org/10.1080/1573062X.2024.2342785.
- **Ferreira, J. P.**, Ferràs, D., Covas, D. I. C., van der Werf, J. A., Kapelan, K. (2024). Air entrapment modelling during pipe filling based on SWMM. *Journal of Hydraulic Research*, 62(1): 39-57. DOI: https://doi.org/10.1080/00221686.2024.2305354.
- **Ferreira, J. P.**, Ferràs, D., Covas, D. I. C., Kapelan, K. (2023). Improved SWMM Modelling for Rapid Pipe Filling Incorporating Air Behavior in Intermittent Water Supply Systems. *Journal of Hydraulic Engineering*, 149(9): 04023004. DOI: https://doi.org/10.1061/JHEND8.HYENG-13137.
- **Ferreira, J. P.**, Ferràs, D., Covas, D.I.C., Kapelan, K. (In preparation). Air pocket modelling and air valve positions in a water network filling events.

International Conferences Publications

- **Ferreira, J. P.**, Ferràs, D., Covas, D. I. C., Kapelan, K. (2023). Modelling entrapped air pockets during pipe-filling process in intermittent water supply systems. In 19th Computing & Control for the Water Industry Conference. Leicester, United Kingdom.
- **Ferreira, J. P.**, Ferràs, D., Covas, D. I. C., Kapelan, K. (2023). Modelling of Pipe Filling Events in Intermittent Water Supply Systems. In 14th International Conference on Pressure Surges. Eindhoven, the Netherlands.
- **Ferreira, J. P.**, Ferràs, D., Covas, D. I. C., Kapelan, K. (2022). Modelling of air pocket entrapment during pipe filling in intermittent water supply systems. In 2nd International Joint Conference on Water Distribution Systems Analysis & Computing and Control in the Water Industry (WDSA/CCWI). Valencia, Spain.

BIBLIOGRAPHY

Alexander, J., Lee, P., Davidson, M., Duan, H. F., Li, Z., Murch, R., Meniconi, S., & Brunone, B. (2019). Experimental validation of existing numerical models for the interaction of fluid transients with in-line air pockets. *Journal of Fluids Engineering, 141*(12), 121101. https://doi.org/10.1115/1.4043776

Alexander, J., Li, Z., Lee, P. J., Davidson, M., & Duan, H.-F. (2021). Comparison of numerical models for the interaction of a fluid transient with an offline air pocket. *Journal of Hydraulic Engineering, 147*(5), 04021014. https://doi.org/doi:10.1061/(ASCE)HY.1943-7900.0001878

Alexander, J. M., Lee, P. J., Davidson, M., Li, Z., Murch, R., Duan, H.-F., Meniconi, S., & Brunone, B. (2020). Experimental investigation of the interaction of fluid transients with an in-line air pocket. *Journal of Hydraulic Engineering, 146*(3), 04019067. https://doi.org/10.1061/(ASCE)HY.1943-7900.0001691

Allievi, L. (1903). Teoria generale del moto perturbato dell'acqua nei tubi in pressione (colpo d'ariete). *Atti dell'Associazione elettrotecnica italiana, 7*, 140–196.

Almeida, A. B., & Koelle, E. (1992). *Fluid transients in pipe networks* (1st Ed.). Computational Mechanics Publications, Elsevier Applied Science, Southampton, UK.

Andey, S., & Kelkar, P. (2007). Performance of water distribution systems during intermittent versus continuous water supply. *American Water Works Association, 99*(8), 99–106. https://doi.org/10.1002/j.1551-8833.2007.tb08011.x

Aureli, F., Dazzi, S., Maranzoni, A., & Mignosa, P. (2015). Validation of single- and two-equation models for transient mixed flows: A laboratory test case. *Journal of Hydraulic Research, 53*(4), 440–451. https://doi.org/10.1080/00221686.2015.1038324

Ayyash, F., Zhang, C., Javadi, A. A., & Farmani, R. (2024). Optimal operation of intermittent water supply systems under water scarcity. *Journal of Water Resources Planning and Management, 150*(3). https://doi.org/10.1061/jwrmd5.Wreng-6227

Ballun, J. V. (2016). *Air valves: Air-release, air/vacuum and combination* (Report). AWWA - American Water Works Association.

Bautista-de Los Santos, Q. M., Chavarria, K. A., & Nelson, K. L. (2019). Understanding the impacts of intermittent supply on the drinking water microbiome. *Curr Opin Biotechnol, 57*, 167–174. https://doi.org/10.1016/j.copbio.2019.04.003

Benjamin, T. B. (1968). Gravity currents and related phenomena. *Journal of Fluid Mechanics, 31*(2), 209–248. https://doi.org/10.1017/s0022112068000133

Bergant, A., Tijsseling, A., Kim, Y.-i., Karadžić, U., Zhou, L., Lambert, M. F., & Simpson, A. R. (2018). Unsteady pressures influenced by trapped air pockets in water-filled pipelines. *Strojniški vestnik - Journal of Mechanical Engineering, 64*(9), 501–512. https://doi.org/10.5545/sv-jme.2018.5238

Bergant, A., Simpson, A., & Tijsseling, A. (2006). Water hammer with column separation: A historical review. *Journal of Fluids and Structures*, *22*(2), 135–171. https://doi.org/10.1016/j.jfluidstructs.2005.08.008

Bergant, A. S., A.Tijsseling, Vitkovsky, J. P., Covas, D. I. C., Simpson, A. R., & Lambert, M. F. (2008). Parameters affecting water-hammer wave attenuation, shape and timing - part 1: Mathematical tools. *Journal of Hydraulic Research*, *46*(3), 373–381. https://doi.org/10.3826/jhr.2008.2848

Bhave, P. R. (1981). Node flow analysis distribution systems. *Transportation Engineering Journal of ASCE*, *107*(4), 457–467. https://doi.org/10.1061/TPEJAN.0000938

Binder, R. C. (1955). *Fluid mechanics* (3rd ed.). Prentice-Hall.

Bonilla-Correa, D. M., Coronado-Hernández, Ó. E., Fuertes-Miquel, V. S., Besharat, M., & Ramos, H. M. (2023). Application of newton–raphson method for computing the final air–water interface location in a pipe water filling. *Water*, *15*(1304).

Bousso, S., Daynou, M., & Fuamba, M. (2013). Numerical modeling of mixed flows in storm water systems: Critical review of literature. *Journal of Hydraulic Engineering*, *139*(4), 385–396. https://doi.org/10.1061/(asce)hy.1943-7900.0000680

Brentan, B., Zanfei, A., Souza, R. G., Menapace, A., Meirelles, G., & Izquierdo, J. (2024). Optimal rehabilitation procedure for intermittent water supply systems. *Journal of Water Resources Planning and Management*, *150*(6). https://doi.org/10.1061/jwrmd5.Wreng-6129

Cabral, M., Ferreira, J. P., Picciochi, S., & Covas, D. I. C. (2023). Experimental and numerical analyses of the effect of entrapped air pockets in pressurised transient flows. *14th International Conference on Pressure Surges*.

Cabrera, E., Abreu, J., Pérez, R., & Vela, A. (1992). Influence of liquid length variation in hydraulic transients. *Journal of Hydraulic Engineering*, *118*(12), 1639–1650. https://doi.org/10.1061/(ASCE)0733-9429(1992)118:12(1639)

Cabrera-Bejar, J. A., & Tzatchkov, V. G. (2009). Inexpensive modeling of intermittent service water distribution networks. *World Environmental and Water Resources Congress 2009: Great Rivers*, 295–304.

Campisano, A., Gullotta, A., & Modica, C. (2019). Using epa-swmm to simulate intermittent water distribution systems. *Urban Water Journal*, *15*(10), 925–933. https://doi.org/10.1080/1573062x.2019.1597379

Chandapillai, J. (1991). Realistic simulation of water distribution system. *Journal of Transportation Engineering*, *117*(2), 258–263. https://doi.org/10.1061/(ASCE)0733-947X(1991)117:2(258)

Charalambous, B., & Laspidou, C. (2017). *Dealing with the complex interrelation of intermittent supply and water losses* (1st Edition, Vol. 16). IWA Publishing. https://doi.org/10.2166/9781780407074

Chaudhry, M. H. (2008). *Open-channel flow* (2n Edition). Springer.

Chaudhry, M. H. (2014). *Applied hydraulic transients* (3rd Ed.). Springer-Verlag New York.

Chepyegon, C., & Kamiya, D. (2018). Challenges faced by the kenya water sector management in improving water supply coverage. *Journal of Water Resource and Protection*, *10*(01), 85–105. https://doi.org/10.4236/jwarp.2018.101006

Christodoulou, S., & Agathokleous, A. (2012). A study on the effects of intermittent water supply on the vulnerability of urban water distribution networks. *Water Science*

and Technology: Water Supply, *12*(4), 523–530. https://doi.org/10.2166/ws.2012.025

Christodoulou, S. E., Christodoulou, C., & Agathokleous, A. (2017). Influence of intermittent water supply operations on the vulnerability of water distribution networks. *Journal of Hydroinformatics*, *19*(6), 838–852. https://doi.org/10.2166/hydro.2017.133

Covas, D., Ramos, H., Lopes, N., & Almeida, A. B. (2006). Water pipe system diagnosis by transient pressure signals. *Water Distribution Systems Analysis Symposium 2006*. https://doi.org/10.1061/40941(247)57

Covas, D., & Ramos, H. (2010). Case studies of leak detection and location in water pipe systems by inverse transient analysis. *Journal of Water Resources Planning and Management*, *136*(2), 248–257. https://doi.org/doi:10.1061/(ASCE)0733-9496(2010)136:2(248)

Covas, D., Ramos, H., & Almeida, A. B. d. (2005). Standing wave difference method for leak detection in pipeline systems. *Journal of Hydraulic Engineering*, *131*(12), 1106–1116. https://doi.org/10.1061/(ASCE)0733-9429(2005)131:12(1106)

Cunge, J. A., & Wegner, M. (1964). Intégration numérique des équations d'écoulement de barré de saint-venant par un schéma implicite de différences finies. *La Houille Blanche*, (1), 33–39. https://doi.org/10.1051/lhb/1964002

Davies, R. M., & Taylor, G. I. (1950). The mechanics of large bubbles rising through extended liquids and through liquids in tubes. *Proceedings of the Royal Society of London. Series A. Mathematical and Physical Sciences*, *200*(1062), 375–390. https://doi.org/10.1098/rspa.1950.0023

Dumitrescu, D. T. (1943). Strömung an einer luftblase im senkrechten rohr. *ZAMM - Journal of Applied Mathematics and Mechanics / Zeitschrift für Angewandte Mathematik und Mechanik*, *23*(3), 139–149. https://doi.org/10.1002/zamm.19430230303

EEA. (2021). *Responding to the health risks of climate change in europe* (Report). European Environment Agency.

Erickson, J. J., Nelson, K. L., & Meyer, D. D. J. (2022). Does intermittent supply result in hydraulic transients? mixed evidence from two systems. *Journal of Water Supply: Research and Technology-Aqua*, *71*(11), 1251–1262. https://doi.org/10.2166/aqua.2022.206

Escarameia, M. (2007). Investigating hydraulic removal of air from water pipelines. *Proceedings of the Institution of Civil Engineers*, *160*(WM1), 25–34.

Escarameia, M. (2004). *Experimental and numerical studies on movement of air in water pipelines* (Report No. SR 661). HR Wallingford.

Farley, M. (2001). *Leakage management and control - a best practice training manual*. World Healt Organization.

Ferrante, M. (2023). A laboratory investigation on the effects of intermittent water supply in a branched system. *Water Resources Management*. https://doi.org/10.1007/s11269-023-03686-8

Ferrante, M., Rogers, D., Mugabi, J., & Casinini, F. (2022). Impact of intermittent supply on water meter accuracy. *Journal of Water Supply: Research and Technology-Aqua*, *71*(11), 1241–1250. https://doi.org/10.2166/aqua.2022.091

Ferreira, J. P., Ferras, D., Covas, D. I. C., & Kapelan, Z. (2022). Modelling of air pocket entrapment during pipe filling in intermittent water supply systems. *2nd International Joint Conference on Water Distribution Systems Analysis and Computing and Control in the Water Industry (WDSA/CCWI)*.

Ferreira, J. P. B. C. C., Martins Nuno, M. C., & Covas Dídia, I. C. (2018). Ball valve behavior under steady and unsteady conditions. *Journal of Hydraulic Engineering*, *144*(4), 04018005. https://doi.org/10.1061/(ASCE)HY.1943-7900.0001434

Ferreira, J. P., Buttarazzi, N., Ferras, D., & Covas, D. I. C. (2021). Effect of an entrapped air pocket on hydraulic transients in pressurized pipes. *Journal of Hydraulic Research*, *59*(6), 1018–1030. https://doi.org/10.1080/00221686.2020.1862323

Ferreira, J. P., Ferras, D., Covas, D. I. C., & Kapelan, Z. (2023). Modelling of pipe filling events in intermittent water supply systems. *14th International Conference on Pressure Surges*.

Ferreri, G. B., Freni, G., & Tomaselli, P. (2010). Ability of preissmann slot scheme to simulate smooth pressurisation transient in sewers. *Water Science Technology*, *62*(8), 1848–58. https://doi.org/10.2166/wst.2010.360

Fontanazza, C. M., Notaro, V., Puleo, V., & Freni, G. (2015). The apparent losses due to metering errors: A proactive approach to predict losses and schedule maintenance. *Urban Water Journal*, *12*(3), 229–239. https://doi.org/10.1080/1573062x.2014.882363

Freni, G., De Marchis, M., & Napoli, E. (2014). Implementation of pressure reduction valves in a dynamic water distribution numerical model to control the inequality in water supply. *Journal of Hydroinformatics*, *16*(1), 207–217. https://doi.org/10.2166/hydro.2013.032

Fuamba, M. (2002). Contribution on transient flow modelling in storm sewers. *Journal of Hydraulic Research*, *40*(6), 685–693. https://doi.org/10.1080/00221680209499915

Fuertes-Miquel, V. S., Coronado-Hernández, O. E., Mora-Meliá, D., & Iglesias-Rey, P. L. (2019). Hydraulic modeling during filling and emptying processes in pressurized pipelines: A literature review. *Urban Water Journal*, *16*(4), 299–311. https://doi.org/10.1080/1573062x.2019.1669188

Fujiwara, O., & Li, J. (1998). Reliability analysis of water distribution networks in consideration of equity, redistribution, and pressure-dependent demand. *Water Resources Research*, *34*(7), 1843–1850. https://doi.org/10.1029/98WR00908

Galaitsi, E. S., Russell, R., Bishara, A., Durant, L. J., Bogle, J., & Huber-Lee, A. (2016). Intermittent domestic water supply: A critical review and analysis of causal-consequential pathways. *Water*, *8*(7), 1–25. https://doi.org/10.3390/w8070274

Gandenberger, W. (1957). *Über die wirtschaftliche und betriebssichere gestaltung von fernwasserleitungen*. Oldenbourg.

Germanopoulos, G. (1985). A technical note on the inclusion of pressure dependent demand and leakage terms in water supply network models. *Civil Engineering Systems*, *2*(3), 171–179. https://doi.org/10.1080/02630258508970401

Giustolisi, O., Savic, D., & Kapelan, Z. (2008). Pressure-driven demand and leakage simulation for water distribution networks. *Journal of Hydraulic Engineering*, *134*(5), 626–635. https://doi.org/10.1061/(ASCE)0733-9429(2008)134:5(626)

Glauser, S., & Wickenhäuser, M. (2009). Bubble movement in downward-inclined pipes. *Journal of Hydraulic Engineering, 135*(11), 1012–1015. https://doi.org/10.1061/(ASCE)HY.1943-7900.0000093

Goldring, B. T. (1979). The use of small-scale siphon models. *Proceedings of the Institution of Civil Engineers, 67*(4), 929–942. https://doi.org/10.1680/iicep.1979.2782

Gonzalez, C. I., Erickson, J., Chavarría, K. A., Nelson, K. L., & Goodridge, A. (2020). Household stored water quality in an intermittent water supply network in panama. *Journal of Water, Sanitation and Hygiene for Development*, 1–11. https://doi.org/10.2166/washdev.2020.156

Gottipati, P. V. K. S. V., & Nanduri, U. V. (2014). Equity in water supply in intermittent water distribution networks. *Water and Environment Journal, 28*(4), 509–515. https://doi.org/10.1111/wej.12065

Guizani, M., Vasconcelos, J., Wright, S. J., & Maalel, K. (2006). Investigation of rapid filling of empty pipes. *Journal of Water Management Modeling, R225-20*, 463–482. https://doi.org/10.14796/jwmm.R225-20

Gullotta, A., Butler, D., Campisano, A., Creaco, E., Farmani, R., & Modica, C. (2021). Optimal location of valves to improve equity in intermittent water distribution systems. *Journal of Water Resources Planning and Management, 147*(5), 04021016. https://doi.org/10.1061/(asce)wr.1943-5452.0001370

Guo, Q., & Song, C. C. S. (1990). Surging in urban storm drainage systems. *Journal of Hydraulic Engineering, 116*(12), 1523–1537.

Haakh, F. (2018). Transient thermodynamic processes in air chambers with a gas cushion for surge protection. *13th International Conference on Pressure Surges*.

Hachem, F. E., & Schleiss, A. J. (2012). Effect of drop in pipe wall stiffness on water-hammer speed and attenuation. *Journal of Hydraulic Research, 50*(2), 218–227. https://doi.org/10.1080/00221686.2012.656838

Hanjahanja, R., & Omuto, C. (2018). Do prepaid water meters improve the quality of water service delivery? the case of nakuru, kenya. *Smart Water, 3*(1), 1–12. https://doi.org/10.1186/s40713-018-0010-9

Hatcher, T. M., Malekpour, A., Vasconcelos, J., & Karney, B. (2015). Comparing unsteady modeling approaches of surges caused by sudden air pocket compression. *Journal of Water Management Modeling, 23*, 1–10. https://doi.org/10.14796/jwmm.c392

He, J., Hou, Q., Lian, J., Tijsseling, A. S., Bozkus, Z., Laanearu, J., & Lin, L. (2022). Three-dimensional cfd analysis of liquid slug acceleration and impact in a voided pipeline with end orifice. *Engineering Applications of Computational Fluid Mechanics, 16*(1), 1444–1463. https://doi.org/10.1080/19942060.2022.2095440

Hodges, B. R. (2020). An artificial compressibility method for 1d simulation of open-channel and pressurized-pipe flow. *Water, 12*(6). https://doi.org/10.3390/w12061727

Hou, Q., Zhang, L. X., Tijsseling, A. S., & Kruisbrink, A. C. H. (2012). Rapid filling of pipelines with the sph particle method. *Procedia Engineering, 31*, 38–43. https://doi.org/10.1016/j.proeng.2012.01.987

Idel'čik, I., & Steinberg, M. (2005). *Handbook of hydraulic resistance*. Jaico Publishing House. https://books.google.nl/books?id=GrcZPQAACAAJ

Ilaya-Ayza, A. E., Martins, C., Campbell, E., & Izquierdo, J. (2018). Gradual transition from intermittent to continuous water supply based on multi-criteria optimization for network sector selection. *Journal of Computational and Applied Mathematics*, *330*, 1016–1029. https://doi.org/10.1016/j.cam.2017.04.025

Ingeduld, P., Svitak, Z., Pradhan, A., & Tarai, A. (2006). Modelling intermittent water supply systems with epanet. *8th annual WD symposium*.

Izquierdo, J., Fuertes, V. S., Cabrera, E., Iglesias, P. L., & Garcia-Serra, J. (1999). Pipeline start-up with entrapped air. *Journal of Hydraulic Research*, *37*(5), 579–590. https://doi.org/10.1080/00221689909498518

Kalinske, A., & Bliss, P. (1943). Removal of air from pipelines by flowing water. *Civil Engineering, ASCE, Vol. 13, No. 10*, 480–482.

Kaur, K., Laanearu, J., & Annus, I. (2023). Air pocket dynamics under bridging of stratified flow during rapid filling of a horizontal pipe. *Journal of Hydraulic Engineering*, *149*(1), 04022030. https://doi.org/10.1061/(asce)hy.1943-7900.0002021

Kent, J. C. (1952). *The entrainment of air by water flowing in circular conduits with downgrade slopes* [Thesis].

Kim, Y. I. (2008). *Advanced numerical and experimental transient modelling of water and gas pipeline flows incorporating distributed and local effects* [Thesis].

Klingel, P. (2012). Technical causes and impacts of intermittent water distribution. *Water Science and Technology: Water Supply*, *12*(4), 504–512. https://doi.org/10.2166/ws.2012.023

Kong, R., Rau, A., Kim, S., Bajorek, S., Tien, K., & Hoxie, C. (2019). A robust image analysis technique for the study of horizontal air-water plug flow. *Experimental Thermal and Fluid Science, 102,* 245–260. https://doi.org/10.1016/j.expthermflusci.2018.12.001

Lauchlan, C. S., Escarameia, M., May, R. W. P., Burrows, R., & Gahan, C. (2005). *Air in pipelines, a literature review* (Report No. SR 649). HR Wallingford.

Lee, N. H. (2005). *Effect of pressurization and expulsion of entrapped air in pipelines* [Thesis].

Leon, A. S., Ghidaoui, M. S., Schmidt, A. R., & García, M. H. (2009). Application of godunov-type schemes to transient mixed flows. *Journal of Hydraulic Research*, *47*(2), 147–156. https://doi.org/10.3826/jhr.2009.3157

Leon, A. S., Ghidaoui, M. S., Schmidt, A. R., & Garcia, M. H. (2010). A robust two-equation model for transient-mixed flows. *Journal of Hydraulic Research*, *48*(1), 44–56. https://doi.org/10.1080/00221680903565911

Liou, C. P., & Hunt, W. A. (1996). Filling of pipelines with undulating elevation profiles. *Journal of Hydraulic Engineering*, *122*(10), 534–539. https://doi.org/10.1061/(ASCE)0733-9429(1996)122:10(534)

Liu, D., & Zhou, L. (2009). Numerical simulation of transient flow in pressurized water pipeline with trapped air mass. *2009 Asia-Pacific Power and Energy Engineering Conference*, 1–4. https://doi.org/10.1109/APPEEC.2009.4918544

Louati, M., Ghidaoui, M. S., Tekitek, M. M., & Jose Lee, P. (2020). Wave-leak interaction in a simple pipe system. *Journal of Hydraulic Engineering*, *146*(4). https://doi.org/10.1061/(asce)hy.1943-7900.0001714

Lubbers, C., & Clemens, F. (2007). Detection of gas pockets in pressurised wastewater mains using dynamic system response analysis. *Water Science and Technology*, *55*(4), 31–38. https://doi.org/10.2166/wst.2007.092

Mahmoud, H. A., Savić, D., & Kapelan, Z. (2017). New pressure-driven approach for modeling water distribution networks. *Journal of Water Resources Planning and Management*, *143*(8), 04017031. https://doi.org/doi:10.1061/(ASCE)WR.1943-5452.0000781

Malekpour, A., & Karney, B. (2014a). A non-oscillatory preissmann slot method based numerical model. *Procedia Engineering*, *89*, 1366–1373. https://doi.org/10.1016/j.proeng.2014.11.461

Malekpour, A., & Karney, B. W. (2011). Rapid filling analysis of pipelines with undulating profiles by the method of characteristics. *ISRN Applied Mathematics*, *2011*, 1–16. https://doi.org/10.5402/2011/930460

Malekpour, A., & Karney, B. W. (2014b). Profile-induced column separation and rejoining during rapid pipeline filling. *Journal of Hydraulic Engineering*, *140*(11), 1–12. https://doi.org/10.1061/(asce)hy.1943-7900.0000918

Malekpour, A., & Karney, B. W. (2016). Spurious numerical oscillations in the preissmann slot method: Origin and suppression. *Journal of Hydraulic Engineering*, *142*(3), 04015060. https://doi.org/10.1061/(asce)hy.1943-7900.0001106

Malekpour, A., Karney, B. W., & Nault, J. (2016). Physical understanding of sudden pressurization of pipe systems with entrapped air: Energy auditing approach. *Journal of Hydraulic Engineering*, *142*(2). https://doi.org/10.1061/(asce)hy.1943-7900.0001067

Malekpour, A., & Karney, B. (2012). Rapid filling in pipe systems with column separation. *11th International Conference on Pressure Surges*, 543–557.

Malekpour, A., & Karney, B. (2014c). Column separation and rejoinder during rapid pipeline filling induced by a partial flow blockage. *Journal of Hydraulic Research*, *52*(5), 693–704. https://doi.org/10.1080/00221686.2014.905502

Marchis, M., Fontanazza, C. M., Freni, G., La Loggia, G., Napoli, E., & Notaro, V. (2010). A model of the filling process of an intermittent distribution network. *Urban Water Journal*, *7*(6), 321–333. https://doi.org/10.1080/1573062X.2010.519776

Marchis, M., Fontanazza, C. M., Freni, G., Loggia, G. L., Napoli, E., & Notaro, V. (2011). Analysis of the impact of intermittent distribution by modelling the network-filling process. *Journal of Hydroinformatics*, *13*(3), 358–373. https://doi.org/10.2166/hydro.2010.026

Marsili, V., Mazzoni, F., Alvisi, S., Maietta, F., Capponi, C., Meniconi, S., Brunone, B., & Franchini, M. (2023). Investigation of pressure transients induced on a real water service line by user's activity. *AQUA — Water Infrastructure, Ecosystems and Society*. https://doi.org/10.2166/aqua.2023.276

Marsili, V., Mazzoni, F., Marzola, I., Alvisi, S., & Franchini, M. (2023). Intermittent water supply system rehabilitation through a multiphase methodology based on network analysis and hydraulic modeling. *Journal of Water Resources Planning and Management*, *149*(9). https://doi.org/10.1061/jwrmd5.Wreng-6116

Martin, C. S. (1976). Entrapped air in pipelines. *Second International Conference on Pressure Surges*, 15–28.

Martins, N. M. C., Delgado, J. N., Ramos, H. M., & Covas, D. I. C. (2017). Maximum transient pressures in a rapidly filling pipeline with entrapped air using a cfd model. *Journal of Hydraulic Research*, *55*(4), 506–519. https://doi.org/10.1080/00221686.2016.1275046

Martins, S. C., Ramos, H. M., & Almeida, A. B. (2015). Conceptual analogy for modelling entrapped air action in hydraulic systems. *Journal of Hydraulic Research*, *53*(5), 678–686. https://doi.org/10.1080/00221686.2015.1077353

McIntosh, A. C. (2003). *Asian water supplies: Reaching the urban poor* (Report). Asian Development Bank and International Water Association.

Meniconi, S., Brunone, B., Ferrante, M., & Capponi, C. (2016). Mechanism of interaction of pressure waves at a discrete partial blockage. *Journal of Fluids and Structures*, *62*, 33–45. https://doi.org/10.1016/j.jfluidstructs.2015.12.010

Mohan, S., & Abhijith, G. R. (2020). Hydraulic analysis of intermittent water-distribution networks considering partial-flow regimes. *Journal of Water Resources Planning and Management*, *146*(8), 04020071. https://doi.org/10.1061/(asce)wr.1943-5452.0001246

Mokssit, A., de Gouvello, B., Chazerain, A., Figuères, F., & Tassin, B. (2018). Building a methodology for assessing service quality under intermittent domestic water supply. *Water*, *10*(9), 2–24. https://doi.org/10.3390/w10091164

Mortensen, J. D., Barfuss, S. L., & Johnson, M. C. (2011a). Scale effects of air entrained by hydraulic jumps within closed conduits. *Journal of Hydraulic Research*, *49*(1), 90–95. https://doi.org/10.1080/00221686.2010.536695

Mortensen, J. D., Barfuss, S. L., & Johnson, M. C. (2011b). Scale effects of air entrained by hydraulic jumps within closed conduits. *Journal of Hydraulic Research*, *49*(1), 90–95. https://doi.org/10.1080/00221686.2010.536695

Nyahora, P. P., Babel, M. S., Ferras, D., & Emen, A. (2020). Multi-objective optimization for improving equity and reliability in intermittent water supply systems. *Water Supply*, *20*(5), 1592–1603. https://doi.org/10.2166/ws.2020.066

Pachaly, R., Vasconcelos, J., Allasia, D., & Minetto, B. (2019). Field evaluation of discretized model setups for the storm water management model. *Journal of Water Management Modeling*, *27*, C463. https://doi.org/10.14796/jwmm.C463

Pachaly, R. L., Vasconcelos, J. G., Allasia, D. G., & Bocchi, J. P. P. (2021). Evaluating swmm capabilities to simulate closed pipe transients. *Journal of Hydraulic Research*, *60*(1), 1–8. https://doi.org/10.1080/00221686.2020.1866695

Pachaly, R. L., Vasconcelos, J. G., & Allasia, D. G. (2021). Surge predictions in a large stormwater tunnel system using swmm. *Urban Water Journal*, *18*(8), 577–584. https://doi.org/10.1080/1573062x.2021.1916828

Pachaly, R. L., Vasconcelos, J. G., Allasia, D. G., Tassi, R., & Bocchi, J. P. P. (2020). Comparing swmm 5.1 calculation alternatives to represent unsteady stormwater sewer flows. *Journal of Hydraulic Engineering*, *146*(7), 1–16. https://doi.org/10.1061/(asce)hy.1943-7900.0001762

Peddu, A., Chakraborty, S., & Kr. Das, P. (2018). Visualization and flow regime identification of downward air–water flow through a 12 mm diameter vertical tube using image analysis. *International Journal of Multiphase Flow*, *100*, 1–15. https://doi.org/10.1016/j.ijmultiphaseflow.2017.11.016

Perron, A., Kiss, L. I., & Poncsák, S. (2006). An experimental investigation of the motion of single bubbles under a slightly inclined surface. *International Journal of Multiphase Flow*, *32*(5), 606–622. https://doi.org/10.1016/j.ijmultiphaseflow.2006.02.001

Politano, M., Odgaard, A. J., & Klecan, W. (2007). Case study: Numerical evaluation of hydraulic transients in a combined sewer overflow tunnel system. *Journal of Hydraulic Engineering*, *133*(10), 1103–1110. https://doi.org/10.1061/åĚśASCEåĚš0733-9429åĚś2007åĚš133:10åĚś1103åĚš

Pothof, I., & Clemens, F. (2010). On elongated air pockets in downward sloping pipes. *Journal of Hydraulic Research*, *48*(4), 499–503. https://doi.org/10.1080/00221686.2010.491651

Pothof, I., & Clemens, F. (2011). Experimental study of air–water flow in downward sloping pipes. *International Journal of Multiphase Flow*, *37*(3), 278–292. https://doi.org/10.1016/j.ijmultiphaseflow.2010.10.006

Pozos, O., Giesecke, J., Marx, W., Rodal, E. A., & Sanchez, A. (2010). Experimental investigation of air pockets in pumping pipeline systems. *Journal of Hydraulic Research*, *48*(2), 269–273. https://doi.org/10.1080/00221681003726262

Rabben, S., Els, H., & Rouve, G. (1983). Investigation on flow aeration at offsets downstream of high-head control structures. *20th IAHR Congress, Vol. 4*, pp 354–360.

Rajaratnam, N. (1967). Hydraulic jumps. In V. T. Chow (Ed.), *Advances in hydroscience* (pp. 197–280, Vol. 4). Elsevier. https://doi.org/10.1016/B978-1-4831-9935-1.50011-2

Ramezani, L., Karney, B., & Malekpour, A. (2015). The challenge of air valves: A selective critical literature review. *Journal of Water Resources Planning and Management*, *141*(10). https://doi.org/10.1061/(asce)wr.1943-5452.0000530

Ramezani, L., Karney, B., & Malekpour, A. (2016). Encouraging effective air management in water pipelines: A critical review. *Journal of Water Resources Planning and Management*, *142*(12), 04016055. https://doi.org/10.1061/(asce)wr.1943-5452.0000695

Roesner, L. A., Aldrich, J. A., Dickinson, R. E., & Barnwell, T. O. (1988). *Storm water management model user's manual, version 4: Extran addendum* (Report No. EPA/600/3-88/00lb). U.S. Environmental Protection Agency.

Romero, G., Fuertes-Miquel, V. S., Coronado-Hernández, Ó. E., Ponz-Carcelén, R., & Biel-Sanchis, F. (2020). Analysis of hydraulic transients during pipeline filling processes with air valves in large-scale installations. *Urban Water Journal*, *17*(6), 568–575. https://doi.org/10.1080/1573062x.2020.1800762

Rossman, L. A. (2022). *Addendum to the storm water management model reference manual, volume ii – hydraulics* (Report No. EPA/600/C-22/016). U.S. Environmental Protection Agency.

Rossman, L. A., Woo, H., Tryby, M., Shang, F., Janke, R., & Haxton, T. (2020). *Epanet 2.2 user manual* (Report No. EPA/600/R-20/133). U.S. Environmental Protection Agency.

Rossman, L. A. (2017). *Storm water management model reference manual volume ii – hydraulics* (Report No. EPA/600/R-17/111). U.S. Environmental Protection Agency.

Schulz, H. E., Vasconcelos, J. G., & Patrick, A. C. (2020). Air entrainment in pipe-filling bores and pressurization interfaces. *Journal of Hydraulic Engineering*, *146*(2), 04019053. https://doi.org/10.1061/(asce)hy.1943-7900.0001672

Sharior, S., Hodges, B. R., & Vasconcelos, J. G. (2023). Generalized, dynamic, and transient-storage form of the preissmann slot. *Journal of Hydraulic Engineering*, *149*(11), 04023046. https://doi.org/10.1061/jhend8.Hyeng-13609

Sharma, S. K., & Vairavamoorthy, K. (2009). Urban water demand management: Prospects and challenges for the developing countries. *Water and Environment Journal*, *23*(3), 210–218. https://doi.org/10.1111/j.1747-6593.2008.00134.x

Simukonda, K., Farmani, R., & Butler, D. (2018a). Causes of intermittent water supply in lusaka city, zambia. *Water Practice and Technology*, *13*(2), 335–345. https://doi.org/10.2166/wpt.2018.046

Simukonda, K., Farmani, R., & Butler, D. (2018b). Intermittent water supply systems: Causal factors, problems and solution options. *Urban Water Journal*, *15*(5), 488–500. https://doi.org/10.1080/1573062x.2018.1483522

Sjöberg, A. (1982a). Sewer network models dagvl-a and dagvl-diff. In B. C. Yen (Ed.), *Urban stormwater hydraulics and hydrology* (pp. 127–136).

Sjöberg, A. (1982b). *On the stability of gradually varied flows in sewers* (Report No. Series B:33). Department of Hydraulics Chalmers Univeristy of Technology.

Song, C. C. S., Cardie, J. A., & Leung, K. S. (1983). Transient mixed-flow models for storm sewers. *Journal of Hydraulic Engineering*, *109*(11), 1487–1504.

Souza, R. G., Meirelles, G., & Brentan, B. (2022). Energy and hydraulic efficiency in intermittent operation of water distribution networks. *Journal of Water Resources Planning and Management*, *148*(5). https://doi.org/10.1061/(asce)wr.1943-5452.0001552

Staff, A. (2001). *Air release, air/vacuum valves and combination air valves (m51)*. American Water Works Association.

Stephenson, D. (1997). Effects of air valves and pipework on water hammer pressures. *Journal of Transportation Engineering*, *123*(2), 101–106. https://doi.org/10.1061/(ASCE)0733-947X(1997)123:2(101)

Tanyimboh, T., Tahar, B., & Templeman, A. (2003). Pressure-driven modelling of water distribution systems. *Water Science and Technology: Water Supply*, *3*(1-2).

Tijsseling, A. S., Hou, Q., & Bozkuş, Z. (2019). Rapid liquid filling of a pipe with venting entrapped gas: Analytical and numerical solutions. *Journal of Pressure Vessel Technology*, *141*(4). https://doi.org/10.1115/1.4043321

Trajkovic, B., Ivetic, M., Calomino, F., & D'Ippolito, A. (1999). Investigation of transition from free surface to pressurized flow in a circular pipe. *Water Science and Technology*, *39*(9), 105–112. https://doi.org/10.2166/wst.1999.0453%JWaterScienceandTechnology

Tukker, M., Kooij, K., & Pothof, I. (2016). *Hydraulic design and management of wastewater transport systems*. IWA Publishing.

USACE. (1980). *Engineering and design: Hydraulic design of reservoir out-let works. engineering manual* (Report No. EM 1110-2-1602). USACE. www.publications.usace.army.mil/Portals/76/Publications/EngineerManuals/EM_1110-2-1602.pdf

Vairavamoorthy, K., Akinpelu, E., Lin, Z., & Ali, M. (2001). Design of sustainable water distribution systems in developing countries. In *Bridging the gap* (pp. 1–10). https://doi.org/doi:10.1061/40569(2001)378

Van der Bruggen, B., Borghgraef, K., & Vinckier, C. (2009). Causes of water supply problems in urbanised regions in developing countries. *Water Resources Management*, *24*(9), 1885–1902. https://doi.org/10.1007/s11269-009-9529-8

Vasconcelos, J., Eldayih, Y., Zhao, Y., & Jamily, J. A. (2018). Evaluating storm water management model accuracy in conditions of mixed flows. *Journal of Water Management Modeling*, *27:C451*, 1–10. https://doi.org/10.14796/jwmm.C451

Vasconcelos, J. G., & Wright, S. J. (2007). Comparison between the two-component pressure approach and current transient flow solvers. *Journal of Hydraulic Research*, *45*(2), 178–187. https://doi.org/10.1080/00221686.2007.9521758

Vasconcelos, J. G., Wright, S. J., & Roe, P. L. (2006). Improved simulation of flow regime transition in sewers: Two-component pressure approach. *Journal of Hydraulic Engineering*, *132*(6), 553–562. https://doi.org/10.1061/(ASCE)0733-9429(2006)132:6(553)

Vasconcelos, J. G., Klaver, P. R., & Lautenbach, D. J. (2014). Flow regime transition simulation incorporating entrapped air pocket effects. *Urban Water Journal*, *12*(6), 488–501. https://doi.org/10.1080/1573062x.2014.881892

Vasconcelos, J. G., & Leite, G. M. (2012). Pressure surges following sudden air pocket entrapment in storm-water tunnels. *Journal of Hydraulic Engineering*, *138*(12), 1081–1089. https://doi.org/10.1061/(asce)hy.1943-7900.0000616

Vasconcelos, J. G., & Marwell, D. T. (2011). Innovative simulation of unsteady low-pressure flows in water mains. *Journal of Hydraulic Engineering*, *137*(11), 1490–1499. https://doi.org/10.1061/(asce)hy.1943-7900.0000440

Wagner, J. M., Shamir, U., & Marks, D. H. (1988). Water distribution reliability: Simulation methods. *114*(2), 276–294.

Walski, T. M., Barnhart, T. S., Driscoll, J. M., & Yencha, R. M. (1994). Hydraulics of corrosive gas pockets in force mains. *Water Environment Research*, *66*(6), 772–778. https://www.jstor.org/stable/25044480

Walter, D., Mastaller, M., & Klingel, P. (2017). Accuracy of single-jet water meters during filling of the pipe network in intermittent water supply. *Urban Water Journal*, *14*(10), 991–998. https://doi.org/10.1080/1573062x.2017.1301505

Wang, L., Wang, F., Karney, B., & Malekpour, A. (2017). Numerical investigation of rapid filling in bypass pipelines. *Journal of Hydraulic Research*, *55*(5), 647–656. https://doi.org/10.1080/00221686.2017.1300193

Wang, X., Lin, J., Ghidaoui, M. S., Meniconi, S., & Brunone, B. (2020). Estimating viscoelasticity of pipes with unknown leaks. *Mechanical Systems and Signal Processing*, *143*. https://doi.org/10.1016/j.ymssp.2020.106821

Wiggert, D. C. (1972). Transient flow in free-surface, pressurized systems. *Journal of the Hydraulics Division*, *98*(1), 11–27. https://doi.org/10.1061/JYCEAJ.0003189

Wisner, P., Mohsen, F., & Kouwen, N. (1975). Removal of air from water lines by hydraulic means. *Journal of the Hydraulics Divison*, *101*(HY2), 243–257. https://doi.org/10.1061/JYCEAJ.0004201

Wylie, E., & Streeter, V. (1993). *Fluid transients in systems* (1st Edition). Prentice Hall, Englewood Cliffs, NJ. https://books.google.pt/books?id=Ep9RAAAAMAAJ

Yan, X. F., Duan, H. F., Wang, X. K., Wang, M. L., & Lee, P. J. (2021). Investigation of transient wave behavior in water pipelines with blockages. *Journal of Hydraulic Engineering*, *147*(2). https://doi.org/10.1061/(asce)hy.1943-7900.0001841

Yen, B. C. (1986). Hydraulics of sewers.

Zhou, F., Hicks, F. E., & Steffler, P. M. (2002). Transient flow in a rapidly filling horizontal pipe containing trapped air. *Journal of Hydraulic Engineering*, *128*(6), 625–634. https://doi.org/10.1061/(asce)0733-9429(2002)128:6(625)

Zhou, L., Liu, D., & Karney, B. (2013). Investigation of hydraulic transients of two entrapped air pockets in a water pipeline. *Journal of Hydraulic Engineering*, *139*(9), 949–959. https://doi.org/10.1061/(asce)hy.1943-7900.0000750

Zhou, L., Liu, D., Karney, B., & Wang, P. (2013). Phenomenon of white mist in pipelines rapidly filling with water with entrapped air pockets. *Journal of Hydraulic Engineering*, *139*(10), 1041–1051. https://doi.org/10.1061/(asce)hy.1943-7900.0000765

Zhou, L., Liu, D., Karney, B., & Zhang, Q. (2011). Influence of entrapped air pockets on hydraulic transients in water pipelines. *Journal of Hydraulic Engineering*, *137*(12), 1686–1692. https://doi.org/10.1061/(asce)hy.1943-7900.0000460

Zhou, L., Liu, D.-y., & Ou, C.-q. (2011). Simulation of flow transients in a water filling pipe containing entrapped air pocket with vof model. *Engineering Applications of Computational Fluid Mechanics*, *5*(1), 127–140. https://doi.org/10.1080/19942060.2011.11015357

Zhou, L., Wang, H., Karney, B., Liu, D., Wang, P., & Guo, S. (2018). Dynamic behavior of entrapped air pocket in a water filling pipeline. *Journal of Hydraulic Engineering*, *144*(8), 04018045. https://doi.org/10.1061/(asce)hy.1943-7900.0001491

Zhou, L., Pan, T., Wang, H., Liu, D., & Wang, P. (2019). Rapid air expulsion through an orifice in a vertical water pipe. *Journal of Hydraulic Research*, *57*(3), 307–317. https://doi.org/10.1080/00221686.2018.1475427

Zhou, L., Cao, Y., Karney, B., Bergant, A., Tijsseling, A. S., Liu, D., & Wang, P. (2020). Expulsion of entrapped air in a rapidly filling horizontal pipe. *Journal of Hydraulic Engineering*, *146*(7), 04020047. https://doi.org/10.1061/(asce)hy.1943-7900.0001773

Zhou, L., Lu, Y., Karney, B., Wu, G., Elong, A., & Huang, K. (2023). Energy dissipation in a rapid filling vertical pipe with trapped air. *Journal of Hydraulic Research*, 1–13. https://doi.org/10.1080/00221686.2022.2132309

Zhu, J., Duan, X., Wu, G., Li, X., & Tang, X. (2022). Numerical investigations of hydraulic transient and thermodynamic characteristics of water flow impacting air pocket inside pipe based on clsvof. *Journal of Hydroinformatics*, *24*(4), 856–874. https://doi.org/10.2166/hydro.2022.020